Less-Visible Contrast Enhancement Based on Human Visual Perception

SUTHUM KEERATIVITTAYANUN

Japan Advanced Institute of Science and Technology

Doctoral Dissertation

Less-Visible Contrast Enhancement Based on Human Visual Perception

SUTHUM KEERATIVITTAYANUN

Supervisor: Professor Kazunori Kotani

School of Information Science
Japan Advanced Institute of Science and Technology

September 2018

Abstract

Typically, conventional image-enhancement methods have a common problem concerning the over-enhancement in an image which contains both less-visible and nicely-visible areas, while preserve such the key-lighting of image or the tone of original image. To solve such problem, we propose two new less-visible-image enhancement schemes, called the less-visible contrast enhancement method (LVCE) and the less-visible contrast enhancement based on human visual perception (LVCEHP). For the LVCE, we propose a new contrast enhancement method based on the singular value decomposition (SVD), an adaptive non-linear scaling function, and a pyramid-based blending method. The SVD is used to decompose an image into several. Based on our investigation, we found that some layers are associated with the less-visible area. Then, the less-visible layers are selected and enhanced by using the proposed logarithm-function. For the LVCEHP, we propose a new contrast enhancement method based on several principles of visual human perception such as the Weber's law in image contrast and the Just-Noticeable-Different (JND). At the beginning, we study the principle of image contrast. Based on this study, we found that the human perception is more sensitive to image contrast rather than absolute luminance values.

The original idea of LVCEHP is to enhance an image by applying several principles of visual human perception such as the Weber's law in image contrast and the Just-Noticeable-Different (JND) to create the algorithm. Then, we apply definition of the Weber's contrast to the proposed non-scaling function. By investigating the characteristic of Weber's equation, there are three possible cases that could be occurred in the entire image. We used these cases as the inspiration to calculate the enhancement rate of the proposed non-linear scaling function. We also use the principle of JND in the image to guarantee that the less-visible areas perceived discriminatory from the previous ones too. Moreover, we used the principle of singular value decomposition (SVD) to propose a new technique for analyze and remove the hidden noise of the input image. We experimentally found that the smaller area-bounded of the singular-value curve implies the higher level of noise. If the area of singular value contains the area-bounded less than the threshold value of the hidden noise value. Then, we remove the noise layer before the enhancement process. Lastly, to recover the nicely-visible area, we propose the pyramid-based blending techniques for fusing two images in order to solve the problem of information missing in the blending process. This recovery process is mandatory because enhancing images in the previous step might cause the over-enhancement. Objective and subjective evaluations were conducted, and experimental results show that our proposed method can successfully improve the less-visible contrast without amplifying noise. It also preserves the tone and texture of original images and produces satisfying results in terms of human preference.

Keywords: less-visible contrast enhancement, human visual perception, singular value decomposition, pyramid-based blending, just-noticeable-different

Acknowledgments

Numerous people helped bring this work to fruition. My deepest gratitude goes first and foremost to Prof. Kazunori Kotani, and Prof. Tosiahki Kondo, my supervisors at SIIT, and JAIST, respectively, for their guidance and support. My heartfelt gratitude is extended to Prof. Waree Kongprawechnon, and Dr. Teera Phatrapornnant for their critical comments and invaluable suggestions. My sincere thanks also go to my friend, Dr. Jessada Karnjana, for giving me time and encouragement. I appreciate the supporting grants in SIIT-JAIST-NECTEC dual degree program. Last but not least, I would like to give many thanks to my parents who have stood by my side for the whole years of education life.

Table of Contents

This dissertation was prepared according to the curriculum for the Collaborative Education Program organized by Japan Advanced Institute of Science and Technology and Sirindhron International Institute of Science and Technology, Thammasat University.

List of Figures

List of Tables

Chapter 1

Introduction

1.1 Less-visible Contrast Enhancement: Importance and Challenge

Over the last few years, one of the challenging problems in digital image processing is to enhance an image which contains both less-visible and nicely-visible areas. In this case, only the former are needed to be enhanced, whereas the latter areas should be preserved. Note that, in this work, we call an image that is correctly exposed a nicely-visible one. In general, a good enhancement method should produce a resulting image in which information in less-visible areas can be easily perceived by our visual system. Also image tone, texture, and other characteristics, e.g. the naturalness, should be similar to those of the original image. Moreover, a good enhancement process should avoid unwanted side effects, such as noise amplification or the halo effect [1].

During the early years, the power-law transformation, the logarithmic transformation, and the histogram equalization (HE) are ones of famous techniques for enhancing images [2]. The power-law and the logarithmic transformations deploy non-linear functions to expand input image ranges, i.e. a smaller input value is amplified with a greater factor. Therefore, the less-visible areas could be enhanced. However, both introduce a side effect, i.e. hidden noise in the less-visible areas is amplified, and nicely-visible areas are unnecessarily amplified as well. Consequently, they cause the noisy and over-exposed image. The HE enhances an input image by expanding its histogram range. However, performance of this method strongly depends on characteristics of the histogram. These three methods are classified as the global enhancement,

and they all share the common problems of noise amplification and over-enhancement.

Later, several local enhancement methods have been proposed. These methods include the histogram-based [3], [4], the just-noticeable-different-based (JND-based) [5], the retinex-based [6], [7], [8], and the singular-value-decomposition-based (SVD-based) methods [9], [10]. For example, the adaptive histogram equalization (AHE) and the contrast limit adaptive histogram equalization (CLAHE) [3] are histogram-based and widely used to improve local contents. However, this approach still suffers from unnecessarily amplifying, and it suppresses values in some regions in the case that distribution of intensity is narrow and intensity values are too high or too low. Recently, X. Fu *et al.* try to solve these problems by implementing an enhancement method based on the multi exposure fusion with a sigmoid function and adoptive histogram equalization [11]. In this paper, we abbreviate the name of this method as MEF. According to this method, the under-exposed images, well-exposed images, and over-exposed images are blended together to generate the resulting image. This method can solve those two problems. However, in some cases, it still amplifies the hidden noise. An example of this case is to be shown in Sect. 3.3.

The JND-based approach employs the Weber's law, which is based on the human visual perception, to create a non-linear function [5]. The advantage of this approach is that an enhanced image looks clearly visible because the average local contrast is increased. Although the less-visible areas can be seen clearly, the contrast in the nicely-visible areas is also strengthened. Hence, in some cases, the resulting image looks different from the original one.

The retinex-based methods, such as the single-scale retinex (SSR) [6], the multi-scale retinex (MSR) [7], and the multi-scale retinex with color restoration (MSRCR) [8], originate from a theory proposed by Edwin H. Land *et al.* [12]. Functions used in these methods are based on the human visual perception. These methods enhance less-visible areas by using logarithmic transformation and the Gaussian surround function. These methods have a critical problem concerning the value of standard deviation of the Gaussian function. That is, if the standard deviation is too small, the nicely-visible parts of an enhanced image will be degraded and look unnatural. Even though the MSR and the MSRCR have tried to solve the problem by using several different standard deviations, the problem still persists, especially when the biggest standard deviation used by the algorithm is smaller than an object size displayed on the image. The multi-scale retinex with chromaticity perservation (MSRCP), which is an improved

MSRCR, was proposed by A. B. Petro *et al.* [13] to solve such problem. In stead of performing the algorithm to each RGB channels, MSRCP performs only on the luminance channel. Then, it computes the scaling factor to restore true color. In most of the cases, resulting images enhanced by the MSRCP are excellent. However, in some cases, this algorithm produces an image which is too colorful, hence an unnatural-looking image. The Frankle and McCann algorithm is another retinex, and this method uses a single pixel to estimate a new value by computing long-distance interactions between pixels and progressively move to short-distance interactions [14]. The benefit of this method is that it can reduce a computational-complexity time. However, it cannot tolerate hidden noise. Another method similar to the retinex-based is fast center surround modification [1]. The algorithm employed concept of the shunting centre-surround cells of the human visual system to modify the under and over-expose regions [1]. To our knowledge, this method produce the best resulting images in terms of tone preservation, detail preservation, and human preference. However, in some cases, it still amplifies the hidden noise. An example of this case is to be shown in Sect. 3.3.

The SVD-based methods enhance an input image by amplifying all singular values of the matrix representing the image [9], [10]. The performance of these methods depends on characteristics of the input image. That is, the algorithm works well only when most pixel of the input image have low intensity values; otherwise, the problem of over-enhancement occurs.

1.2 Motivation and Research Goal

As stated in the previous section, this work aims to propose a new method based on adaptive non-linear mapping function of the averaged-pixel values. Also it should not suffer from amplifying hidden noise and distort the original tone, texture, key-lighting, etc. We choose to investigate the Singular Vector Decomposition (SVD) because according to its advantages: either the possibility to enhance the visible areas without amplifying the hidden noise or the ability to remove the hidden noise along the input image.

This paper proposes a new less-visible enhancement method based on the human visual perception using an adaptive none-linear scaling function. The proposed method aims to satisfy the following properties.

- The less-visible areas are enhanced to be visible without amplifying noise.

- The tone, texture, and key-lighting of the enhanced image should be similar to those of the original one.
- The enhancement method should not cause unwanted side effects, such as the halo effect, over-enhancement, etc.
- The enhancement method should create the resulting image that is preferred by participants in a preference test.

1.3 Thesis Outline

The outline of the rest of this thesis, which consists of five chapters, is as follows. Chapter 2 details on the proposed methods. The first one is called the less-visible contrast enhancement (LVCE) which it mainly focused on on a non-linear scaling function and the singular value decomposition (SVD). The SVD is used to decompose the image into several layers. Some layers are associated with the less-visible areas. Then, such layers are strengthened by using the proposed logarithmic-scaling function. The second one is called the less-visible contrast enhancement based on human-visual perception (LVCEHP). At this techniques, we first analyze a hidden noise level of an image in order to avoid such a hidden noise. If the level of hidden is greater than a predefined value, an SVD-based technique will be used to remove the noise. Then, we use that image to create the result. We believe that a function used to enhance an pixel value should depend not only the pixel value but also on its neighbors. Also, this enhancement function should be based on a human perception model.

Chapter 3 reports from our simulations in implementation and evaluation of the proposed methods. The explanation of evaluation methods, and parameters are also describe in this chapter. Chapter 4 discuss about the strength and weakness of the proposed methods as well as the reason for choosing different kinds of objective and subjective method.

Chapter 5 summarizes this work. It emphasizes the contributions and discusses possibilities for further improvement.

Chapter 2

Proposed method

We proposed two methods in this chapter, an our scheme are based on adaptive non-linear scaling function, the singular value decomposition (SVD), and the pyramid-based blending method. The first one is called the less-visible contrast enhancement (LVCE) in which only the associated layers obtained from the SVD will be used to enhanced the less-visible areas. The second one is called the less-visible contrast enhancement based on human visual perception, which is constructed by generating the non-linear scaling function for each pixel values. The just-noticeable-different (JND) is used to control the slope of scaling function along each pixel. To recover the visible-area of the image, the pyramid-based blending method is applied.

2.1 Less-visible contrast enhancement based on Singular Value Decomposition

In this method, we study a characteristic of the singular value decomposition (SVD) which it can decompose the original image into several layers. Based on our investigation, some layers may associate with the less-visible areas. Hence, if we can extract and enhance such layers, our goal may be achieved.

To enhance the less-visible contrast without amplifying noise, we use the SVD to decompose an input image into three additive layers: main body, less-visible areas, and noise. Only the less-visible areas are strengthened before all three layers are combined to produce the enhanced image. Then, the pyramid-based blending method is used to reduce the brightness of over-enhanced areas due to the selective enhancement and to make the resulting image smooth. The

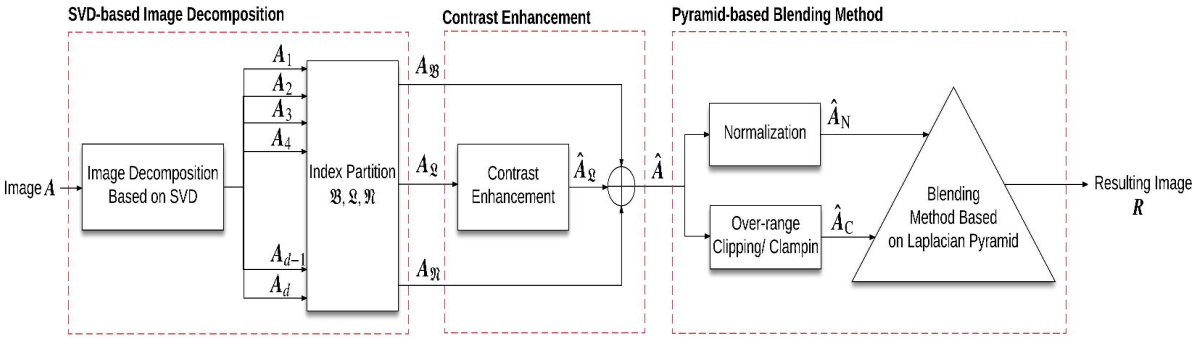

Figure 2.1: Less-visible contrast enhancement method.

block diagram of our proposed method for the less-visible contrast enhancement is shown in Fig.2.1. The details are provided in the following subsections.

2.1.1 Singular Value Decomposition

In linear algebra, the SVD is a factorization of a matrix. Let $\boldsymbol{X}_{m\times n}$ denote a matrix $\boldsymbol{X}$ of size $m\times n$. The SVD decomposes the matrix $\boldsymbol{X}_{m\times n}$ into a product of three matrices $\boldsymbol{U}_{m\times m}$, $\boldsymbol{D}_{m\times n}$, and $\boldsymbol{V}_{n\times n}$ with the following relationship.

$$\boldsymbol{X} = \boldsymbol{U}\boldsymbol{D}\boldsymbol{V}^{\mathrm{T}}, \tag{2.1}$$

where $\boldsymbol{X}$ is a matrix being decomposed, $\boldsymbol{U}$ and $\boldsymbol{V}$ are orthogonal matrices, and $\boldsymbol{D}$ is a diagonal matrix whose non-zero elements are called the *singular values*.

Let U_i and V_i denote vectors at the column i of $\boldsymbol{U}$ and $\boldsymbol{V}$, respectively, i.e. $\boldsymbol{U} = [U_1\ U_2\ U_3\ ...\ U_m]$ and $\boldsymbol{V} = [V_1\ V_2\ V_3\ ...\ V_n]$. Let λ_i denote the *eigenvalues* of $\boldsymbol{X}\boldsymbol{X}^{\mathrm{T}}$ (or $\boldsymbol{X}^{\mathrm{T}}\boldsymbol{X}$). The vectors U_i and V_i are the *eigenvectors* of $\boldsymbol{X}\boldsymbol{X}^{\mathrm{T}}$ and $\boldsymbol{X}^{\mathrm{T}}\boldsymbol{X}$, respectively, and are sorted in descending order of the corresponding eigenvalues. The elements on the main diagonal of $\boldsymbol{D}$ are then the square root of these eigenvalues. Mathematically, the matrix $\boldsymbol{X}$ can be expressed in the following expansion.

$$\boldsymbol{X} = \boldsymbol{X}_1 + \boldsymbol{X}_2 + ... + \boldsymbol{X}_d. \tag{2.2}$$

$$\boldsymbol{X}_i = \sqrt{\lambda_i} \times U_i \times V_i^{\mathrm{T}}, \tag{2.3}$$

where $d = \max\{i, \text{such that } \lambda_i > 0\}$.

In this work, the SVD is used to decompose a gray scale image $\boldsymbol{A}$ into several additive $\boldsymbol{A}_i$. In other words,

$$\boldsymbol{A} = \sum_{i=1}^{d} \boldsymbol{A}_i. \tag{2.4}$$

We experimentally discovered that the set of singular-value indices, $\mathfrak{I} = \{1, 2, 3, ..., d\}$, can be partitioned into three disjoint subsets $\mathfrak{B}$, $\mathfrak{L}$, and $\mathfrak{R}$ such that the image $\boldsymbol{A}$ can be decomposed into three images $\boldsymbol{A}_{\mathfrak{B}}$, $\boldsymbol{A}_{\mathfrak{L}}$, and $\boldsymbol{A}_{\mathfrak{R}}$, where they are the main-body image, the less-visible-area image, and the noise, respectively, and each of them can be reconstructed by the following equations: $\boldsymbol{A}_{\mathfrak{B}} = \sum_{i\in\mathfrak{B}} \boldsymbol{A}_i$, $\boldsymbol{A}_{\mathfrak{L}} = \sum_{i\in\mathfrak{L}} \boldsymbol{A}_i$, and $\boldsymbol{A}_{\mathfrak{R}} = \sum_{i\in\mathfrak{R}} \boldsymbol{A}_i$.

To determine these three subsets, we first extract the singular values of the matrix $\boldsymbol{A}$. An example of the singular values is shown in Fig. 2.2. The singular values in this figure are linearly normalized such that the new values cover the range from 0 to 1, where the new minimum and maximum values are 0 and 1, respectively. Then, we investigate the distribution of the singular values on the binary-logarithmic scale. That is, on the linear scale, we divide the range [0, 1] of normalized singular values into b bins of which their width is equal to 2^{-j}, where j is the bin index. An example is shown in Fig. 2.3(a). Let $f(\sqrt{\lambda_i})$ denote the normalized log-singular-value of the singular value $\sqrt{\lambda_i}$. It is defined as follows.

$$f(\sqrt{\lambda_i}) = 1 + \frac{1}{b}\log_2\left(\frac{\sqrt{\lambda_i} - \sqrt{\lambda_d}}{\sqrt{\lambda_1} - \sqrt{\lambda_d}}\right), \tag{2.5}$$

for all i such that $\sqrt{\lambda_i} > \sqrt{\lambda_d}$. Otherwise, $f(\sqrt{\lambda_i}) = 0$

The plot of $f(\sqrt{\lambda_i})$ against i is shown in Fig. 2.3(b). Subsequently, we plot the numbers of the singular values that fall within each bin. Fig. 2.5 (left) shows the distribution of singular-values illustrated in Fig. 2.2. Note that when the number of bins increased, the distribution looks more similar to the normal distribution. In our experiment, we set the value of b to 21.

We observed that the first eight to ten bins associate with the main-body image, whereas the last five to seven bins always associate with the noise. Fig. 2.4 demonstrates examples of these observations. We made use of these findings to propose an algorithm that automatically determines the subsets $\mathfrak{B}$, $\mathfrak{L}$, and $\mathfrak{R}$ as follows.

1. The distribution of singular values of the image on the binary-logarithmic scale is plotted.
2. The maximum bin is determined. We denote the index of this bin by q.
3. An index $p \in \mathfrak{L}$ if and only if the normalized $\sqrt{\lambda_p}$ is in the range of bin $S_t h$ as $[q + d_{\min}, q + d_{\max}]$.

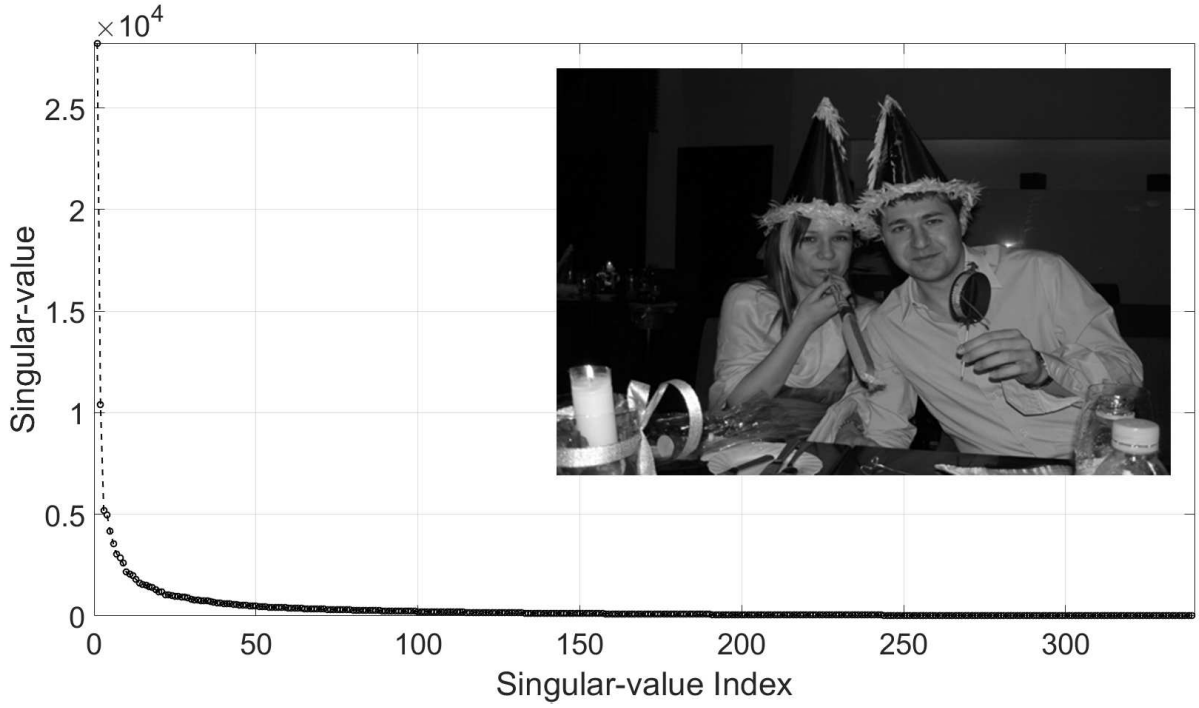

Figure 2.2: Singular values of the image displayed on the top-right.

4. The subset $\mathfrak{B}$ contains all indices that are less than the smallest member of $\mathfrak{L}$, then the subset $\mathfrak{N} = \mathfrak{I} - (\mathfrak{B} \cup \mathfrak{L})$.

Fig. 2.5 shows an example of these three subsets. The subset $\mathfrak{B}$ contains the indices in the black bins, the subset $\mathfrak{L}$ contains the indices in the white bin, and the subset $\mathfrak{N}$ contains the rest. Fig. 2.5(b), 2.5(c), and 2.5(d) show $\boldsymbol{A}_{\mathfrak{B}}$, $\boldsymbol{A}_{\mathfrak{L}}$, and $\boldsymbol{A}_{\mathfrak{N}}$, respectively.

2.1.2 Contrast Enhancement

To enhance only the less-visible areas on the image without amplifying noise, only the less-visible-area layer, i.e. $\boldsymbol{A}_{\mathfrak{L}} = \sum_{i \in \mathfrak{L}} \boldsymbol{A}_i$, obtained from the previous step is strengthened. Our proposed enhancement method is similar to and based on the *Retinex algorithm*.

Conventionally, the Retinex algorithm utilizes a non-linear scale to increase smaller values (i.e. the less-visible areas on the image) with the factors that are greater than those used to increase the larger values (i.e. the clearly-visible areas). According to this algorithm, the enhanced image $\boldsymbol{R}^{\mathrm{SSR}}$ of the input image $\boldsymbol{I}$ is produced by the following equations [12].

$$\boldsymbol{R}^{\mathrm{SSR}}_{xy} = \ln \boldsymbol{I}_{xy} - \ln (\boldsymbol{F}_{xy} * \boldsymbol{I}_{xy}), \tag{2.6}$$

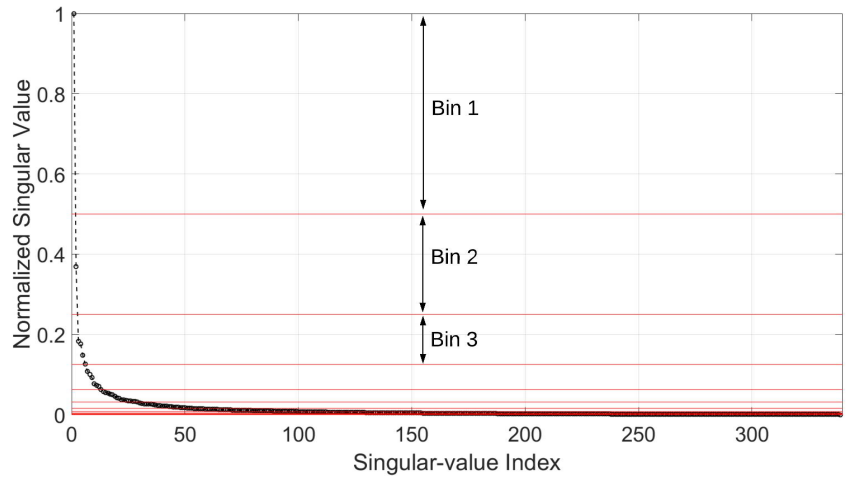

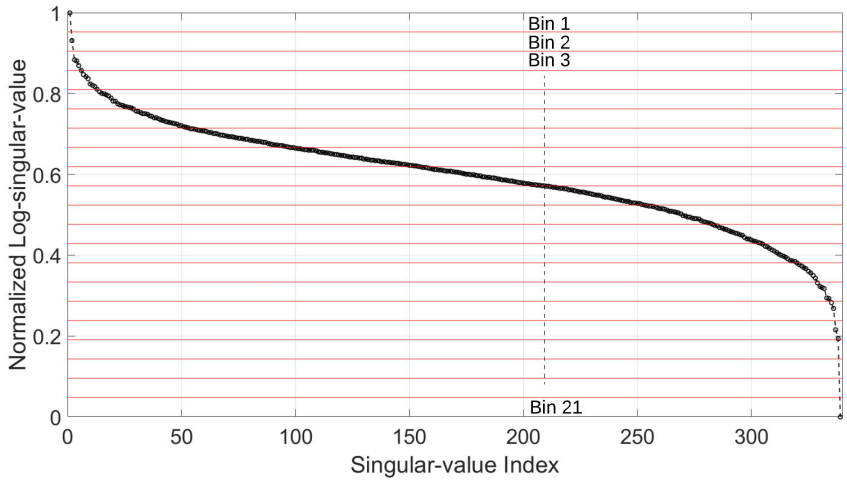

(b)

Figure 2.3: Normalized singular values against the indices: (a) on the linear scale and (b) on binary-logarithmic scale.

where $\boldsymbol{F}_{xy}$ is the Gaussian surround function given by

$$\boldsymbol{F}_{xy} = e^{-\frac{1}{\sigma^2}(x^2+y^2)} \tag{2.7}$$

with the property

$$\iint \boldsymbol{F}_{xy}\, dx\, dy = 1.$$

Note that the subscript x and y of the matrices represent the matrix elements at the row x and column y.

Similarly, to produce the enhanced layer $\hat{\boldsymbol{A}}_{\mathfrak{L}}$, we deploy the following formulae:

$$\hat{\boldsymbol{A}}_{\mathfrak{L},xy} = \left(55 \times \left(\frac{\tilde{\boldsymbol{A}}_{\mathfrak{L},xy} - \tilde{\boldsymbol{A}}_{\mathfrak{L},\min}}{\tilde{\boldsymbol{A}}_{\mathfrak{L},\min} - \tilde{\boldsymbol{A}}_{\mathfrak{L},\max}}\right) + 255\right) \times \tilde{\boldsymbol{A}}_{\mathfrak{L},xy}, \tag{2.8}$$

$$\tilde{\boldsymbol{A}}_{\mathfrak{L},xy} = \frac{\log_{15}\left(\alpha \breve{\boldsymbol{A}}^2_{\mathfrak{L},xy} + \beta \breve{\boldsymbol{A}}_{\mathfrak{L},xy} + \gamma\right)}{2}, \tag{2.9}$$

$$\breve{\boldsymbol{A}}_{\mathfrak{L},xy} = \boldsymbol{A}_{\mathfrak{L},xy} + |\boldsymbol{A}_{\mathfrak{L},\min}|. \tag{2.10}$$

where $\tilde{\boldsymbol{A}}_{\mathfrak{L},\min}$, $\tilde{\boldsymbol{A}}_{\mathfrak{L},\max}$, and $\boldsymbol{A}_{\mathfrak{L},\min}$ are the minimum value of the matrix $\tilde{\boldsymbol{A}}_{\mathfrak{L}}$, the maximum value of the matrix $\tilde{\boldsymbol{A}}_{\mathfrak{L}}$, and the minimum value of the matrix $\boldsymbol{A}_{\mathfrak{L}}$, respectively. The values of α, β, and γ are the scaling function as set in the predefined values as shown in section 3.2.1. We do not need the subtraction in eq. (2.6) because we enhance only the less-visible-area layer. Finally, the enhanced image $\hat{\boldsymbol{A}}$ is created by

$$\hat{\boldsymbol{A}} = \boldsymbol{A}_{\mathfrak{B}} + \hat{\boldsymbol{A}}_{\mathfrak{L}} + \boldsymbol{A}_{\mathfrak{R}}. \tag{2.11}$$

2.1.3 Pyramid-based Blending Method

The resulting image from the contrast enhancement described in the previous subsection sometimes can be over-enhanced because some pixel values may be greater than 1. This problem can be solved by adopting a blending technique. In this work, we adopt a scheme based on the Laplacian pyramid to reduce the over-enhancement effect.

The method based on Gaussian and Laplacian pyramids was originally proposed by Burt *et al.* [15]. Let $\mathbb{G}^n$ and $\mathbb{L}^n$ denote the n-level Gaussian and Laplacian operators, respectively. Then, the n-level Gaussian pyramid of the image $\boldsymbol{I}$, $\mathbb{G}^n(\boldsymbol{I})$, returns $n+1$ images $(\boldsymbol{G}_0, \boldsymbol{G}_1, ..., \boldsymbol{G}_n)$, where $\boldsymbol{G}_0$ is $\boldsymbol{I}$, and $\boldsymbol{G}_i$, for $i \geq 1$, are output images obtained from the low-pass filter with the decimation at the layer i. The n-level Laplacian pyramid of the image $\boldsymbol{I}$, $\mathbb{L}^n(\boldsymbol{I})$, returns $n+1$ images $(\boldsymbol{L}_0, \boldsymbol{L}_1, ..., \boldsymbol{L}_n)$, where $\boldsymbol{L}_n$ is $\boldsymbol{G}_n$, and $\boldsymbol{L}_i = \boldsymbol{G}_i - \uparrow \boldsymbol{G}_{i+1}$ for $i < n$. The symbol $\uparrow \boldsymbol{G}_{i+1}$ represents the image $\boldsymbol{G}_{i+1}$ after it is upsampled by a factor of 2.

We can reconstruct the image $\boldsymbol{I}$ by the inverse Laplacian $\mathbb{L}^{-n}$, which is defined as

$$\mathbb{L}^{-n}(\mathbb{L}^n(\boldsymbol{I})) = \boldsymbol{L}_0 + \uparrow \boldsymbol{L}_1 + \uparrow\uparrow \boldsymbol{L}_1 + ... + \uparrow^n \boldsymbol{L}_n, \tag{2.12}$$

where $\uparrow^n$ denotes the upsampling by a factor of 2^n.

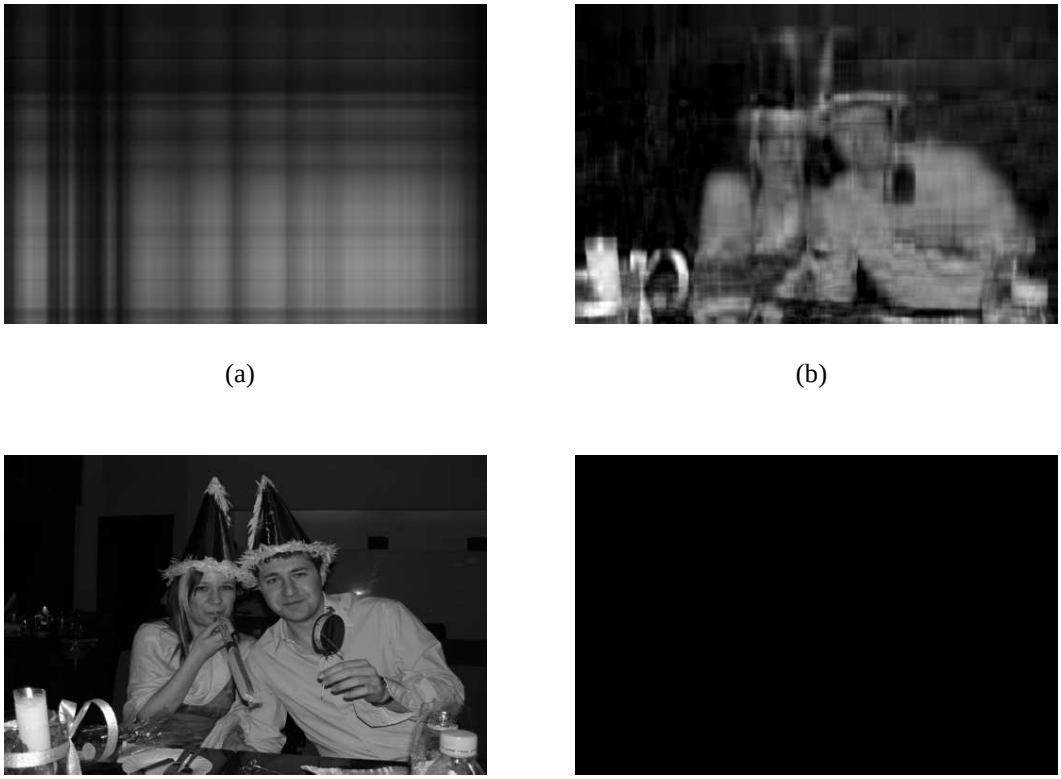

(a) (b)

(c) (d)

Figure 2.4: Reconstructed images $\sum_{i \in \mathfrak{T}} \boldsymbol{A}_i$, where the set $\mathfrak{T}$ contains indices (a) in the first bin, (b) in the first four bins, (c) in the first twelve bins, and (d) in the last six bins.

We previously proposed a variant of the Laplacian operation, which was employed in our improved Laplacian-pyramid-based blending method [16]. We denote our operator by $\mathbb{K}^n$ and define it as follows.

$$\mathbb{K}^n(\boldsymbol{I}) = \mathbb{L}^n(\boldsymbol{I}) \triangle \mathbb{L}^n(\zeta(\boldsymbol{I})), \tag{2.13}$$

where $\zeta(\boldsymbol{I})$ is the Dodge and Burn function, which adaptively reduces values of the image $\boldsymbol{I}$ [16]. Given that $\mathbb{L}^n(\boldsymbol{I}) = (\boldsymbol{S}_0, \boldsymbol{S}_1, ..., \boldsymbol{S}_n)$ and $\mathbb{L}^n(\zeta(\boldsymbol{I})) = (\boldsymbol{T}_0, \boldsymbol{T}_1, ..., \boldsymbol{T}_n)$, the operator $\triangle$ is defined as

$$(\boldsymbol{S}_0, \boldsymbol{S}_1, ..., \boldsymbol{S}_n) \triangle (\boldsymbol{T}_0, \boldsymbol{T}_1, ..., \boldsymbol{T}_n) = (\boldsymbol{S}_0, \boldsymbol{T}_1, ..., \boldsymbol{T}_n). \tag{2.14}$$

The blending image $\boldsymbol{R}$ from two source images $\boldsymbol{I}_1$ and $\boldsymbol{I}_2$ is calculated by our blending function, which is adapted from the function proposed by Mertens *et al.* [17], as follows.

$$\mathbb{L}^n(\boldsymbol{R}) = \sum_{i=1}^{2} \mathbb{G}^n(\boldsymbol{W}_i) \circ \mathbb{K}^n(\boldsymbol{I}_i), \tag{2.15}$$

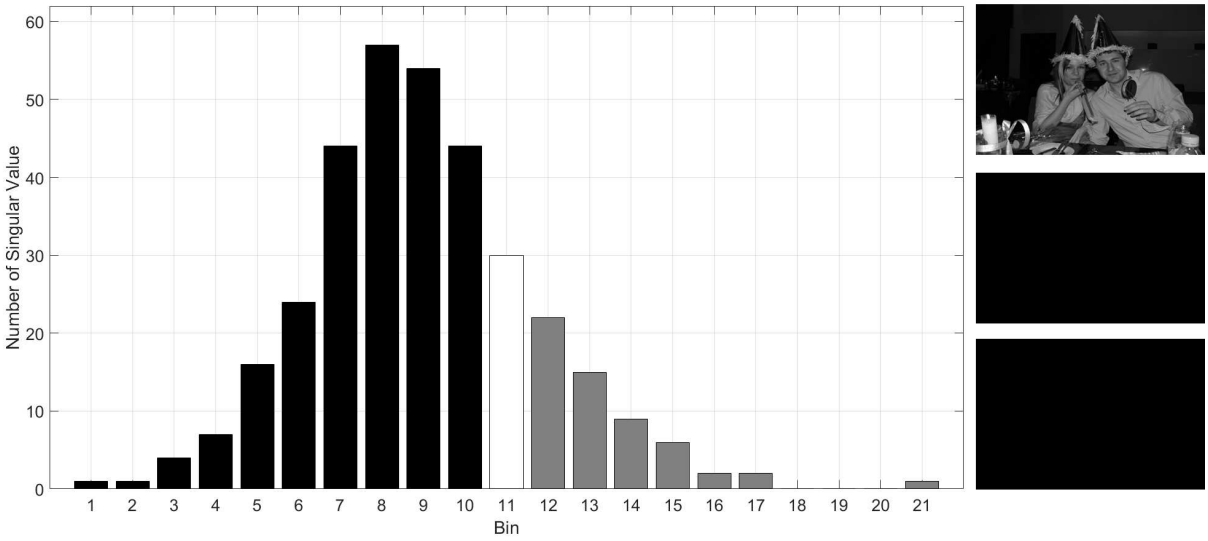

Figure 2.5: Histogram and the reconstructed images: (left) the subset $\mathfrak{B}$, $\mathfrak{F}$, and $\mathfrak{R}$ contain indices in the black, gray, and white bins, respectively, (top-right) the main-body layer $\boldsymbol{A}_{\mathfrak{B}}$, (middle-right) the less-visilble-area layer $\boldsymbol{A}_{\mathfrak{L}}$, and (bottom-right) the noise layer $\boldsymbol{A}_{\mathfrak{R}}$.

$$\boldsymbol{W}_{i,xy} = \frac{1}{\boldsymbol{W}_{1,xy} + \boldsymbol{W}_{2,xy}} \times e^{-\frac{1}{2\sigma^2}\left(\boldsymbol{I}_{i,xy} - 0.5\right)^2}, \tag{2.16}$$

where $\boldsymbol{W}_{i,xy}$ denotes the elements of the matrix $\boldsymbol{W}_i$ at the row x and column y, σ is a standard deviation of the Gaussian function, and the operator $\circ$ is the *Hadamard* product (i.e. element-wise multiplication).

In this work, the resulting image $\boldsymbol{R}$ is produced by blending two images $\hat{\boldsymbol{A}}_{\mathrm{N}}$ and $\hat{\boldsymbol{A}}_{\mathrm{C}}$, where $\hat{\boldsymbol{A}}_{\mathrm{N}}$ is the normalization of the enhanced image $\hat{\boldsymbol{A}}$, and $\hat{\boldsymbol{A}}_{\mathrm{C}}$ is the $\hat{\boldsymbol{A}}$ after its over-range values are clipped or clamped.

2.2 Less-visible contrast enhancement based on human visual perception

The proposed method consists of three stages: noise-level analysis, less-visible-area improvement, and image blending. The block diagram of our proposed algorithm is shown in Fig. 2.6. To enhance the less-visible contrast without amplifying the hidden noise, we first determine a noise level of the input image. If the hidden-noise level of the image is greater than a threshold value, the SVD-based technique is used to remove the noise before moving forward to the

less-visible-area improvement stage; otherwise, the original input image is inputted into the next stage. Then, a non-linear scaling function and a human-perception-based improvement technique are used to enhance the contrast of the image. Finally, the pyramid-based blending method is used to reduce the brightness of over-enhanced areas due to the selective enhancement and to make the resulting image smoother.

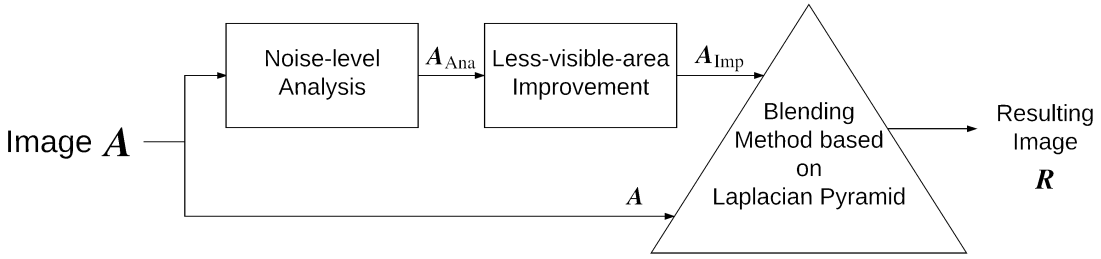

Figure 2.6: Less-visible contrast enhancement based on human visual perception.

2.2.1 Noise-level Analysis

Basically, the less-visible areas of an image contain hidden noise. We simply define the hidden noise as the noise hidden in the less-visible areas. That is, we normally cannot perceive the noise unless it is enhanced by any typical enhancement method. The hidden noise can be chromatic or achromatic, and it can be additive or multiplicative [18]. There are many sources that can cause the hidden noise, for example, a camera sensor with low quality, inappropriate camera settings, or some limitations of a capturing device. To avoid enhancing the hidden noise, we adopt the Singular Value Decomposition (SVD) to analyze the noise level of the input image.

In general, the SVD is a factorization of a matrix. Let $\boldsymbol{X}_{m\times n}$ denote a matrix $\boldsymbol{X}$ of size $m\times n$. The SVD decomposes the matrix $\boldsymbol{X}_{m\times n}$ into a product of three matrices $\boldsymbol{U}_{m\times m}$, $\boldsymbol{D}_{m\times n}$, and $\boldsymbol{V}_{n\times n}$ with the following relationship.

$$\boldsymbol{X} = \boldsymbol{U}\boldsymbol{D}\boldsymbol{V}^{\mathrm{T}}, \tag{2.17}$$

where $\boldsymbol{U}$ and $\boldsymbol{V}$ are orthogonal matrices, and $\boldsymbol{D}$ is a diagonal matrix whose non-zero elements are called the *singular values*.

Let U_i and V_i denote the vectors at the column i of $\boldsymbol{U}$ and $\boldsymbol{V}$, respectively, i.e. $\boldsymbol{U} = [U_1\ U_2\ U_3\ ...\ U_m]$ and $\boldsymbol{V} = [V_1\ V_2\ V_3\ ...\ V_n]$. Let λ_i denote the *eigenvalues* of $\boldsymbol{X}\boldsymbol{X}^{\mathrm{T}}$ (or $\boldsymbol{X}^{\mathrm{T}}\boldsymbol{X}$). The vectors U_i and V_i are the *eigenvectors* of $\boldsymbol{X}\boldsymbol{X}^{\mathrm{T}}$ and $\boldsymbol{X}^{\mathrm{T}}\boldsymbol{X}$, respectively, and are sorted

in descending order of the corresponding eigenvalues. The elements on the main diagonal of $\boldsymbol{D}$ are then the square root of these eigenvalues. Mathematically, the matrix $\boldsymbol{X}$ can be expressed in the following expansion.

$$\boldsymbol{X} = \boldsymbol{X}_1 + \boldsymbol{X}_2 + ... + \boldsymbol{X}_d. \tag{2.18}$$

$$\boldsymbol{X}_i = \sqrt{\lambda_i} \times U_i \times V_i^{\mathrm{T}}, \tag{2.19}$$

where $d = \max\{i, \text{ such that } \lambda_i > 0\}$.

In this work, the SVD is used to decompose each channel of a color image $\boldsymbol{A}$ into several additive layers $\boldsymbol{A}_i$. In other words,

$$\boldsymbol{A} = \sum_{i=1}^{d} \left(\sqrt{\lambda_i} \times U_i \times V_i^{\mathrm{T}} \right) = \sum_{i=1}^{d} \boldsymbol{A}_i. \tag{2.20}$$

Konstatinides *et al.* [19] observed the effect of SVD under the additive noise model and found that the group of latter singular values can be represented the image noise. Our analysis of the noise level is based on this finding.

First, we extract the singular values of the matrix $\boldsymbol{A}$ representing the input image. An example of the plot of singular values is shown in Fig. 2.7. Then, given a set of singular values $\{\sqrt{\lambda_1}, \sqrt{\lambda_2}, ..., \sqrt{\lambda_d}\}$, we calculate the summation of all singular values:

$$S = \sum_{i=1}^{d} \sqrt{\lambda_i}. \tag{2.21}$$

The summation S can be used to estimate the area bounded by the singular-value curve and the singular-value-index axis. We experimentally found that the smaller area implies the higher level of noise.

Based on our experiments, if S is less than a threshold value of hidden-noise level S_{th}, which is set the hidden-noise level in the input image is too high. When the contrast of the input image is enhanced, in this case, the noise will be noticeable. Hence, the noise of such image should be removed before the enhancement process. Fig. 2.8 (a) shows an example of the input image where its value of S is less than S_{th}. If we enhance this image without removing the hidden noise, the noise will appear, and the resulting image looks noisy, as shown in Fig. 2.8 (b). However, when the noise is removed before the enhancement, the resulting image looks better, as shown in Fig. 2.8 (c).

To remove the noise, the singular values are firstly normalized such that the new values cover the range from 0 to 1, where the new minimum and maximum values are 0 and 1, respectively.

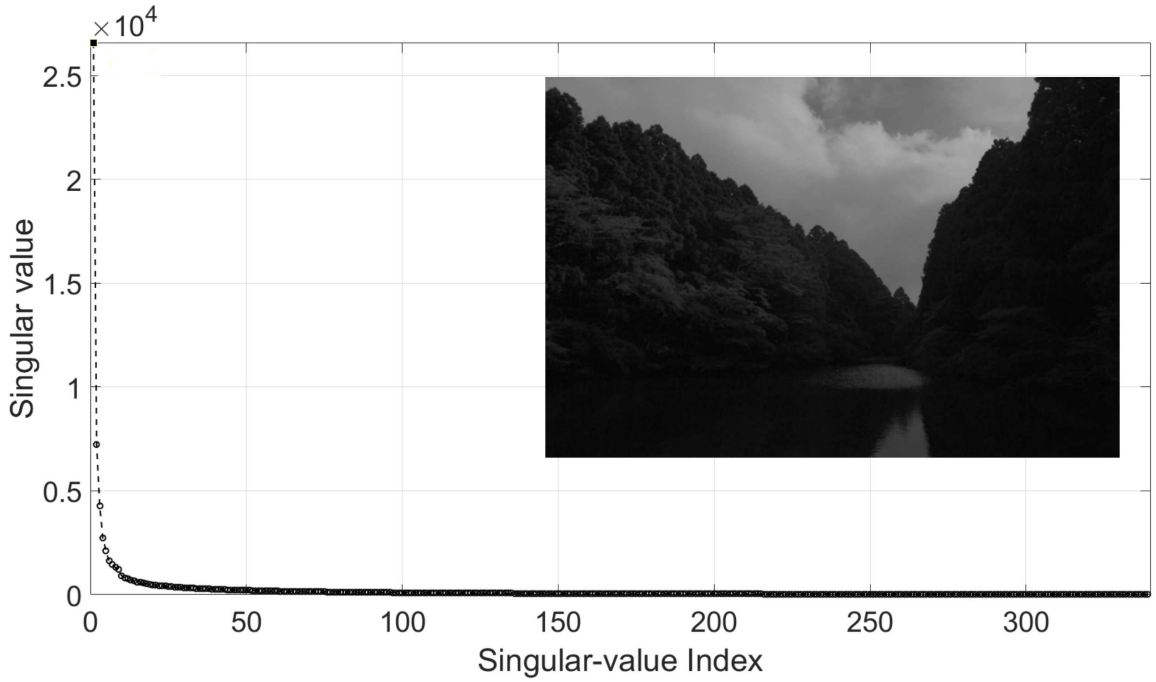

Figure 2.7: Plot of singular values of the image displayed on the top-right.

The set of singular-value indices, $\Im = \{1, 2, 3, ..., d\}$, is partitioned into two disjoint subsets $\mathfrak{B}$ and $\mathfrak{R}$ such that the image $\boldsymbol{A}$ can be decomposed into two images $\boldsymbol{A}_{\mathfrak{B}}$ and $\boldsymbol{A}_{\mathfrak{R}}$, where they are the main-body image and the noise, respectively.

$$\boldsymbol{A}_{\mathfrak{B}} = \sum_{i \in \mathfrak{B}} \boldsymbol{A}_i, \tag{2.22}$$

and

$$\boldsymbol{A}_{\mathfrak{R}} = \sum_{i \in \mathfrak{R}} \boldsymbol{A}_i. \tag{2.23}$$

Then, we plot the distribution of the singular values on the binary-logarithmic scale. That is, on the linear scale, we divide the range [0, 1] of the normalized singular values into b bins of which their width is equal to 2^{-j}, where j is the bin index. Let $f(\sqrt{\lambda_i})$ denote the normalized log-singular-value of the singular value $\sqrt{\lambda_i}$. It is defined as follows.

$$f(\sqrt{\lambda_i}) = 1 + \frac{1}{b} \log_2\left(\frac{\sqrt{\lambda_i} - \sqrt{\lambda_d}}{\sqrt{\lambda_1} - \sqrt{\lambda_d}}\right), \tag{2.24}$$

for all i where $\sqrt{\lambda_i} > \sqrt{\lambda_d}$. Otherwise, $f(\sqrt{\lambda_i}) = 0$.

Then, we plot the numbers of the singular values that fall within each bin. Note that when the number of bins increases, the distribution looks more similar to the normal distribution. In

(a)

(b)

(c)

Figure 2.8: Example of resulting images when the input image is enhanced with and without hidden noise removal: (a) input image with its value of S is less than S_{th}, (b) the resulting image (only the area in the red box of Fig. 2.8 (a)) in the case that the input image is enhanced without the noise removal, (c) the resulting image in the case that the hidden noise is removed before the enhancement process.

our experiment, we set the value of b to 21. We define the singular-value indices of the singular values from the bin with the maximum number of singular values to the last bin as the members of the subset $\mathfrak{N}$. Then, the subset $\mathfrak{B}$ is determined by $\mathfrak{I} - \mathfrak{N}$. In the case $S \leq S_{\text{th}}$, only the $\boldsymbol{A}_{\mathfrak{B}}$ is inputted into the next stage.

Fig. 2.9 (a) shows an example of these two subsets: the subset $\mathfrak{B}$ is indicated by the light bars, whereas the subset $\mathfrak{N}$ is indicated by the dark bars. Fig. 2.9 (b) and Fig. 2.9 (c) show $\boldsymbol{A}_{\mathfrak{B}}$ and $\boldsymbol{A}_{\mathfrak{N}}$, respectively.

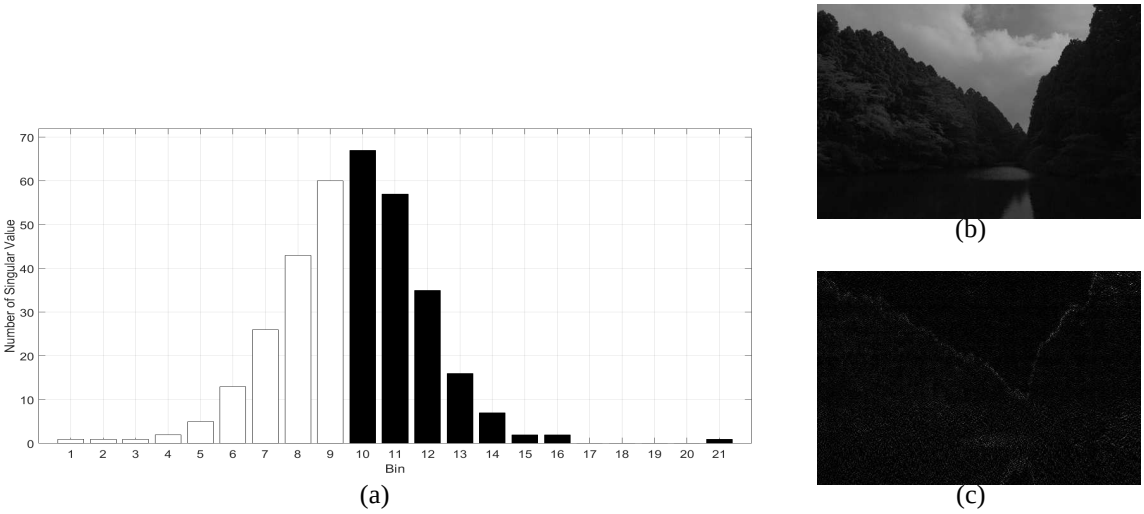

Figure 2.9: Histogram and the reconstructed images: (a) the subsets $\mathfrak{B}$ and $\mathfrak{R}$ contain the indices of singular values in the light bars and in the dark bars, respectively, (b) the main-body image $\boldsymbol{A}_{\mathfrak{B}}$, (c) the noise $\boldsymbol{A}_{\mathfrak{R}}$.

On the other hand, if S is equal to or greater than S_{th}, the original input image is directly inputted into the less-visible-area improvement process. In this case, if we remove the noise layer $\boldsymbol{A}_{\mathfrak{R}}$ before the enhancement process, the resulting image will be distorted as shown in Fig. 2.10 (c).

In short, the noise-level analysis takes the input image $\boldsymbol{A}$ as an input and returns image $\boldsymbol{A}_{\text{Ana}}$ as an output, where $\boldsymbol{A}_{\text{Ana}} = \boldsymbol{A}$ if $S \geq S_{\text{th}}$; otherwise, $\boldsymbol{A}_{\text{Ana}} = \boldsymbol{A}_{\mathfrak{B}}$. This analysis is summarized by the flowchart illustrated in Fig. 2.11.

2.2.2 Less-visible-area Improvement

The less-visible-area improvement process enhances the contrast of less-visible areas of the image $\boldsymbol{A}_{\text{Ana}}$ and outputs the improved image $\boldsymbol{A}_{\text{Imp}}$. We intentionally enhance the less-visible areas of the image $\boldsymbol{A}_{\text{Ana}}$ considerably, thus this process causes the over-enhancement as shown in Fig. 2.12. This over-enhancement will be removed by the blending method, which will be detailed in Sect. 2.2.3.

Our improvement process consists of two subprocesses. The first one is based on a non-linear scaling function. The second one is based on the concept of human perception, i.e. the concept of just noticeable difference (JND). The block diagram of these two subprocesses are shown in Fig. 2.13.

(a)

(b)

(c)

Figure 2.10: Example of resulting images when the input image is enhanced with and without hidden noise removal: (a) input image with its value of S is equal to or greater than S_{th}, (b) the resulting image (only the area in the red box of Fig. 2.10 (a)) in the case that the input image is enhanced without the noise removal, (c) the resulting image in the case that the hidden noise is removed before the enhancement process.

The reason we have two subprocesses is that our proposed non-linear scaling function deployed in the first subprocess causes the foggy effect as shown in Fig. 2.14 (b). Therefore, the normalization is used to mitigate this effect. Consequently, the enhancement function is compressed so that the image $\boldsymbol{A}_{\text{Norm}}$ looks a bit darker than the image $\boldsymbol{A}_{\text{Non}}$. Therefore, we enhance the image $\boldsymbol{A}_{\text{Norm}}$ for the second time by using a JND-based concept.

According to our proposed non-linear scaling function, which will be discussed in details in Sect. 2.2.2, an output of this function covers the range from 46.76 to 347.7. Hence, we

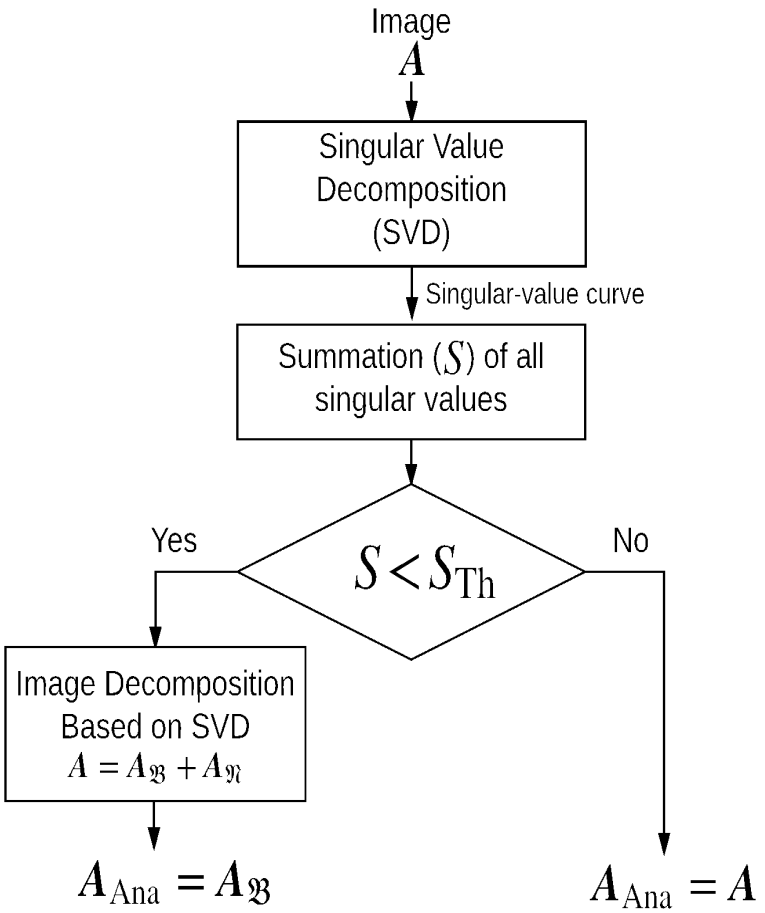

Figure 2.11: Flowchart of the noise-level analysis.

(a) (b)

Figure 2.12: Example of an over-enhance improved image: (a) original image and (b) improved image.

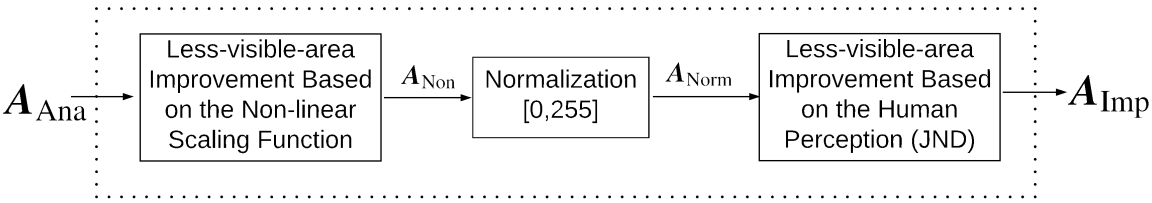

Figure 2.13: Block diagram of the less-visible-area improvement process.

(a)

(b)

(c)

Figure 2.14: Foggy effect due to the non-linear scaling function: (a) original image $\boldsymbol{A}_{\text{Ana}}$, (b) the image $\boldsymbol{A}_{\text{Non}}$, and (c) the image $\boldsymbol{A}_{\text{Imp}}$.

normalized the range $[46.76, 347.7]$ to the range $[0, 255]$ before inputting it into the JND-based improvement process. The JND-based improvement is based on the concept that we can perceive a pixel value easily when the pixel value increased by its JND value.

Less-visible-area Improvement Based on the Non-linear Scaling Function

Our scaling function is proposed based on the assumption that it should be not only a function of the input pixel value but also the input pixel's neighbors. If it is the function of only the pixel value, it might produce image noise due to the difference between the pixel and its neighbors.

Let $\boldsymbol{A}_{\text{Ana}}(x, y)$ denote the pixel values of the image $\boldsymbol{A}_{\text{Ana}}$ at the position (x, y) as illustrated in

Fig. 2.15 (a). In this work, the neighbors of $\boldsymbol{A}_{\text{Ana}}(x,y)$ are defined as the eight pixels surrounding the $\boldsymbol{A}_{\text{Ana}}(x,y)$. We first calculate the average value ($\bar{N}$) of the neighbors of $\boldsymbol{A}_{\text{Ana}}(x,y)$.

$$\bar{N}(x,y) = \frac{1}{8} \times \left[\left(\sum_{i=x-1}^{x+1} \sum_{j=y-1}^{y+1} \boldsymbol{A}_{\text{Ana}}(i,j) \right) - \boldsymbol{A}_{\text{Ana}}(x,y) \right]. \tag{2.25}$$

Then, our proposed non-linear scaling function is defined as follows.

$$\boldsymbol{A}_{\text{Non}}(x,y) = \frac{\log(B(x,y))}{\log(F(x,y))}, \tag{2.26}$$

where

$$\boldsymbol{F}(x,y) = \begin{cases} 20 - 17\sqrt{\frac{|127 - \boldsymbol{A}_{\text{Ana}}(x,y)|}{127}}, & \text{if } \boldsymbol{A}_{\text{Ana}}(x,y) \leq 127, \\ \frac{3}{128}\left(|127 - \boldsymbol{A}_{\text{Ana}}(x,y)| + 1\right), & \text{otherwise,} \end{cases} \tag{2.27}$$

and

$$\boldsymbol{B}(x,y) = \begin{cases} 20 - 17\sqrt{\frac{\bar{N}(x,y)}{127}}, & \text{if } \bar{N}(x,y) \leq 127, \\ \frac{3}{128}\left(\bar{N}(x,y) + 1\right), & \text{otherwise.} \end{cases} \tag{2.28}$$

Note that these equations, especially the forms of eq. (2.27) and eq. (2.28), are inspired by the JND formula proposed by Chou *et al.* [20].

The plot of this function $f\left(\boldsymbol{A}_{\text{Ana}}(x,y), \bar{N}(x,y)\right)$ is shown in Fig. 2.16. The idea behind this formula is that we want to enhance the pixel value, and we try to reduce the difference between the pixel value and the neighbors' values at the same time. If the pixel value $\boldsymbol{A}_{\text{Ana}}(x,y)$ is equal to the average value $\bar{N}(x,y)$, as illustrated in Fig. 2.15 (b), the enhancement function is indicated by the red curve shown in Fig. 2.16.

It can be seen clearly from this figure that, if $\bar{N}(x,y)$ is lesser than $\boldsymbol{A}_{\text{Ana}}(x,y)$, as illustrated in Fig. 2.15 (c), the enhancement rate is lower than that of the case $\boldsymbol{A}_{\text{Ana}}(x,y) = \bar{N}(x,y)$. On the other hand, if $\bar{N}(x,y)$ is greater than $\boldsymbol{A}_{\text{Ana}}(x,y)$, as illustrated in Fig. 2.15 (d), the enhancement rate is greater than that of the case $\boldsymbol{A}_{\text{Ana}}(x,y) = \bar{N}(x,y)$.

Since the range of this function is not from 0 to 255, it is normalized by the following formula before inputting to the next subprocess.

$$\boldsymbol{A}_{\text{Norm}}(x,y) = \frac{255}{327.94} \times \left(\boldsymbol{A}_{\text{Non}}(x,y) - 46.76\right). \tag{2.29}$$

Less-visible-area Improvement Based on JND

In image processing, the JND is defined as the minimum visibility threshold when visual contents are altered [21]. Our idea behind this JND-based improvement process is that, if we

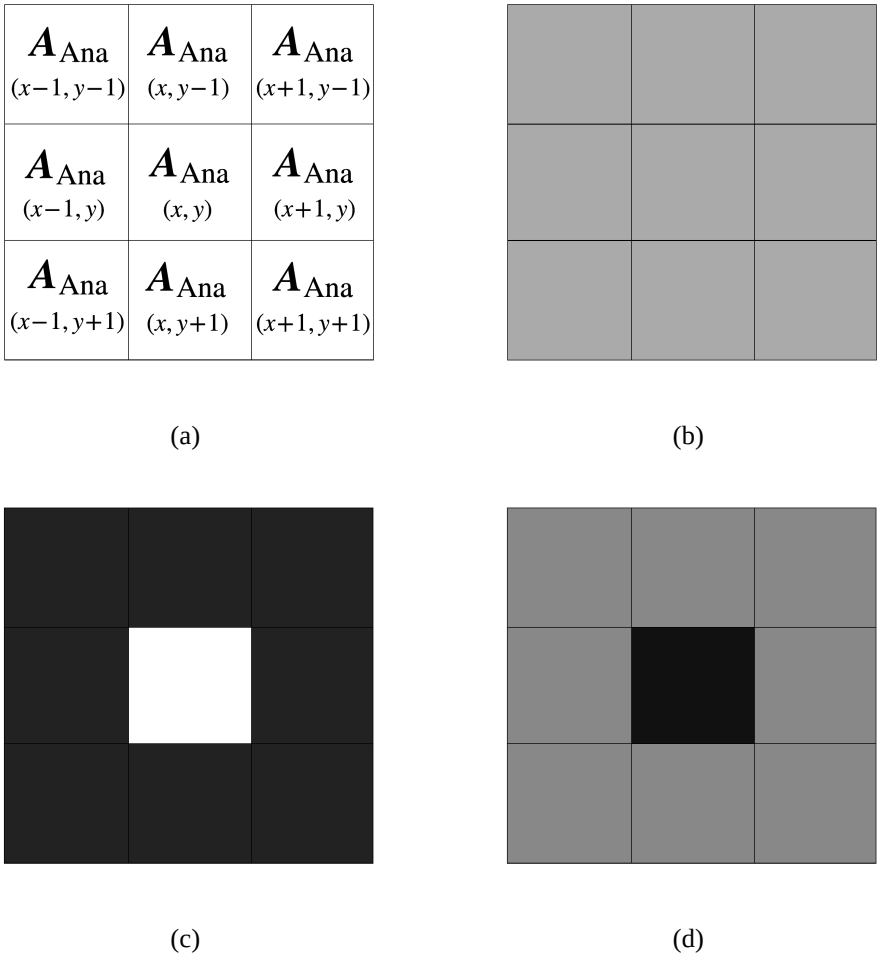

Figure 2.15: Pixel value $\boldsymbol{A}_{\text{Ana}}(x,y)$ and its neighbors: (a) the positions of an area surrounded $\boldsymbol{A}_{\text{Ana}}(x,y)$, (b) the case that $\boldsymbol{A}_{\text{Ana}}(x,y) = \bar{N}(x,y)$, (c) the case that $\boldsymbol{A}_{\text{Ana}}(x,y) > \bar{N}(x,y)$, and (d) the case that $\boldsymbol{A}_{\text{Ana}}(x,y) < \bar{N}(x,y)$

increase the pixel values of the less-visible areas by at least their JND values, such areas are easier to perceive by the human perception. This is because, by the definition of JND, the new values cause the less-visible areas perceived discriminatorily from the previous ones. Therefore, we propose the following formula:

$$\boldsymbol{A}_{\text{Imp}}(x,y) = \boldsymbol{A}_{\text{Norm}}(x,y) + k \times \text{JND}\left(\boldsymbol{A}_{\text{Norm}}(x,y)\right), \tag{2.30}$$

where k is a factor, which is greater than 1, and $\text{JND}\left(\boldsymbol{A}_{\text{Norm}}(x,y)\right)$ is the JND of $\boldsymbol{A}_{\text{Norm}}(x,y)$, which is modeled by Chou *et al.* [20] as follows.

$$\text{JND}\left(\boldsymbol{A}_{\text{Norm}}(x,y)\right) = \begin{cases} \left\lfloor 17 \times \left(1 - \sqrt{\frac{\boldsymbol{A}_{\text{Norm}}(x,y)}{127}}\right)\right\rfloor + 3, & \text{if } \boldsymbol{A}_{\text{Norm}}(x,y) \leq 127, \\ \left\lfloor \frac{3}{128} \times \left(\boldsymbol{A}_{\text{Norm}}(x,y) - 127\right)\right\rfloor + 3, & \text{otherwise.} \end{cases} \tag{2.31}$$

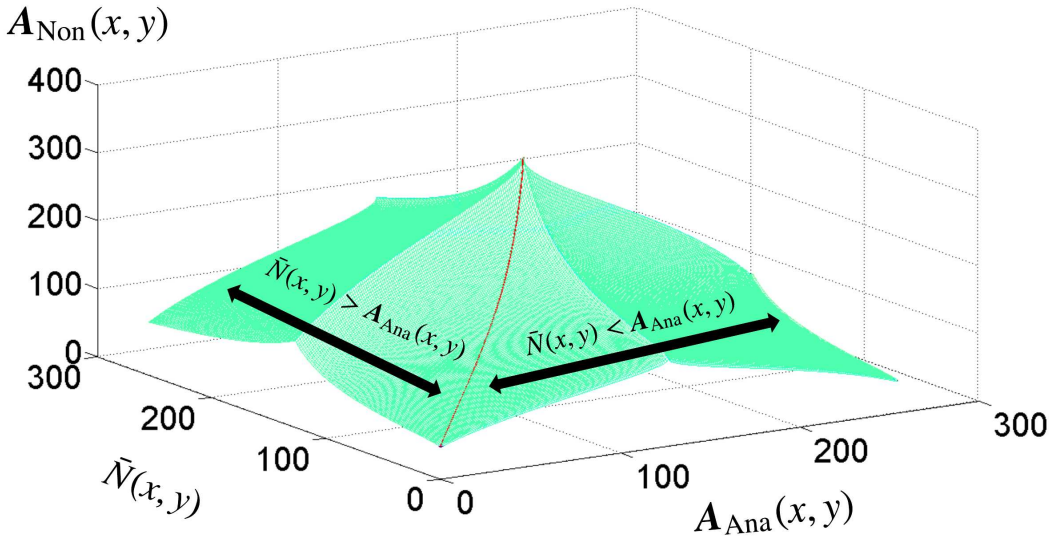

Figure 2.16: Non-linear scaling function $f(\boldsymbol{A}_{\mathrm{Ana}}(x,y), \bar{N})$ for the less-visible-area improvement.

In this work, we assume that k is a function of $\boldsymbol{A}_{\mathrm{Ana}}$ and $\mathrm{JND}\,(\boldsymbol{A}_{\mathrm{Norm}})$. We experimentally found that the relation

$$k = \frac{\boldsymbol{A}_{\mathrm{Ana}}(x,y)}{\mathrm{JND}\,(\boldsymbol{A}_{\mathrm{Norm}}\,(x,y))} + 1 \tag{2.32}$$

works well for our purpose.

2.2.3 Pyramid-based Blending Method

We use a blending technique to resolve the over-enhancement problem caused by the less-visible-area improvement process described in the previous subsection. We adopt the technique based on the Gaussian and Laplacian pyramids, which is proposed by Burt *et al.* [15]. We do not use a conventional pyramid-based blending method, which is proposed by Mertens *et al.* [17], because some information is lost after blending, especially the information in small areas [16]. Thus, we propose a more sophisticated technique to overcome such problem. Our proposed blending method is summarized by a flowchart shown in Fig2.17 and consists of five steps as follows.

First, let $\mathbb{G}^n$ and $\mathbb{L}^n$ denote the n-level Gaussian and Laplacian operators, respectively. The n-level Gaussian pyramid of the image $\boldsymbol{I}$, $\mathbb{G}^n(\boldsymbol{I})$, returns $n+1$ images $(\boldsymbol{G}_0, \boldsymbol{G}_1, ..., \boldsymbol{G}_n)$, where $\boldsymbol{G}_0$ is $\boldsymbol{I}$, and $\boldsymbol{G}_i$, for $i \geq 1$, are output images obtained from the low-pass filter with the decimation

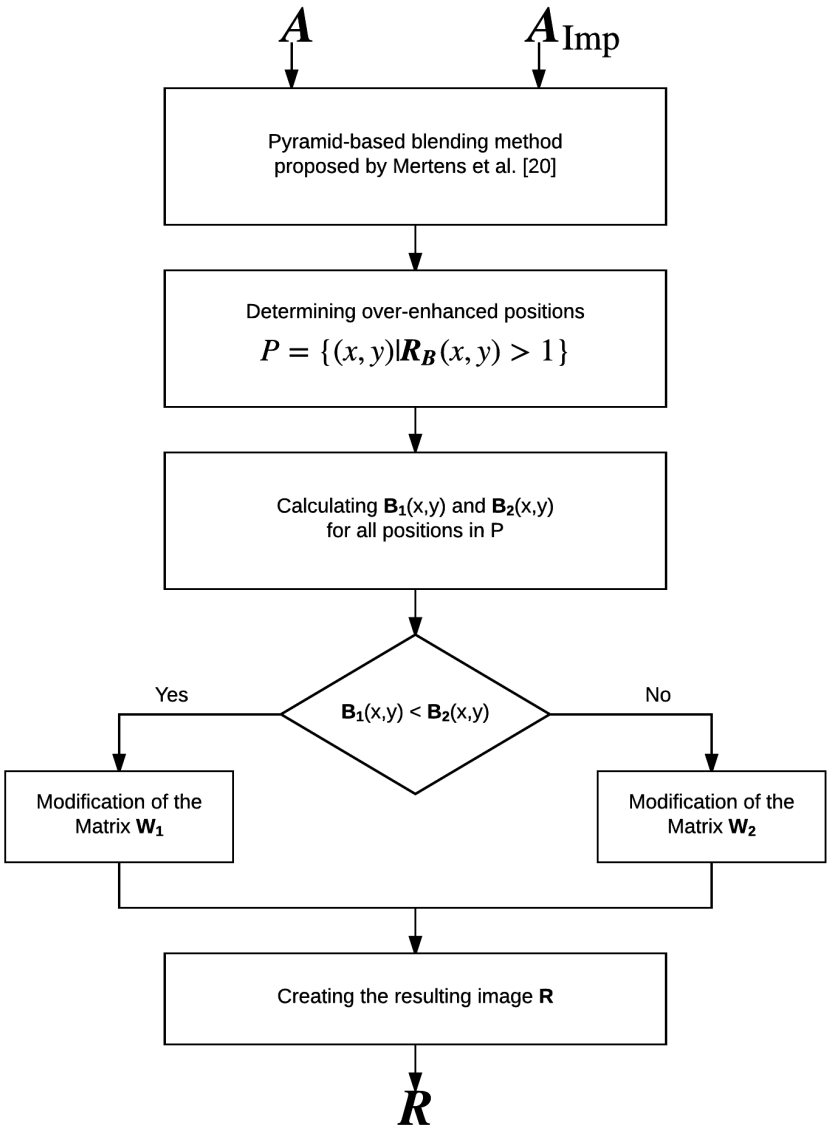

Figure 2.17: Flowchart of pyramid-based blending method.

at the layer i. The n-level Laplacian pyramid of the image $\boldsymbol{I}$, $\mathbb{L}^n(\boldsymbol{I})$, returns $n + 1$ images $(\boldsymbol{L}_0, \boldsymbol{L}_1, ..., \boldsymbol{L}_n)$, where $\boldsymbol{L}_n$ is $\boldsymbol{G}_n$, and $\boldsymbol{L}_i = \boldsymbol{G}_i - \uparrow \boldsymbol{G}_{i+1}$ for $i < n$. The symbol $\uparrow \boldsymbol{G}_{i+1}$ represents the image $\boldsymbol{G}_{i+1}$ after it is upsampled by a factor of 2.

We can reconstruct the image $\boldsymbol{I}$ by the inverse Laplacian $\mathbb{L}^{-n}$, which is defined as

$$\mathbb{L}^{-n}(\mathbb{L}^n(\boldsymbol{I})) = \boldsymbol{L}_0 + \uparrow \boldsymbol{L}_1 + \uparrow\uparrow \boldsymbol{L}_1 + ... + \uparrow^n \boldsymbol{L}_n, \tag{2.33}$$

where $\uparrow^n$ denotes the upsampling by a factor of 2^n.

The resulting image $\boldsymbol{R}_\mathrm{B}$ of the pyramid-based blending method proposed by Mertens *et al.*

is then calculated as follows [17].

$$\mathbb{L}^n(\boldsymbol{R}_{\mathrm{B}}) = \mathbb{G}^n(\boldsymbol{W}_1) \circ \mathbb{L}^n(\boldsymbol{A}) + \mathbb{G}^n(\boldsymbol{W}_2) \circ \mathbb{L}^n(\boldsymbol{A}_{\mathrm{Imp}}), \tag{2.34}$$

where $\boldsymbol{A}$ and $\boldsymbol{A}_{\mathrm{Imp}}$ are two source images. $\boldsymbol{W}_1$ and $\boldsymbol{W}_2$ are weighting matrices, and the operator $\circ$ is the Hadamard product (i.e., element-wise multiplication).

The matrices $\boldsymbol{W}_1$ and $\boldsymbol{W}_2$ are constructed by the following formulae.

$$\boldsymbol{W}_1(x,y) = \frac{e^{-\frac{1}{2\sigma^2}(\boldsymbol{A}(x,y)-0.5)^2}}{e^{-\frac{1}{2\sigma^2}(\boldsymbol{A}(x,y)-0.5)^2} + e^{-\frac{1}{2\sigma^2}(\boldsymbol{A}_{Imp}(x,y)-0.5)^2}}, \tag{2.35}$$

and

$$\boldsymbol{W}_2(x,y) = \frac{e^{-\frac{1}{2\sigma^2}\left(\boldsymbol{A}_{Imp}(x,y)-0.5\right)^2}}{e^{-\frac{1}{2\sigma^2}(\boldsymbol{A}(x,y)-0.5)^2} + e^{-\frac{1}{2\sigma^2}(\boldsymbol{A}_{Imp}(x,y)-0.5)^2}}, \tag{2.36}$$

where $\boldsymbol{W}_i(x,y)$ denotes the element of the matrix $\boldsymbol{W}_i$ at row x and column y, and σ is a constant and set to 0.2.

Second, over-enhanced positions are determined. The over-enhanced positions are defined as the positions of which their pixel values are greater than 1. Let P denote a set of the over-enhanced positions. Thus, $P = \{(x,y)|\boldsymbol{R}_{\mathrm{B}}(x,y) > 1\}$.

Third, for all (x,y) in P, we calculate $\boldsymbol{B}_1(x,y)$ and $\boldsymbol{B}_2(x,y)$ by

$$\boldsymbol{B}_1(x,y) = \mathbb{L}^{-n}\Big(\mathbb{G}^n\Big(\boldsymbol{W}_2(x,y)\Big) \circ \mathbb{L}^n\Big(\boldsymbol{A}(x,y)\Big)\Big), \tag{2.37}$$

and

$$\boldsymbol{B}_2(x,y) = \mathbb{L}^{-n}\Big(\mathbb{G}^n\Big(\boldsymbol{W}_2(x,y)\Big) \circ \mathbb{L}^n\Big(\boldsymbol{A}_{Imp}(x,y)\Big)\Big). \tag{2.38}$$

Forth, we compare $\boldsymbol{B}_1(x,y)$ and $\boldsymbol{B}_2(x,y)$, for all (x,y) in P. If $\boldsymbol{B}_1(x,y) < \boldsymbol{B}_2(x,y)$, the matrix $\boldsymbol{W}_1$ is modified; otherwise, the matrix $\boldsymbol{W}_2$ is modified. Our idea behind this modification is as follows. Since $\boldsymbol{W}_i$ is a Gaussian function of input-pixel values, a high value of $\boldsymbol{W}_i(x,y)$ indicates that the input-pixel value at the position (x,y), $\boldsymbol{A}(x,y)$ or $\boldsymbol{A}_{\mathrm{Imp}}(x,y)$, is not too low or not too high. As a result, it is less likely to cause the over-enhancement, compared with a low value of $\boldsymbol{W}_i(x,y)$. Therefore, a value of $\boldsymbol{W}_1(x,y)$ is decreased in order to mitigate the over-enhancement effect when $\boldsymbol{B}_1(x,y) < \boldsymbol{B}_2(x,y)$. Otherwise, a value of $\boldsymbol{W}_2(x,y)$ is decreased. Note that, in this

situation, we can ignore the case that an input-pixel value is too low due to the definition of the set P.

The modified weighting matrix $\boldsymbol{W}_{mi}(x, y)$ is determined by the following equation.

$$\boldsymbol{W}_{mi}(x, y) = \boldsymbol{W}_i(x, y) - |\boldsymbol{W}_i(x, y) - \boldsymbol{B}_i(x, y)| \tag{2.39}$$

Fifth, the modified weighting matrices $\boldsymbol{W}_{m1}$ and $\boldsymbol{W}_{m2}$ obtained from the previous step are used to create the resulting image $\boldsymbol{R}$.

$$\begin{aligned} \boldsymbol{R} &= \mathbb{L}^{-n}\left(\mathbb{L}^{n}\left(\boldsymbol{R}\right)\right) \\ &= \mathbb{L}^{-n}\left(\mathbb{G}^{n}\left(\boldsymbol{W}_{m1}\right) \circ \mathbb{L}^{n}\left(\boldsymbol{A}\right) + \mathbb{G}^{n}\left(\boldsymbol{W}_{m2}\right) \circ \mathbb{L}^{n}\left(\boldsymbol{A}_{\mathrm{Imp}}\right)\right) \end{aligned} \tag{2.40}$$

According to eq. (2.39), it is possible that there exists $\boldsymbol{R}(x, y)$ such that its value is less than 0. In this case, the value of $\boldsymbol{R}(x, y)$ is clipped to 0. In other words, if $\boldsymbol{R}(x, y) < 0$, then $\boldsymbol{R}(x, y) = 0$.

Chapter 3

Dataset, Implementation and Evaluation of the Proposed Methods

3.1 Dataset

In this work, two datasets in which their images contain different levels of noise were used in our experiments. The first one was provided by the authors of this work. It consists of 30 photos captured from various devices. The second one was suggested by V. Vonikakis *et al.* [1], and it consists of 20 photos. However,to avoid the dizzy effect to the evaluation, only 20 images between the first and second sets were selected to evaluate the performance of proposed algorithm. In the dataset, some areas of these images are correctly-exposed, whereas other areas are under-exposed or over-exposed. All images were downsampled to a size of 512×339 in order to reduce the computational time-complexity of the SVD and of the pyramid-based blending method.

3.2 Implementation of the Proposed Methods

As described in Chapter 2, both proposed methods have some predefined parameters. This section described those parameters we used in our simulations. Note that values of those parameters are empirical, and we obtain them from our preliminary experiments.

3.2.1 LVCE Implementation

To evaluation the performance of LVCE, we implement the method described in Section 2.1 which the following parameters. The scaling factor for enhance the less-visible layers (α, β, and γ) are set to 1, 3.7, and 2.7, respectively. The range for selecting an appropriate bin [$q + d_{\min}$, $q + d_{\max}$] is set into single indexed-bin [$q + 3$]. Lastly, the standard deviation of the Gaussian function (σ) is set to 0.2.

3.2.2 LVCEHP Implementation

To evaluation the performance of LVCEHP, we implement the method described in Section 2.2 which the following parameters. The threshold value of hidden-noise level (S_{th}) and the standard deviation of the Gaussian function (σ) are set to 9×10^4 and 0.2.

3.3 Evaluation of the Proposed Methods

In this experiment, we compared our proposed method with six conventional methods: LVCE [22], FCSM [1], MSRCP [13], MEF [11], MSRCR [8], and CLAHE [3]. To test the FCSM, we used the software called Orasis [23]. For MSRCP, we used an online application provided by the IPOL journal [24]. The rest were implemented with MATLAB. The parameters used in the CLAHE were set as follow: the Rayleigh distribution with the contrast enhancement limit of 0.02. Parameters used in the LVCE, FCSM, MSRCP, and MEF methods were set to the values suggested by their authors. The ratio between color values in each color channel and the luminance values are kept in order to reconstruct the color images in the MSRCP and the CLAHE. Comparison examples of resulting images obtained from all methods are shown in Fig.3.1 - Fig. 3.20.

As mentioned in the introduction, it can be seen from these figures that the images #15 and #21 obtained from the MEF and the FCSM contain image noise. The images obtained from the LVCE have the foggy effect. The images #3, #8 and #11 obtained from the MSRCP suffer from the over-enhancement. The images obtained from the MSRCR lose some details, and they look like over-exposed images. The images obtained from the CLAHE suffer from the over-enhancement problem similar to the MSRCP.

The performance of our proposed algorithm was evaluated objectively and subjectively. Objective measures and subjective tests are detailed in the following subsection.

3.3.1 Objective Evaluation

Four measures were used to evaluate the performance of our proposed algorithm: image enhancement metric (IEM) [26], universal image quality index (QI) [27], entropy, and homogeneity.

The IEM is a full-reference metric. Normally, the higher the value of IEM, the better the improvement in contrast. However, this work aims to improve the contrast only in the less-visible areas. Thus, we expected that this values should not be too close to 1 because if it is too close to 1, a resulting image seems not to be enhanced. On the other hand, if the value is too far from 1, the resulting image will be over-enhanced.

Basically, the QI is based on the mathematical model of image distortion using three factors, which are the loss of correlation, the luminance distortion, and the contrast distortion. The closer the QI to 1, the image quality of the enhanced image is closer to that of the original image.

The calculations of entropy and homogeneity are based on the gray level co-occurence matrix (GLCM) [28]. The entropy was used to evaluate the texture and key-lighting of an enhanced image. The homogeneity was used to evaluate the similarity of the pixels in the neighborhood area. We do not want the enhancement process to damage image tone and to amplify the hidden noise. Therefore, both measurements should be as close to those of the original image as possible. Because the great difference in entropy between the original and the enhanced images can imply the over-enhancement. Ideally, the homogeneity of the enhanced image should be the same as that of the original one.

The results from the objective evaluations for IEM, QI, entropy, and homogeneity are shown in Table 3.2. It can be seen that the average IEM of the LVCE is the lowest, whereas that of the CLAHE is the highest. The average IEM of our proposed algorithm is 1.431. We will discuss in Sect. 4 that the number 1.431, as well as that of the MEF, is in an appropriate range for the purpose of this work. In terms of image distortion, the LVCE is the best with the average QI of 0.558. The average QI of the images obtained from our proposed algorithm is 0.529, which is third rank compares to those of the other methods.

The average entropy of LVCE is the best since it is closest to that of the original images while LVCEHP holds the fifth place for the detail preservation criterion. For the noise amplification, the average homogeneity of LVCE is the best since it is closest to that of the original images while LVCEHP holds the second place.

We will discuss what should be an appropriate range for the good resulting image in Sect. 4 because the interpretation of these numbers should be done after we have subjective test results.

3.3.2 Subjective Evaluation

To measure an image quality by human beings, we conducted subjective experiments with respect to three aspects that we want to measure: noise amplification, tone preservation, and detail preservation.

The subjective tests were conducted as follows. We showed 8 images to participants, where one of these image is the original image, and the rest are enhanced images obtained from 7 methods including our proposed one. We asked the participants to select three enhanced images that they thought those three images contain less noise compared with the others, as well as the original image, and to sort them from the least-noise image to the noisiest image. Similarly, we also asked the participants to select and rank the first three preferred images in terms of tone preservation and detail preservation. Finally, we asked the participants to select and rank the first three preferred images with respect to the combination of these three criteria, where they could assign weights to each criterion according to their preference.

Note that the term of detail preservation is used instead of over-enhancement. Since lot of participants have confused in the term of over-enhancement and could not complete the evaluations. The participants did not know how much of the brightness is called over-enhancement. Thus, some dataset did not clearly distinguish the problem of over-enhancement. Sometimes, it is hard to measure which resulting image can avoid the over-enhancement problem. Based on these problems, the participants are difficult to finish the subjective measurement. In that case, we re-arrange the term of over-enhancement to detail preservation. Since, the term of detail preservation has had the relationships to the term of over-enhancement. When the enhanced images have the highest rank to preserve the detail preservation, it can be implied that those images are also far apart to create such the over-enhancement problem too. In other word, the images that contain the lowest rank of detail preservation, it means that those images are facing

Table 3.1: Subjective-evaluation results.

Method	Noise amplification			Tone preservation			Detail preservaton			Preference testing		
	Rank #1	Rank #2	Rank #3	Rank #1	Rank #2	Rank #3	Rank #1	Rank #2	Rank #3	Rank #1	Rank #2	Rank #3
Proposed method	58	77	41	84	70	32	36	47	55	52	61	58
LVCE [22]	66	32	28	21	34	49	16	11	23	5	16	31
FCSM [1]	30	38	48	51	39	60	41	59	44	56	47	48
MSRCP [13]	27	30	38	11	19	23	9	16	19	18	29	17
MEF [11]	18	21	42	31	37	30	56	46	42	66	45	40
MSRCR [8]	0	0	2	1	1	1	10	11	13	1	1	3
CLAHE [3]	1	2	1	1	0	5	32	10	4	2	1	3

the problem of over-enhancement.

In this experiment, ten subjects who have an experience with taking the photography are participated. Their ages were ranging from 21 to 45 years. The results from the subjective evaluations are shown in Table 3.1.

It can be seen from the table that the enhanced images obtained from the LVCE got 66 votes (or 33%) for the first rank in the noise-amplification criterion. That is, one-third of the participants thought these images contained least noise compared with the others. The LVCEHP hold the second place for the first rank in this criterion, and it also hold the first place for the second rank. In terms of tone preservation, 42% of the participants thought the proposed method was the best compared with the others. In terms of detail preservation, the MEF, the MSRCP, and the proposed method got 56, 41, and 36 votes for the first rank, respectively. However, the MEF and the LVCEHP got approximately the same votes for the second rank in the detail preservation. For the preference testing, 33%, 28%, and 26% of the participants thought that the MEF, the MSRCP, and the LVCEHP were the best, respectively. Also, 30.5% of the participants thought that the LVCEHP should be the second rank in the preference testing. In short, the subjective evaluation results show that the LVCEHP can achieve one of the first three ranks in all criteria.

Table 3.2: Results from the objective evaluations.

Image Enhancement Metric (IEM)								
	Input	LVCEHP [25]	LVCE [22]	FCSM [1]	MSRCP [13]	MEF [11]	MSRCR [8]	CLAHE [3]
Avg	1.000	1.431	1.044	2.109	1.812	2.307	2.000	2.512
Std	0.000	0.215	0.067	0.991	0.625	1.207	1.280	0.994

Quality Index (QI)								
	Input	LVCEHP [25]	LVCE [22]	FCSM [1]	MSRCP [13]	MEF [11]	MSRCR [8]	CLAHE [3]
Avg	1.000	0.529	0.558	0.548	0.397	0.487	0.311	0.374
Std	0.000	0.226	0.227	0.238	0.138	0.224	0.136	0.156

Entropy								
	Input	LVCEHP [25]	LVCE [22]	FCSM [1]	MSRCP [13]	MEF [11]	MSRCR [8]	CLAHE [3]
Avg	6.178	6.864	6.220	6.804	6.781	7.076	6.799	6.839
Std	1.371	0.963	1.222	1.034	0.999	0.761	0.827	0.998

Homogeneity								
	Input	LVCEHP [25]	LVCE [22]	FCSM [1]	MSRCP [13]	MEF [11]	MSRCR [8]	CLAHE [3]
Avg	0.954	0.929	0.950	0.911	0.920	0.902	0.919	0.886
Std	0.042	0.046	0.041	0.047	0.050	0.051	0.035	0.055

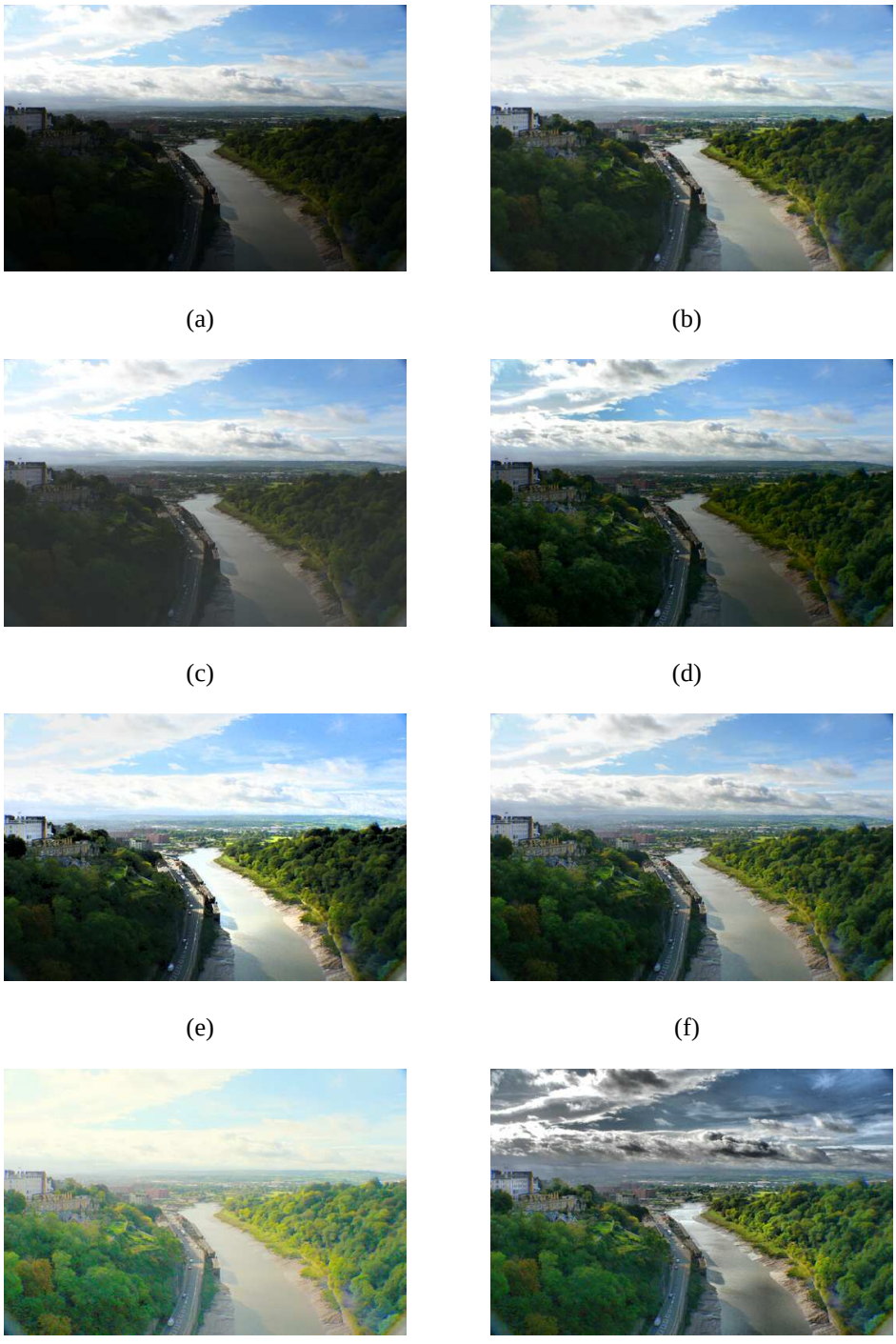

(a) (b) (c) (d) (e) (f) (g) (h)

Figure 3.1: Image comparison with the existing method: (a) input image, (b) LVCEHP [25], (c) LVCE [22], (d) FCSM [1], (e) MSRCP [13], (f) MEF [11], (g) MSRCR [8], (h) CLAHE [3]

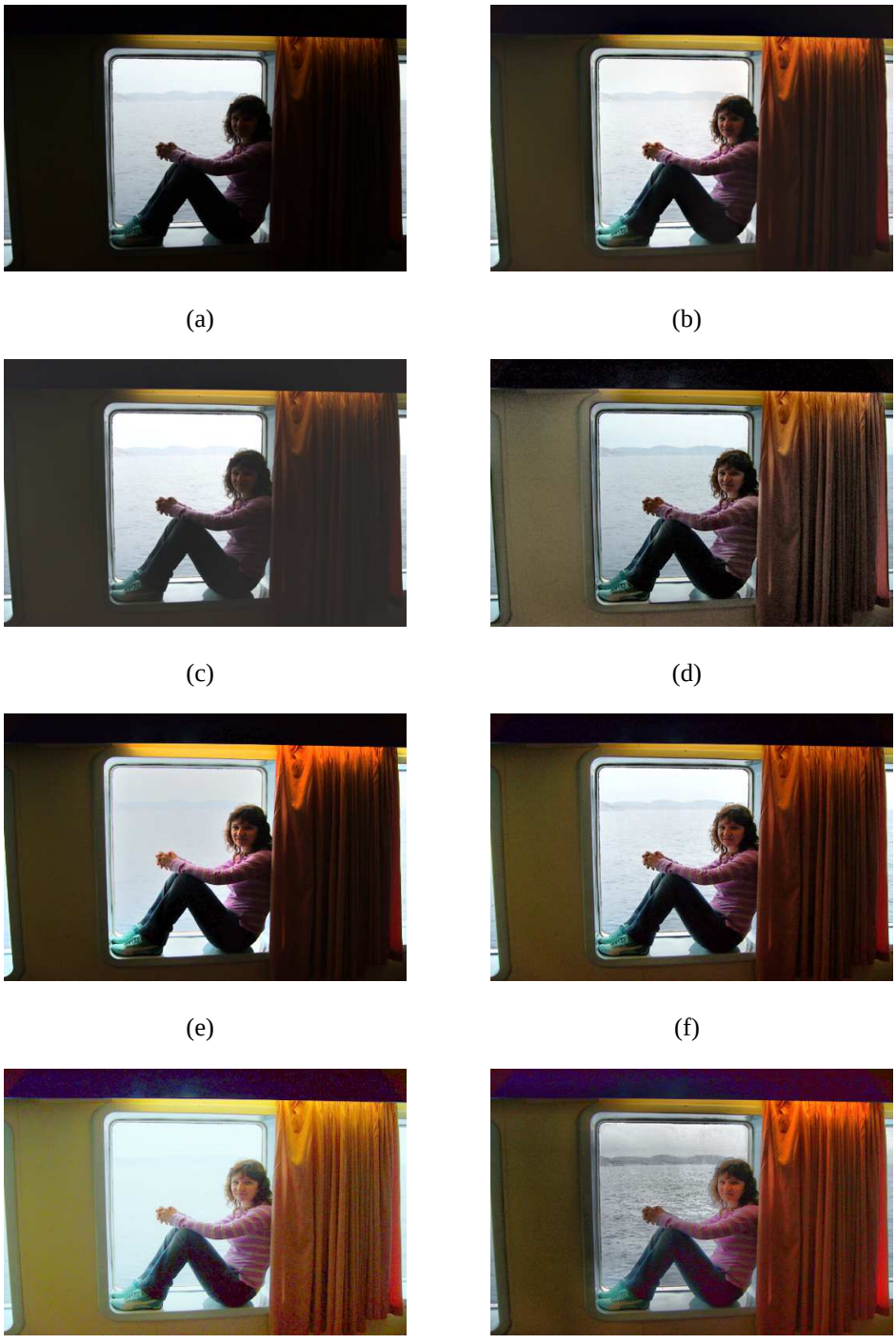

Figure 3.2: Image comparison with the existing method: (a) input image, (b) LVCEHP [25], (c) LVCE [22], (d) FCSM [1], (e) MSRCP [13], (f) MEF [11], (g) MSRCR [8], (h) CLAHE [3]

(a) (b) (c) (d) (e) (f) (g) (h)

Figure 3.3: Image comparison with the existing method: (a) input image, (b) LVCEHP [25], (c) LVCE [22], (d) FCSM [1], (e) MSRCP [13], (f) MEF [11], (g) MSRCR [8], (h) CLAHE [3]

(a) (b) (c) (d) (e) (f) (g) (h)

Figure 3.4: Image comparison with the existing method: (a) input image, (b) LVCEHP [25], (c) LVCE [22], (d) FCSM [1], (e) MSRCP [13], (f) MEF [11], (g) MSRCR [8], (h) CLAHE [3]

Figure 3.5: Image comparison with the existing method: (a) input image, (b) LVCEHP [25], (c) LVCE [22], (d) FCSM [1], (e) MSRCP [13], (f) MEF [11], (g) MSRCR [8], (h) CLAHE [3]

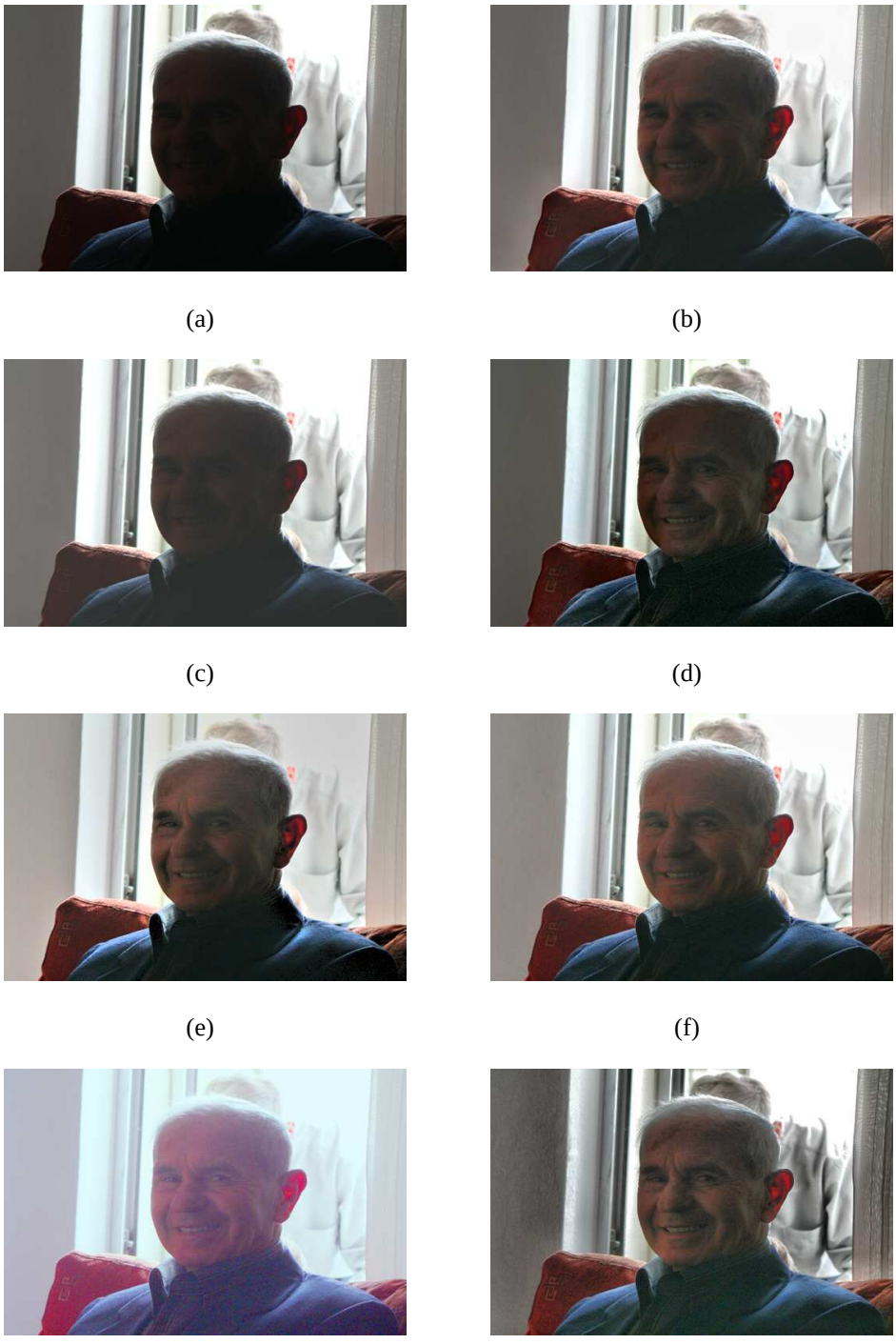

(a) (b) (c) (d) (e) (f) (g) (h)

Figure 3.6: Image comparison with the existing method: (a) input image, (b) LVCEHP [25], (c) LVCE [22], (d) FCSM [1], (e) MSRCP [13], (f) MEF [11], (g) MSRCR [8], (h) CLAHE [3]

(a) (b) (c) (d) (e) (f) (g) (h)

Figure 3.7: Image comparison with the existing method: (a) input image, (b) LVCEHP [25], (c) LVCE [22], (d) FCSM [1], (e) MSRCP [13], (f) MEF [11], (g) MSRCR [8], (h) CLAHE [3]

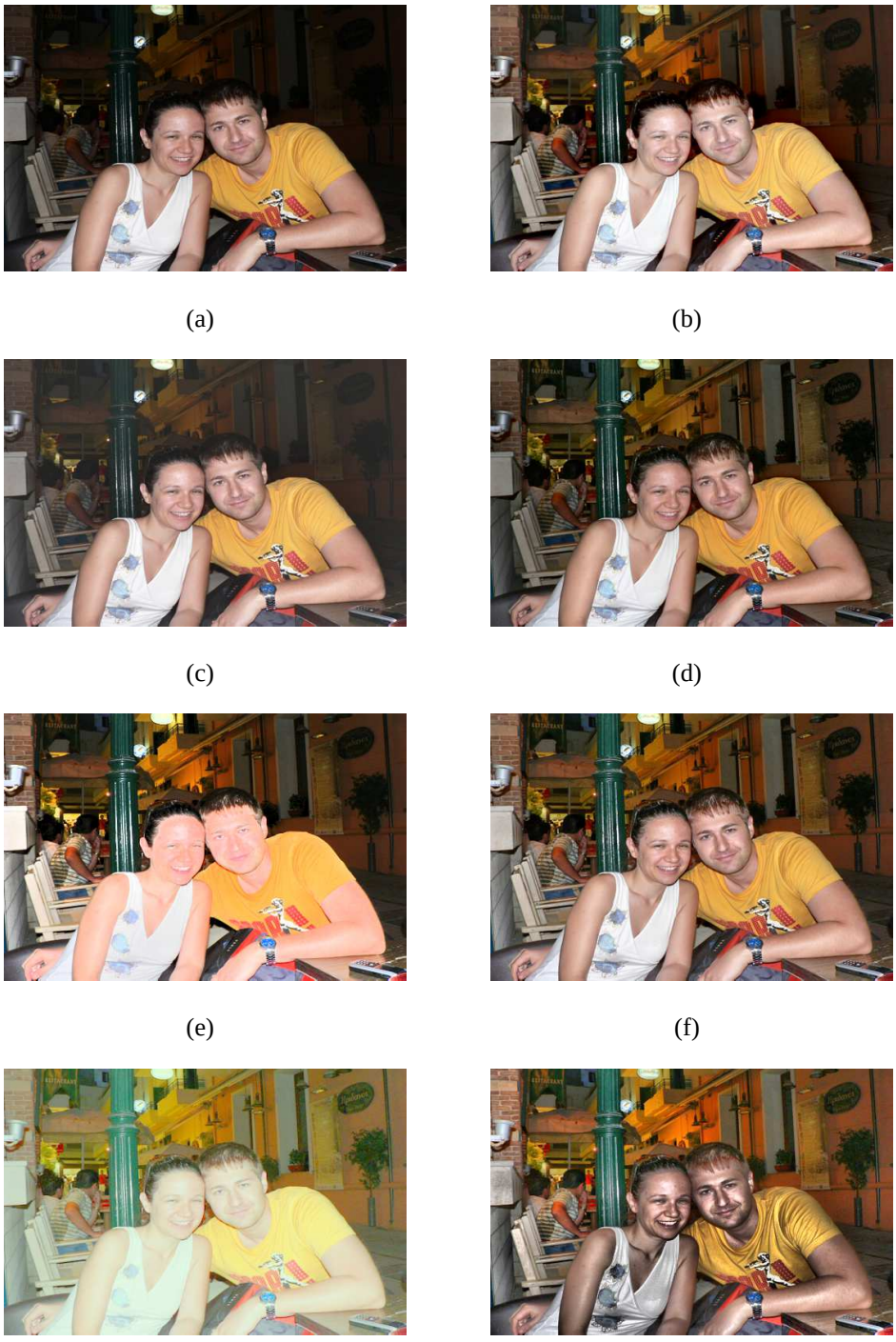

(a) (b)

(c) (d)

(e) (f)

(g) (h)

Figure 3.8: Image comparison with the existing method: (a) input image, (b) LVCEHP [25], (c) LVCE [22], (d) FCSM [1], (e) MSRCP [13], (f) MEF [11], (g) MSRCR [8], (h) CLAHE [3]

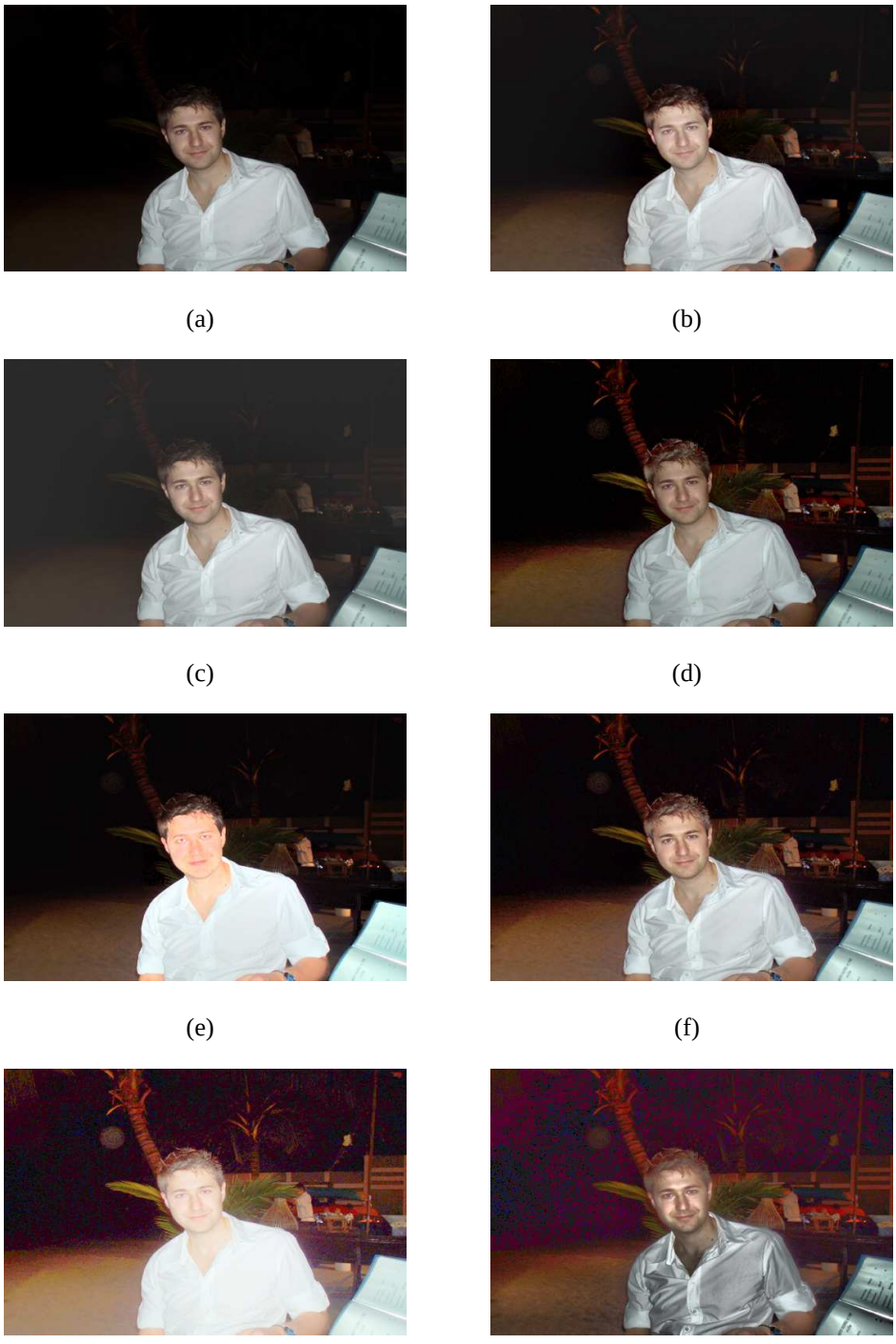

(a) (b)

(c) (d)

(e) (f)

(g) (h)

Figure 3.9: Image comparison with the existing method: (a) input image, (b) LVCEHP [25], (c) LVCE [22], (d) FCSM [1], (e) MSRCP [13], (f) MEF [11], (g) MSRCR [8], (h) CLAHE [3]

(a) (b) (c) (d) (e) (f) (g) (h)

Figure 3.10: Image comparison with the existing method: (a) input image, (b) LVCEHP [25], (c) LVCE [22], (d) FCSM [1], (e) MSRCP [13], (f) MEF [11], (g) MSRCR [8], (h) CLAHE [3]

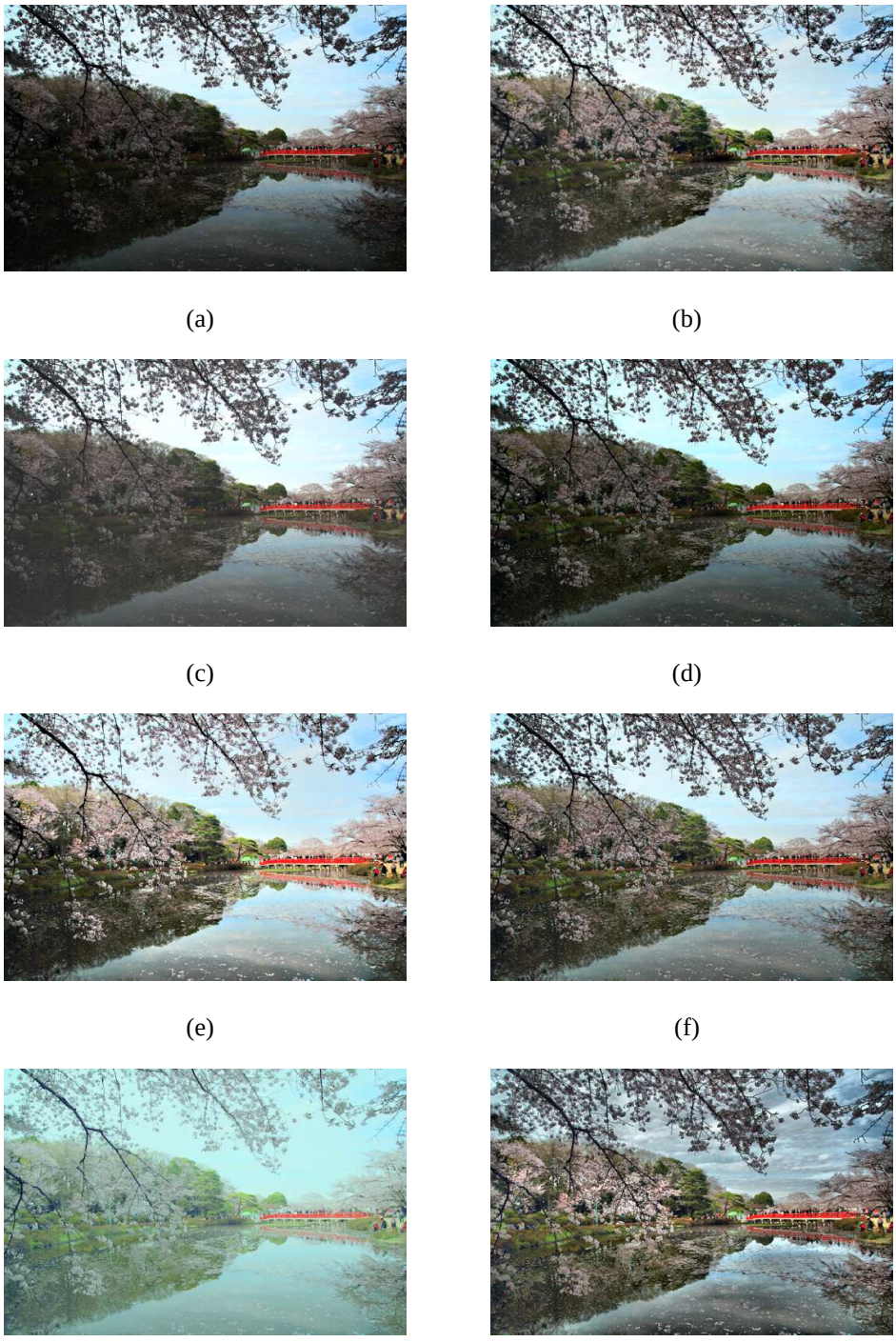

(a) (b) (c) (d) (e) (f) (g) (h)

Figure 3.11: Image comparison with the existing method: (a) input image, (b) LVCEHP [25], (c) LVCE [22], (d) FCSM [1], (e) MSRCP [13], (f) MEF [11], (g) MSRCR [8], (h) CLAHE [3]

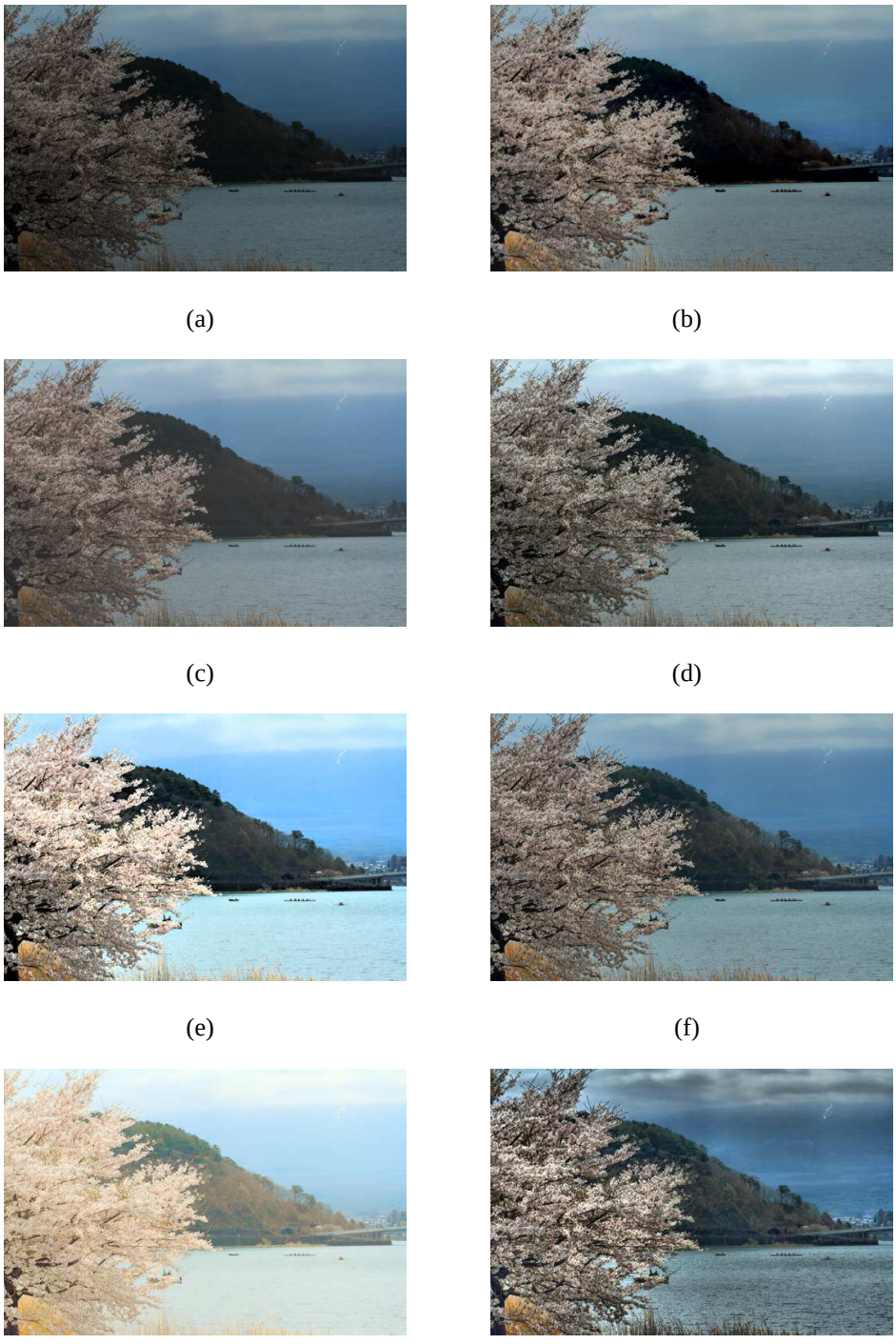

(a) (b) (c) (d) (e) (f) (g) (h)

Figure 3.12: Image comparison with the existing method: (a) input image, (b) LVCEHP [25], (c) LVCE [22], (d) FCSM [1], (e) MSRCP [13], (f) MEF [11], (g) MSRCR [8], (h) CLAHE [3]

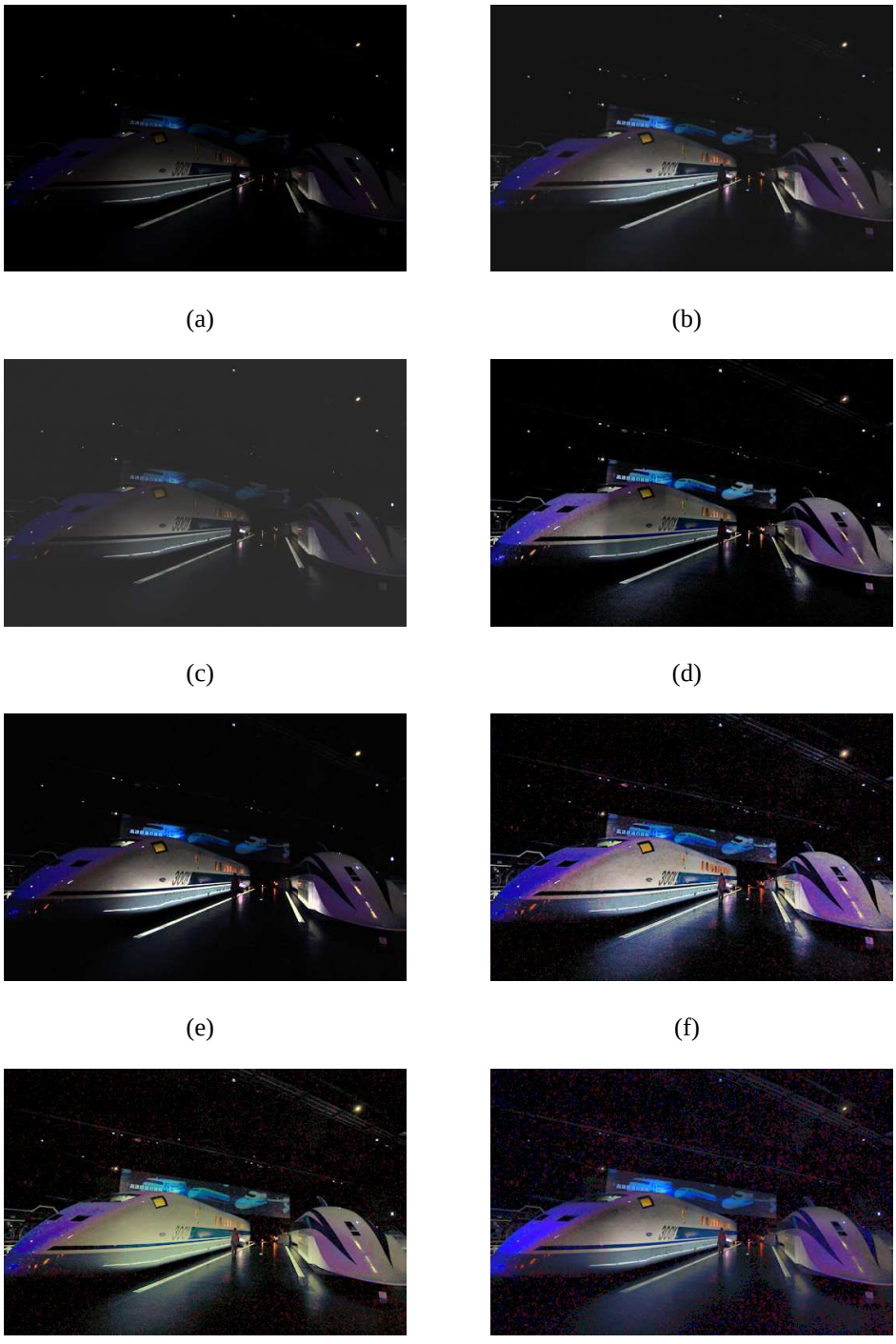

Figure 3.13: Image comparison with the existing method: (a) input image, (b) LVCEHP [25], (c) LVCE [22], (d) FCSM [1], (e) MSRCP [13], (f) MEF [11], (g) MSRCR [8], (h) CLAHE [3]

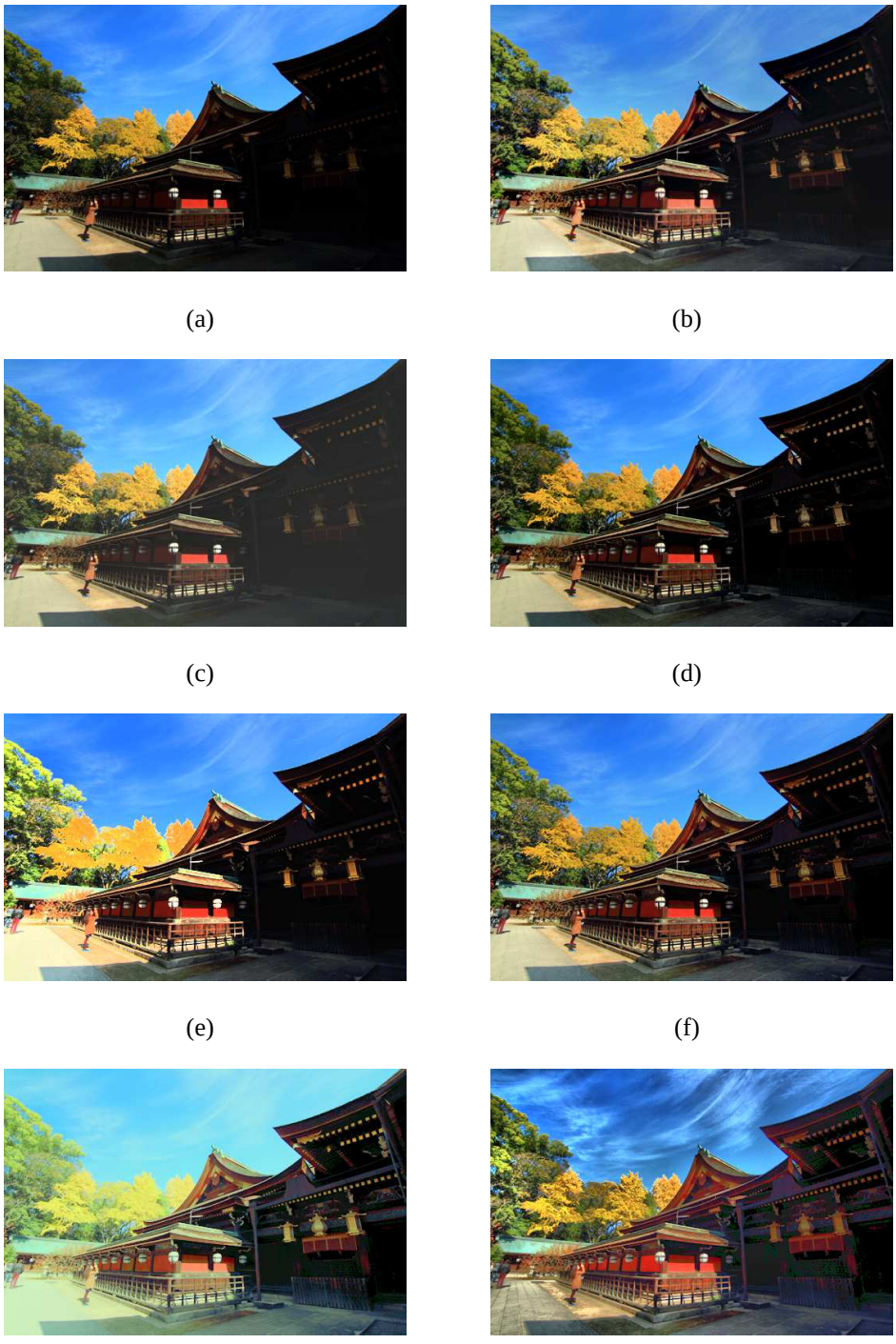

(a) (b) (c) (d) (e) (f) (g) (h)

Figure 3.14: Image comparison with the existing method: (a) input image, (b) LVCEHP [25], (c) LVCE [22], (d) FCSM [1], (e) MSRCP [13], (f) MEF [11], (g) MSRCR [8], (h) CLAHE [3]

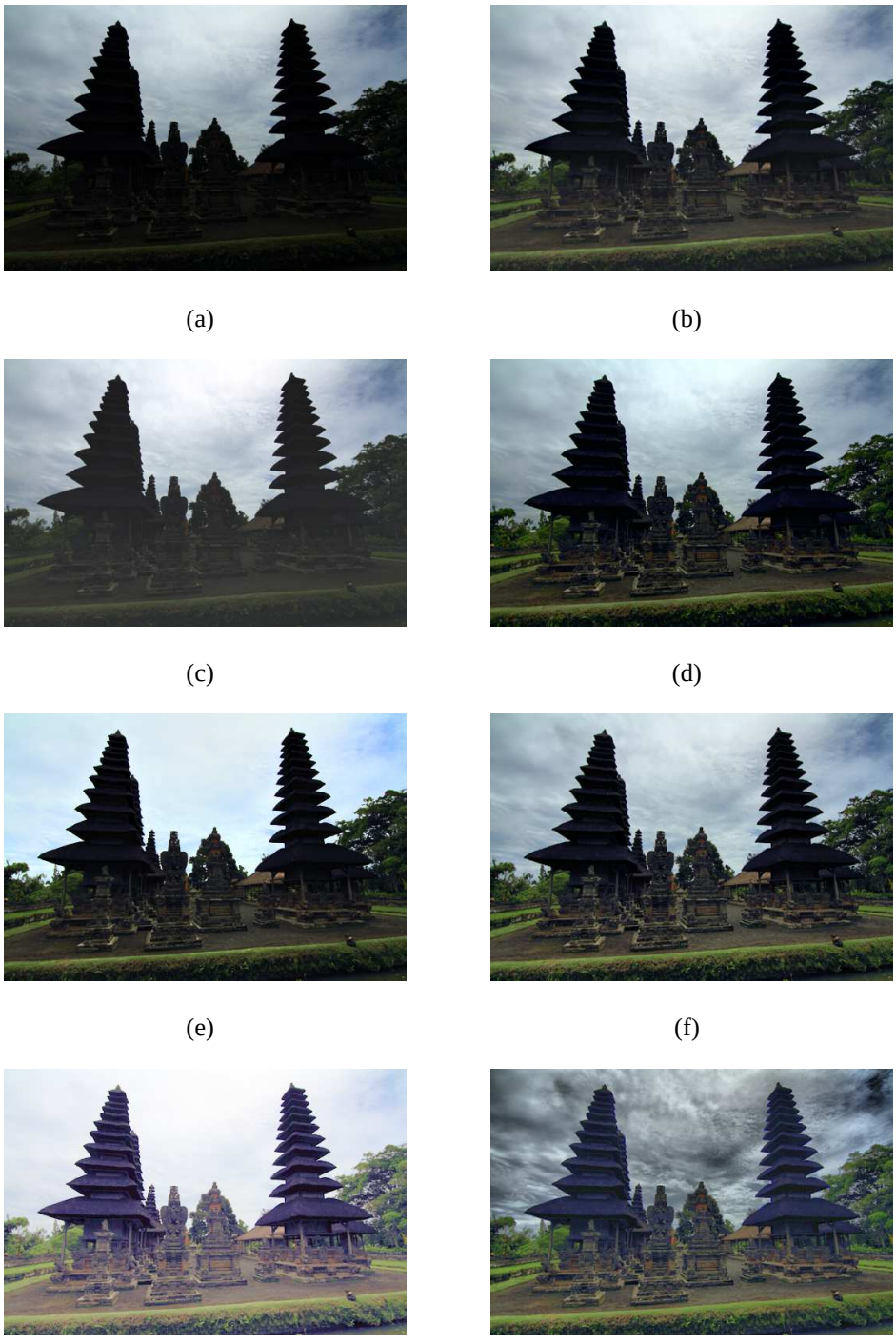

Figure 3.15: Image comparison with the existing method: (a) input image, (b) LVCEHP [25], (c) LVCE [22], (d) FCSM [1], (e) MSRCP [13], (f) MEF [11], (g) MSRCR [8], (h) CLAHE [3]

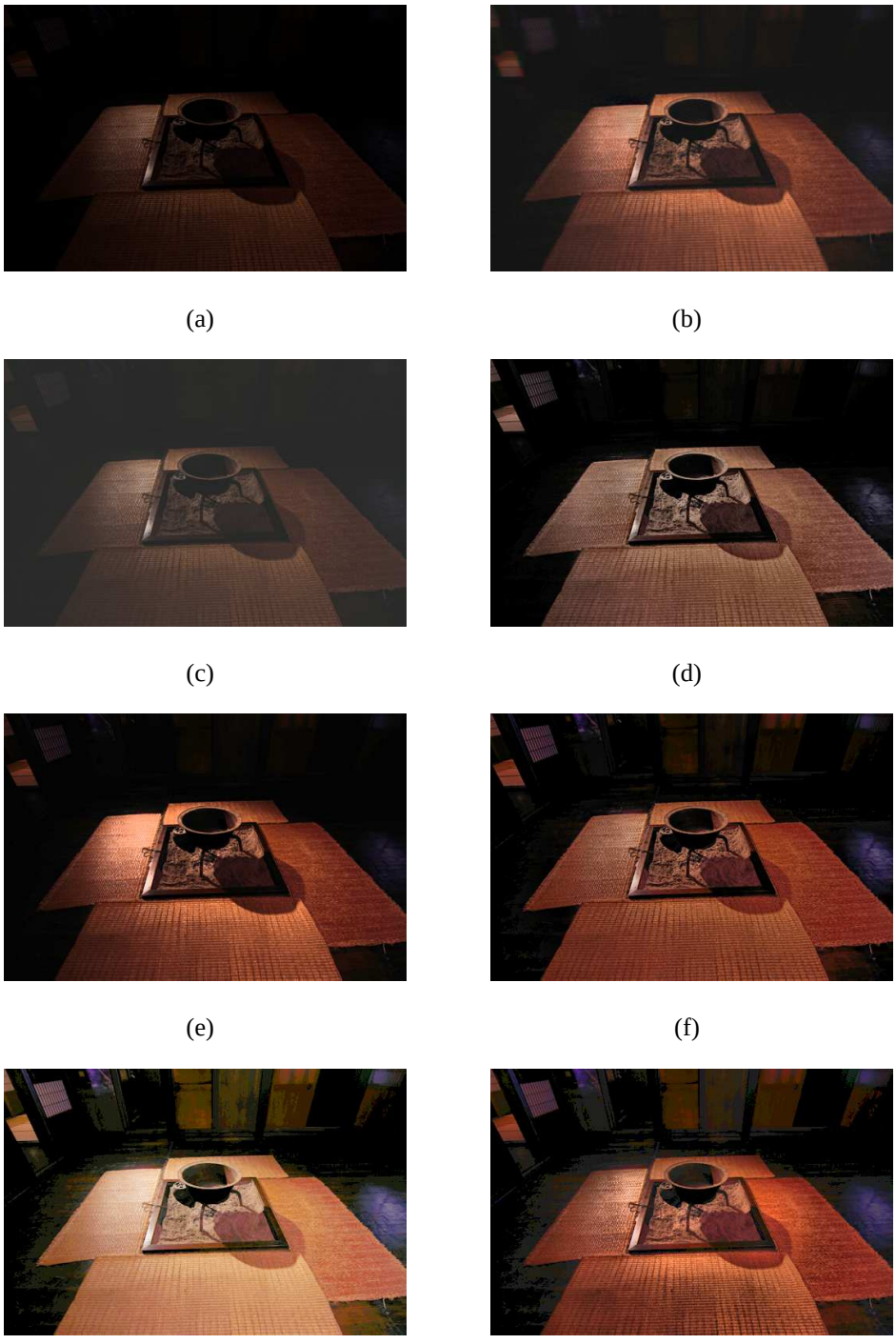

Figure 3.16: Image comparison with the existing method: (a) input image, (b) LVCEHP [25], (c) LVCE [22], (d) FCSM [1], (e) MSRCP [13], (f) MEF [11], (g) MSRCR [8], (h) CLAHE [3]

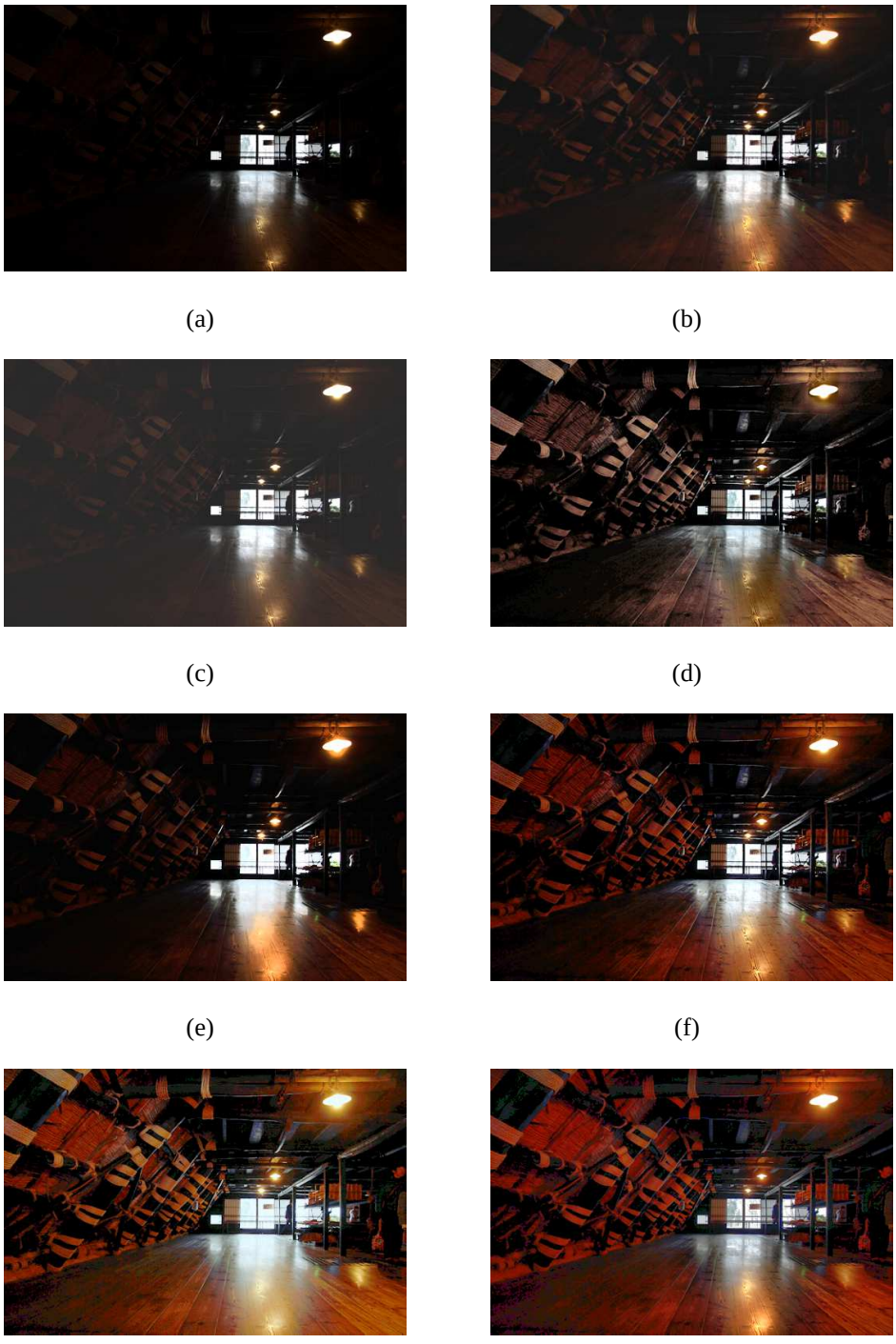

(a) (b) (c) (d) (e) (f) (g) (h)

Figure 3.17: Image comparison with the existing method: (a) input image, (b) LVCEHP [25], (c) LVCE [22], (d) FCSM [1], (e) MSRCP [13], (f) MEF [11], (g) MSRCR [8], (h) CLAHE [3]

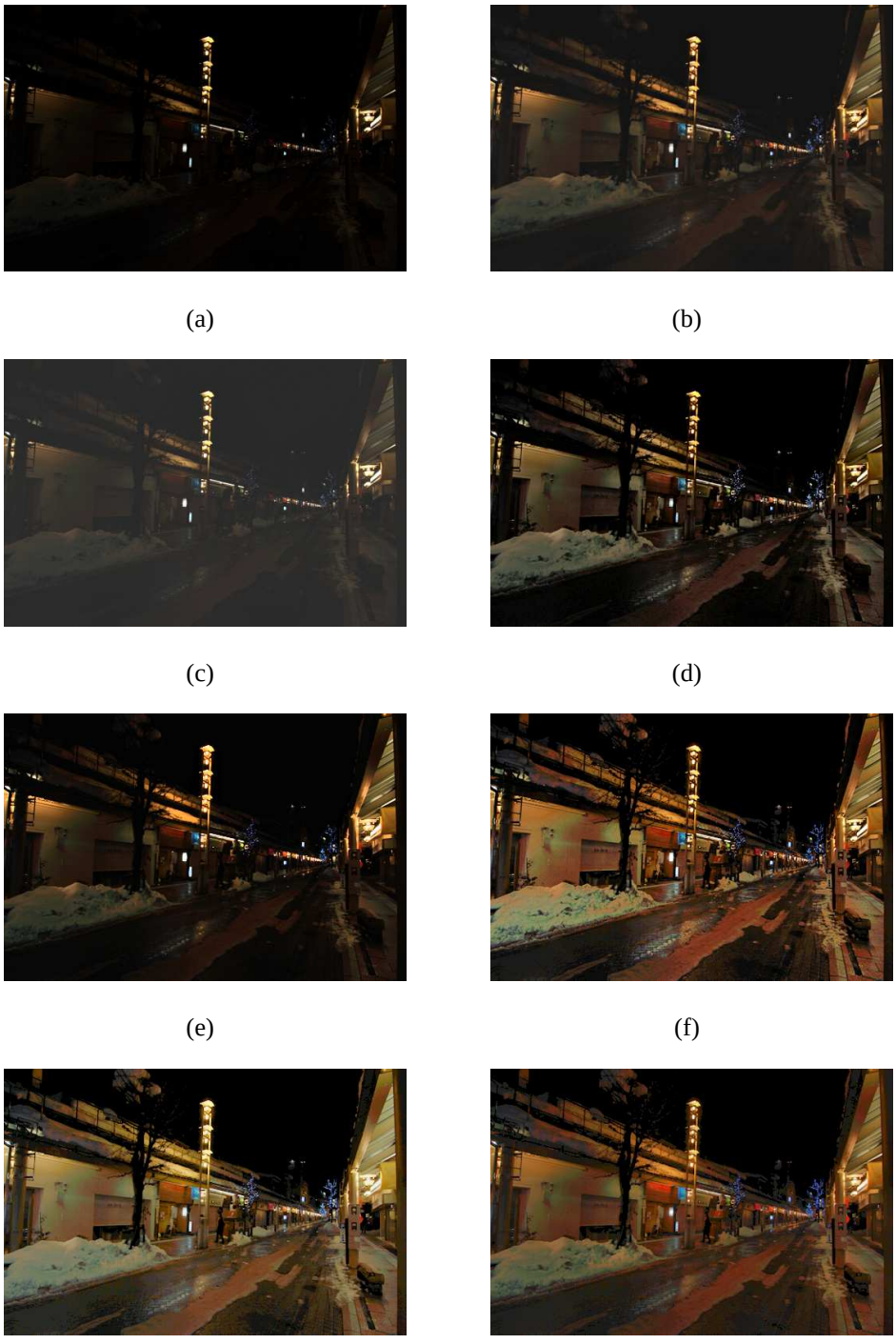

(a) (b) (c) (d) (e) (f) (g) (h)

Figure 3.18: Image comparison with the existing method: (a) input image, (b) LVCEHP [25], (c) LVCE [22], (d) FCSM [1], (e) MSRCP [13], (f) MEF [11], (g) MSRCR [8], (h) CLAHE [3]

(a) (b) (c) (d) (e) (f) (g) (h)

Figure 3.19: Image comparison with the existing method: (a) input image, (b) LVCEHP [25], (c) LVCE [22], (d) FCSM [1], (e) MSRCP [13], (f) MEF [11], (g) MSRCR [8], (h) CLAHE [3]

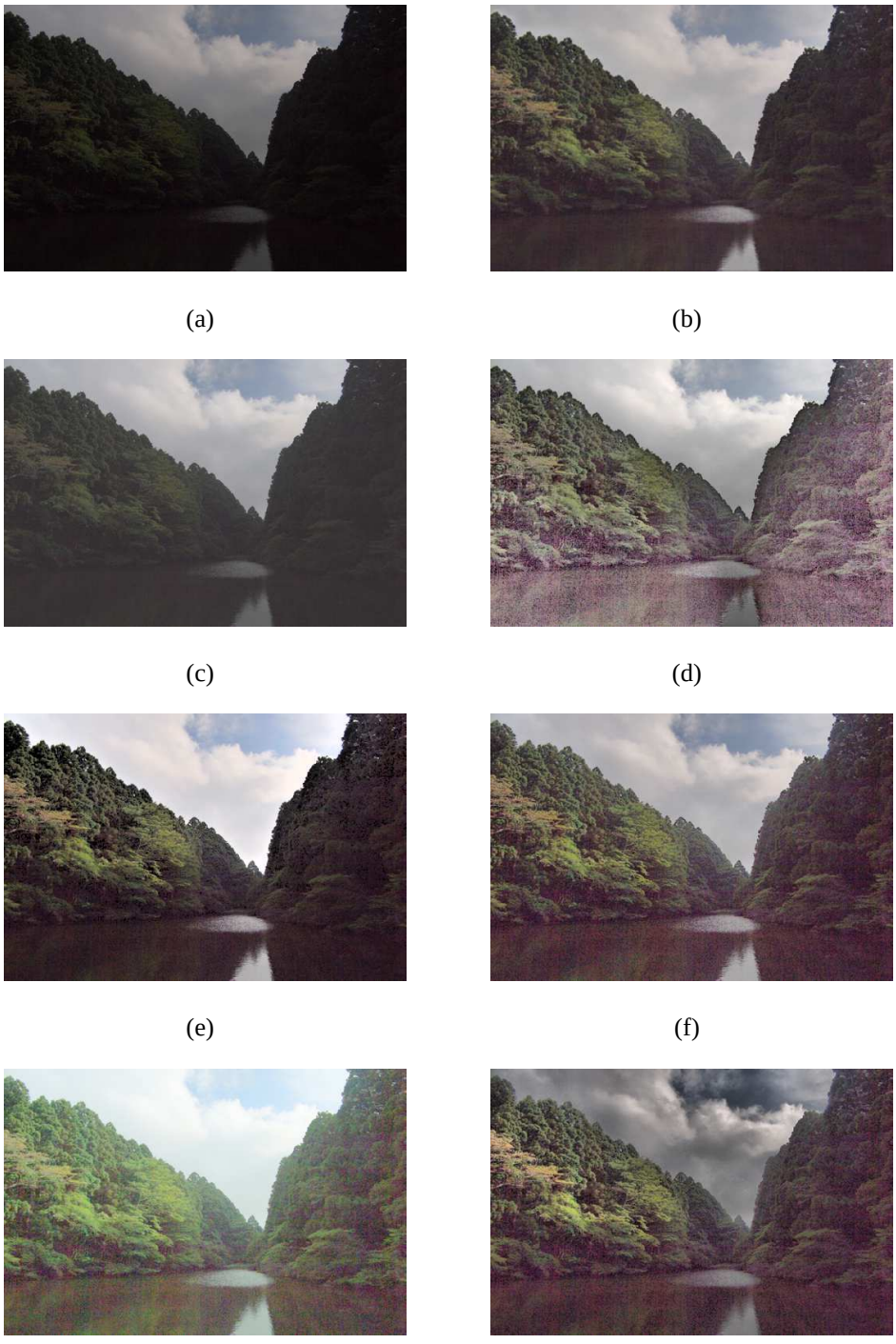

(a) (b) (c) (d) (e) (f) (g) (h)

Figure 3.20: Image comparison with the existing method: (a) input image, (b) LVCEHP [25], (c) LVCE [22], (d) FCSM [1], (e) MSRCP [13], (f) MEF [11], (g) MSRCR [8], (h) CLAHE [3]

Chapter 4

Analysis and Discussion of the Proposed Method

4.1 Analysis the Flexibility of the Proposed Method

4.1.1 Adjust the Parameter on LVCE

In LVCE, there are five parameters which can be adjusted; the first-two parameters (Sel_{bin} and σ) come from the range of selected bin to assign as the less-visible areas and the standard deviation of the Gaussian low-pass filter in the processes of SVD-based image decomposition and pyramid-based blending method. The latter-three parameters (α, β, and γ) come from the scaling factor in the non-linear contrast enhancement process.

Parameter setting in SVD-based Decomposition Process

In SVD-based decomposition process, it allows the users to select the range (Sel_{bin}) to define the less-visible areas of the input image. The range (Sel_{bin}) of less-visible image is calculated by plotting the distribution of singular values on the binary-logarithmic scale. Then, the maximum bin, q, is determined. Finally, we can adjust the range of Sel_{bin} from $q + d_{min}$ to $q + d_{max}$

To adjust an appropriate range (Sel_{bin}) of less-visible areas, there are few factors that users need to consider.

1. The range of selection is one of the major factor that we need to concern. Even through, the wider range of Sel_{bin} may create the higher chance for improving the less-visible areas

as shown in Fig. 4.1(b)- 4.1(d). Too wider range may cause some distortion effect to the resulting image as shown in Fig. 4.1(b).

(a) (b)

(c) (d)

Figure 4.1: Image comparison with different ranges of Sel_{bin}. (a) Input image, (b)-(d) Resulting images obtained from the different ranges of Selbin; $[q-1, q+3]$, $[q+1, q+3]$, and $[q+3, q+3]$, respectively.

2. The position of selected bin, Sel_{bin}, is another factor that might affect the quality of resulting image.

   (a) Select the bin on the highest bin or left-hand side of the highest bin (q): too far apart from the highest bin may cause the over-enhancement and distortion problems to the resulting image. Thus, in our experiment, selecting the appropriate bin at the highest bin (q) may cause the problems too as shown in Fig. 4.2(b)- 4.2(c).

   (b) Select the bin on right-hand side of the highest bin (q): too far apart from the highest bin (q) might not cause any problem. However, due to the less pixel values on the less-visible areas image, the enhancement process cannot be scaled up the targeted

pixel to improve the less-visible areas of the resulting image as expected. Figure 4.2(b)- 4.2(c) show the example of the image with different positions of Sel_{bin}.

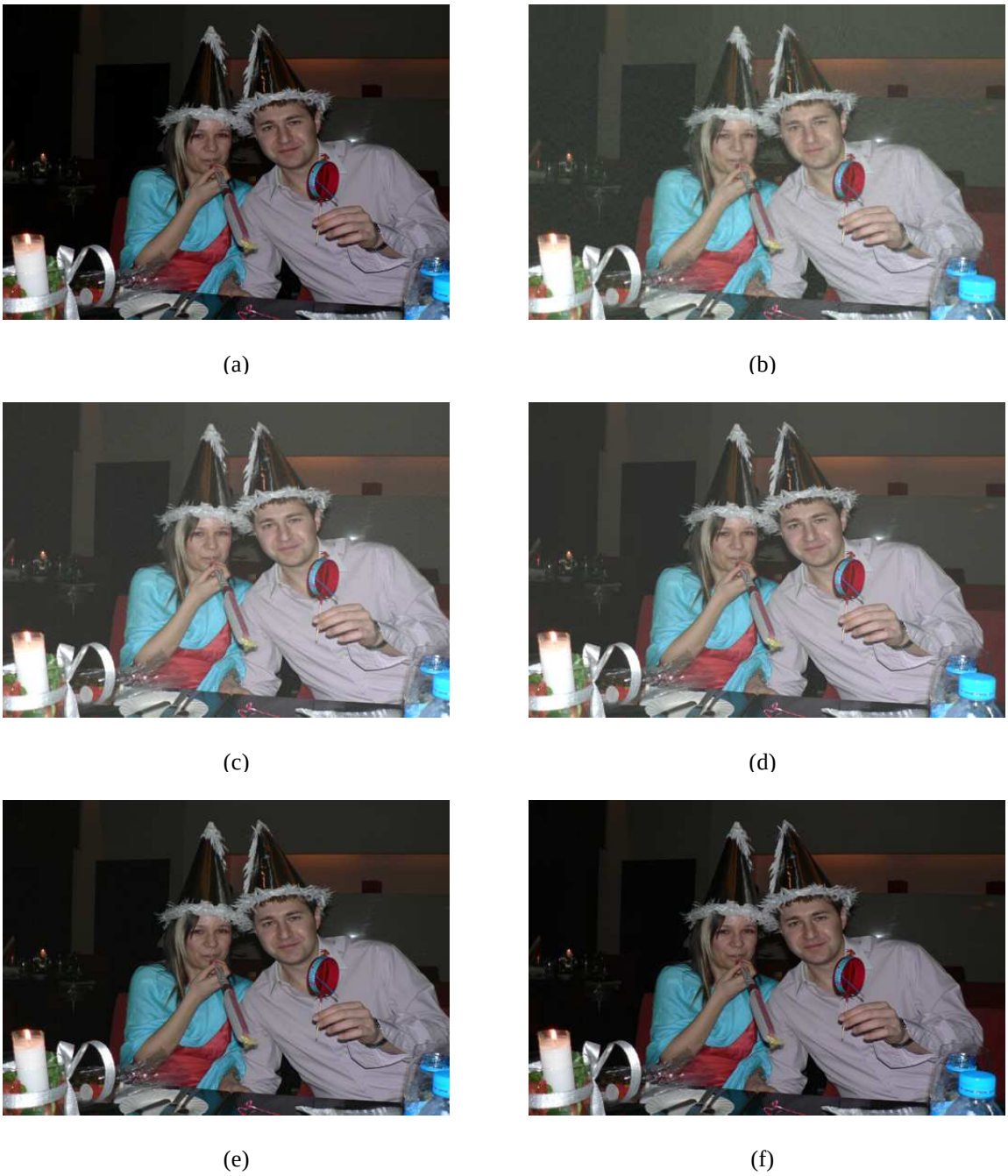

(a) (b)

(c) (d)

(e) (f)

Figure 4.2: Image comparison with different positions of Sel_{bin}. (a) Input image, (b)-(f) Resulting images obtain from the different position of Selbin; $[q - 1]$, $[q + 0]$, $[q + 3]$, $[q + 5]$, and $[q + 7]$, respectively.

Parameters setting in Non-linear Contrast Enhancement Process

In the non-linear contrast enhancement process, there are three parameters (α, β, and γ) that can be adjusted in the following non-linear equation.

$$\tilde{\boldsymbol{A}}_{\varrho,xy} = \frac{\log_{15}\left(\alpha \breve{\boldsymbol{A}}_{\varrho,xy}^{2} + \beta \breve{\boldsymbol{A}}_{\varrho,xy} + \gamma\right)}{2}, \tag{4.1}$$

$$\breve{\boldsymbol{A}}_{\varrho,xy} = \boldsymbol{A}_{\varrho,xy} + |\boldsymbol{A}_{\varrho,\min}|. \tag{4.2}$$

where $\boldsymbol{A}_{\varrho,\min}$ and the minimum value of the matrix $\boldsymbol{A}_{\varrho}$.

By substituting the predefined value into α, β, and γ in eq.4.1, we can rearrange the equation as follow.

$$\begin{aligned}
\tilde{\boldsymbol{A}}_{\varrho,xy} &= \frac{\log_{15}\left(1\breve{\boldsymbol{A}}_{\varrho,xy}^{2} + 3.7\breve{\boldsymbol{A}}_{\varrho,xy} + 2.7\right)}{2} \\
&= \frac{\log_{15}\left((1\breve{\boldsymbol{A}}_{\varrho,xy} + 1)(\breve{\boldsymbol{A}}_{\varrho,xy} + 2.7)\right)}{2} \\
&= \frac{\log_{15}\left((1\breve{\boldsymbol{A}}_{\varrho,xy} + 1) + \log_{15}(\breve{\boldsymbol{A}}_{\varrho,xy} + 2.7)\right)}{2} \\
&= \frac{1}{2} \times \frac{\log_{15}\left((1\breve{\boldsymbol{A}}_{\varrho,xy} + 1) + \log_{15}(\breve{\boldsymbol{A}}_{\varrho,xy} + 2.7)\right)}{\log_{15}}
\end{aligned} \tag{4.3}$$

Note that $\log_b xy = log_b x + log_b y$ and $\log_b x = \frac{\log_k x}{\log_k b}$

From the rearrange equation, the parameter β can be calculated by summation between α, and γ.

$$\breve{\boldsymbol{A}}_{\varrho,xy} = \frac{1}{2} \times \frac{\log_{15}\left((1\breve{\boldsymbol{A}}_{\varrho,xy} + 1) + \log_{15}(\breve{\boldsymbol{A}}_{\varrho,xy} + 2.7)\right)}{\log_{15}}. \tag{4.4}$$

In such case, it is possible to adjust the parameters α and γ as follow:

1. Improve the less-visible areas without concerning the Just-Noticeable-Different (JND) in the dark area: based on the experiment, it found that the summation of α and γ or parameter is proportion to the scaling factor. Greater value of β, higher information on less-visible area to be improved. However, the users need to carefully adjust the values of α and γ. If the summation of α and γ is greater than 4, the over-enhancement may occur in the resulting image. Thus, the proposed non-linear contrast enhancement is a pixel-based approach which separately apply into each red, green and blue (R,G,B) channel. If

the pixel value (R,G,B) is closely to $(0, 0, 0)$ or black, the proposed contrast enhancement will produce the increment value with the same amount or closely to each channel. Based on principle of digital image processing, when the pixel value in red, green, and blue channel are produced the same amount or closely to each other, it will generate the shade of gray (dark gray to gray). Finally, the foggy effect could be occurred in the resulting image as shown in Fig. 4.3(c)- 4.3(d).

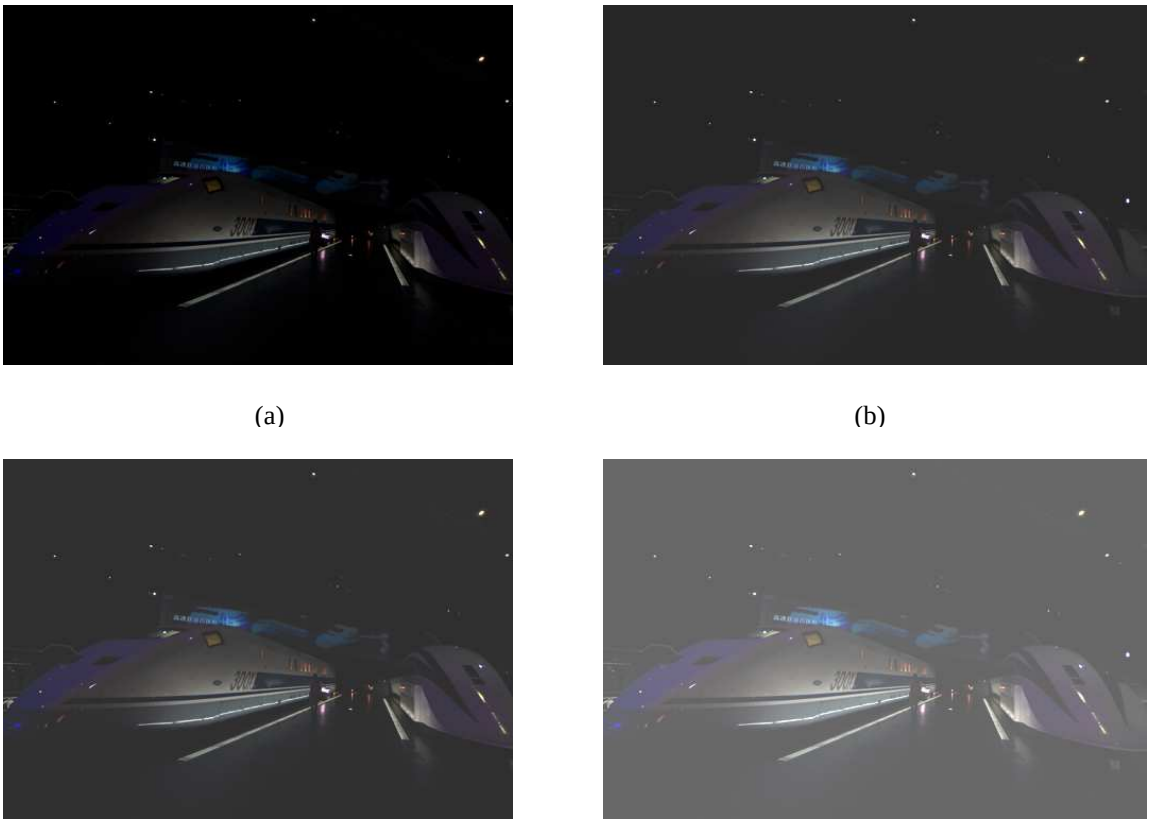

(a) (b)

(c) (d)

Figure 4.3: Image comparison with different values of the summation between α and γ. (a) Input image, (b)-(d) Resulting images obtained from the summation values of α and γ; 3.75, 5, and 6, respectively.

2. Improve the less-visible areas by concerning Just-Noticeable-Different (JND) in the dark areas. Based on JND in digital image processing, JND is defined as the minimum visibility threshold when visual contents are altered. In this work, the JND model from Chou et al [20]. is used to find the appropriate range for scaling the pixel value in less-visible image without create any foggy effect.

   In the enhancement process, the pixel value (R,G,B), which closes to $(0, 0, 0)$, should not be enhanced exceed the minimum visibility that the human can notice. Otherwise, the foggy effect might be occurred. By investigating the characteristic of JND, we found that the JND at intensity equal to 0 produces the highest JND values. In that case, we take an advantage of its values to avoid the foggy effect. By setting the suitable values of summation between α and γ regards to $JND(0)$, we found that it can avoid such the foggy effect and other areas also successfully enhance the less-visible area. In the experiment, suitable value of summation between and are around 2.01 – 2.5. Anyway, due to limitation of scaling factor, the less-visible area in resulting image may not be improved as much as we expected (Fig. 4.4(c)- 4.4(d)).

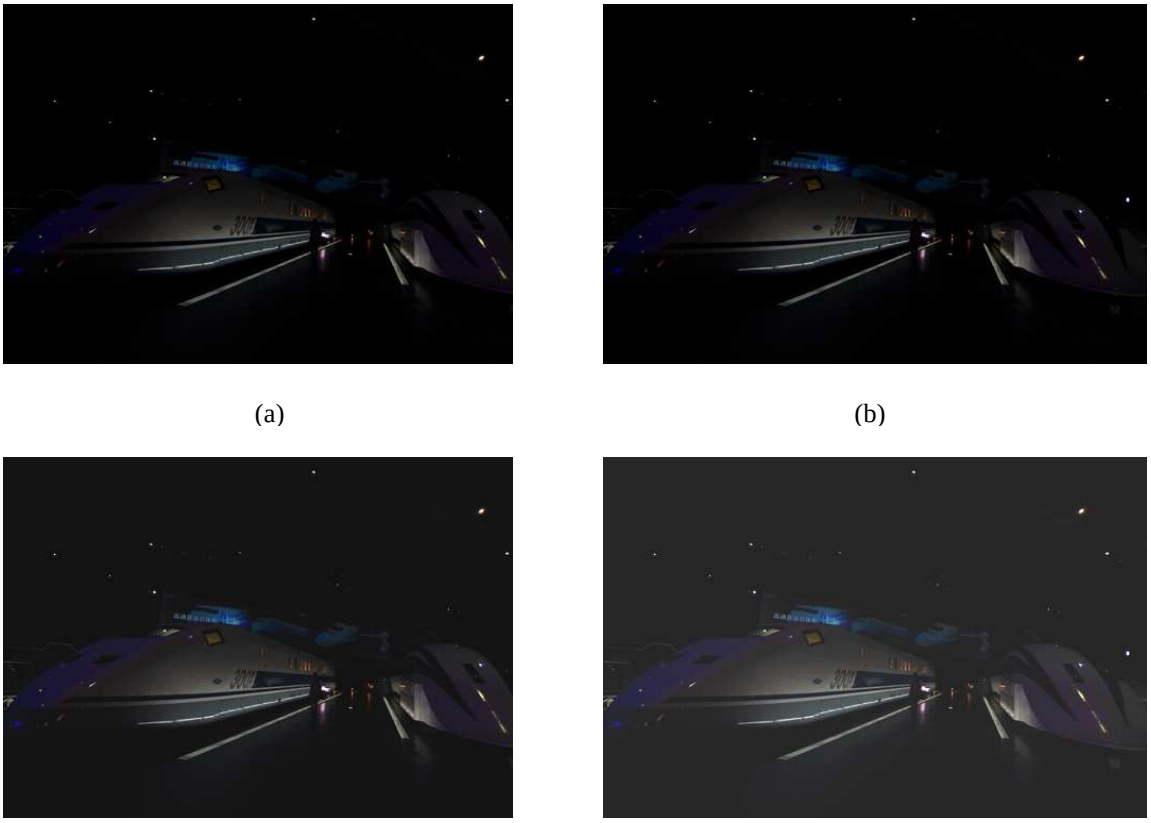

(a) (b)

(c) (d)

Figure 4.4: Image comparison with different values of the summation between α and γ. (a) Input image, (b)-(d) Resulting images obtained from the summation values of α and γ; 2, 2.5, and 3, respectively.

Parameter setting in Pyramid-based Blending Process

In the pyramid-based blending process, the standard deviation of the Gaussian function (σ) in the local exposure weight can be adjusted. By increasing the parameter σ, the width of the Gaussian function will be expanded. As consequent, the exposure weights at the small pixel values are also gradually scaled up, and allow the blending algorithm hard to find the most saliency pixel (x,y) along the dataset. Finally, the resulting image obtained from blending function cannot recover the less-visible areas from enhanced image as shown in Fig. 4.5. Consequently, the resulting image is not improved as much as we expected.

(a)

(b)

(c)

(d)

Figure 4.5: Image comparison with different values of standard deviation (σ) in pyramid-based blending method. (a) Input image, (b)-(d) Resulting images obtained from the summation values of ; 0.2, 0.4, and 0.6, respectively.

4.1.2 Adjust the Parameter on LVCEHP

In LVCEHP, there are two parameters which can be adjusted; the first parameter,S_{th}, is the threshold value to indicate whether the input image has a risk to contain the high level of noise or not. Another parameter is the standard deviation,σ , of the Gaussian low-pass filter in the processes of pyramid-based blending method which is similarly to LVCE.

Parameter setting in Noise-level Analysis Process

In the process of noise-level analysis, the algorithm analyzes the level of noise in the input images using the Singular Value Decomposition (SVD). Firstly, we decompose the input image using SVD. Then, we calculate the summation of all singular values, S, which is used to estimate the area bounded by the singular-value curve and the singular-value-index axis. If the S value

is less than a threshold value of hidden-noise level S_{th}, the algorithm will eliminate the latter group of singular value. However, the users need to carefully set the parameter S_{th}. By setting the high threshold value S_{th}, sometimes, it may distort the information which is contained in the latter group of singular value. Finally, the resulting image may cause some unwanted effects as shown in Fig. 4.6(c). In the other hand, setting the low threshold value S_{th}, may allow the image that contains the high level of noise to be enhanced. Finally, the resulting image may look noisy as shown in Fig. 4.7(b).

(a)

(b)

(c)

Figure 4.6: Image comparison with different threshold values S_{th} in noise-level analysis process. (a) Input image, (b)-(c) Resulting images obtained from the threshold values; 9×10^4, and 9×10^20, respectively.

(a)

(b)

(c)

Figure 4.7: Image comparison with different threshold values S_{th} in noise-level analysis process. (a) Input image, (b)-(c) Resulting images obtained from the threshold values; 9×10^3, and 9×10^4, respectively.

4.2 Discussion

There are six issues that we would like to discuss in this section. Also, the interpretation of the evaluation results is to be explained. First, the predefined value of several parameters from the proposed methods e.g. the range of the less-visible bin Sel_{bin}, the scaling factor for enhance the less-visible layers (α, β, and γ), and the threshold value of hidden-noise level (S_{th}), etc. that used in our simulation are based on a process of trial and error, and it might depend upon a data set. To improve the proposed algorithm further, we need a general process that can determine those parameters automatically.

Second, in this work, we used the IEM, QI, entropy, and homogeneity as our objective measurements. We did not use the measure of enhancement (EMEE), the measure of enhancement by entropy (EMEE), the logarithmic Michelson contrast measure (AME), and the second

derivative the measure of enhancement (SDME). Even though these measurements are popular for measuring the enhanced image, but they are not good at measuring the enhancement only in some specifics areas, especially the less-visible areas. In general, these measurements are calculated from the summation of the ratio between the minimum and the maximum values of each block of the enhanced image.

Third, since the first three prefered methods, according to the subjective tests, are the MEF, the FCSM, and the proposed method, the value of IEM and QI should be in the ranges of $[1.4 - 2.3]$ and $[0.4, 0.6]$, respectively. The value of entropy should be greater than 6.8, and lesser than 7.0, and the value of homogeneity should be greater than 0.9, and lesser than 0.93.

Forth, from the evaluation results, it can conclude that the LVCE is quite effective to enhance the less-visible areas of the input image without amplifying the hidden noise. However, the property of this proposed method may be a two-edged sword. Since the LVCE select only some layers that to modify or enhance, sometimes, such layers are not contain enough pixel value to increase the luminance or intensity of the less-visible areas. However, increasing the number of selected bin may enhance the targeted areas, but it may cause the effect of amplifying the hidden noise.

Fifth, the LVCEHP is one of the most effective compare to the existing methods. The LVCEHP can achieve one of the first three ranks in all criteria from the subjective evaluation. Anyway, the LVCEHP still suffer to preserve the intensity of the improved image A_{Imp}. The problem occur in the step of image blending which the resulting image are such degraded the intensity at the less-visible areas when compare to the improved image A_{Imp} as shown in Fig. 4.8. This limitation will be improved in the near future.

Sixth, we would like to discuss about limitation of the proposed method. Even though the proposed algorithm can solve the various problems, e.g., over-enhancement, noise-amplification, and tone and texture modification as shown in Fig. 4.9, 4.10, 4.11, the proposed algorithm cannot restore true color information in some cases. The example of this problem is shown in Fig. 4.12.

(a)

(b)

(c)

Figure 4.8: Limitation of the LVCEHP: comparison of the improved image A_{Imp} and the resulting image. (a) Input Image, (b) Improved image and (c) LVCEHP.

(a) (b) (c) (d)

(e) (f) (g) (h)

Figure 4.9: Examples of the over-enhancement problem: comparison of an enlarged area of the images obtained from (a) Input Image, (b) LVCEHP [25], (c) LVCE [22], (d) FCSM [1], (e) MSRCP [13], (f) MEF [11], (g) MSRCR [8] and (h) CLAHE [3].

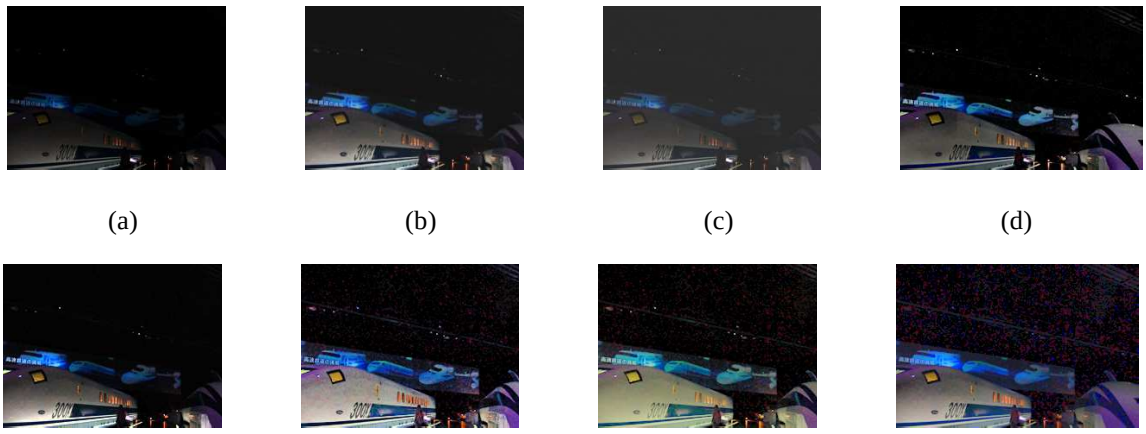

(a) (b) (c) (d)

(e) (f) (g) (h)

Figure 4.10: Examples of the noise amplification problem: comparison of an enlarged area of the images obtained from (a) Input Image, (b) [25], (c) LVCE [22], (d) FCSM [1], (e) MSRCP [13], (f) MEF [11], (g) MSRCR [8] and (h) CLAHE [3].

(a) (b) (c) (d)

(e) (f) (g) (h)

Figure 4.11: Examples of the tone and texture modification problem: comparison of an enlarged area of the images obtained from (a) Input Image, (b) [25], (c) LVCE [22], (d) FCSM [1], (e) MSRCP [13], (f) MEF [11], (g) MSRCR [8] and (h) CLAHE [3].

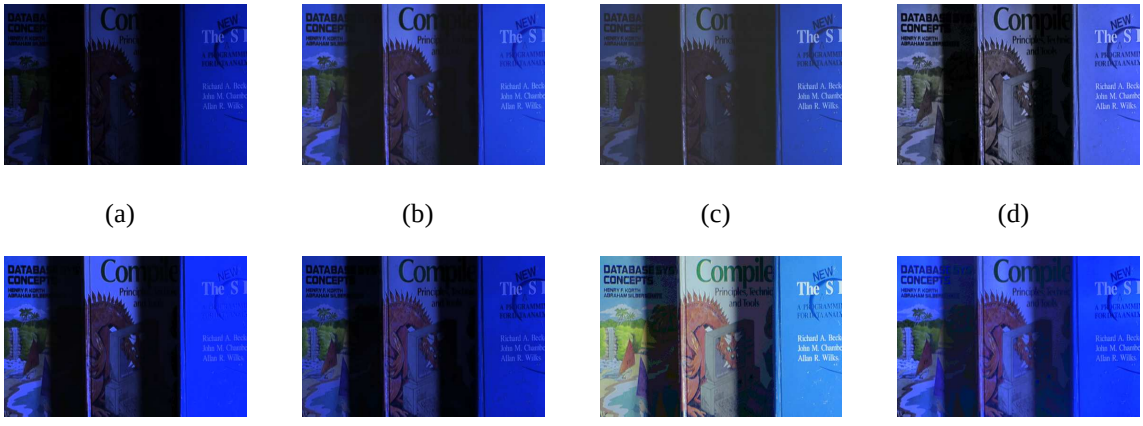

(a) (b) (c) (d)

(e) (f) (g) (h)

Figure 4.12: Examples of the limitation of the proposed method: comparison of an enlarged area of the images obtained from (a) Input Image, (b) [25], (c) LVCE [22], (d) FCSM [1], (e) MSRCP [13], (f) MEF [11], (g) MSRCR [8] and (h) CLAHE [3].

Chapter 5

Conclusion

5.1 Summary

5.1.1 Unique and New Concept from This Work

The conventional image enhancement methods suffer to enhance an image which contains both less-visible and nicely-visible areas while preserve such the key-lighting of image or the tone of original image. In this work, we propose two new less-visible-image enhancement schemes, called the less-visible contrast enhancement method (LVCE) and the less-visible contrast enhancement based on human visual perception (LVCEHP). For the LVCE, we propose the new image enhancement techniques based on a non-linear scaling function and the singular value decomposition (SVD). The SVD is used to decompose the image into several layers. We found that, some layers are associated with the less-visible areas. Then, such layers are selected and strengthened by using the proposed logarithmic-scaling function. For the LVCEHP, we propose a new technique for enhancing each pixel with the different non-linear scaling functions. Since, the targeted pixel is constructed based on Just-Noticeable-Different (JND) of the average-pixel value, with this approach, the pixel that has the same pixel value may use different non-linear scaling functions. Moreover, we also propose a new techniques for analyze and remove the hidden noise of the input image. We experimentally found that the smaller area-bounded of the singular-value curve implies the higher level of noise. If the area of singular value contains the area-bounded less than the threshold value of the hidden noise value ($S < S_{\text{th}}$). Then, we remove the noise layer $\boldsymbol{A}_{\mathfrak{N}}$ before the enhancement process. Lastly, we also propose the pyramid-based blending techniques for fusing two images in order to solve

the problem of information missing in the blending process.

The original idea of this research is to model precisely to the algorithm based on on human vision system while the existing methods always mention to the human visual system as the inspiration to create the algorithm, but they never use the principle of human vision system precisely in their models.

5.1.2 Advantages and Disadvantages of the Proposed Methods

- Less-visible contrast Enhancement (LVCE): The strengthen point of LVCE is its ability to enhance the less-visible area without amplifying the hidden noise, and distort the original tone of the input image. According to the noise-compressing criterion from objective and subject evaluation, the LVCE get the first rank. However, it has a problem concerning the foggy effect due to number of selection and the position for choosing the less-visible-area's layers in the SVD.

- Less-visible contrast enhancement based on human visual perception (LVCEHP): The advantage of the LVCEHP is it can enhance the less-visible areas while preserve the tone, texture, and the key-lighting of visible parts from the input image. The concept of the LVCEHP comes from the concept of human sensitivity which relates to the image contrast rather than absolute intensity values. An increase of pixel values with the same scaling function may not satisfy the human visual perception. By enhancing each pixel with the different non-linear scaling functions based on Just-Noticeable-Different (JND), the resulting image looks more natural and satisfies the human perception. According to the evaluation results, the LVCEHP always places in the first three-ranked of all criterion. However, the LVCEHP still suffers to preserve the intensity of the improved image A_{Imp}. The example of this limitation is shown in Fig. 4.8. The intensities of resulting image at the less-visible areas look darker when compared to the improved image A_{Imp}.

5.2 Contributions

The contribution of this research is to enhance the less-visible areas while preserve the tone, texture, and the key-lighting of visible parts from the input image. Therefore, compared with the existing methods in literature, one of the successful method is to enhance the less-visible

area based on human visual perception (LVCEHP). In this work, it has three contributions as follows. First, it proposes a new noise-reduction technique, which is the preprocessing of the proposed method. Second, we introduce a new adaptive non-scaling function based on the human visual perception. This function compromises a trade-off between tone preservation and detail preservation, and it is used in the contrast enhancement process.

Last, as a part of the proposed method, we propose a new pyramid-based blending technique for fusing two images.

5.3 Future Work

Despite the success of the LVCEHP framework which can enhance the less-visible areas while preserve the tone, texture, and the key-lighting of visible parts from the input image, there are rooms for further improvement.

- The LVCEHP algorithm has suffered to preserve the intensity of less-visible areas compare to the improved image A_{Imp}. To solve the problem, it is necessary to investigate the structure of conventional pyramid-based blending method for fusing two high hidden-noise-level images.

- In addition, we would like to apply our proposed method in other color models such as exact Hue, Saturation and Intensity (eHSI) color space to improve the detail and color information from the foggy image. Since, the foggy images always contain lot of gray color, applying the concept of adaptive non-scaling function based on the human visual perception in saturation channel may recover the detail and true color information. We will keep investigation this challenge problem in the future.

Appendices

Appendix A

Image comparison

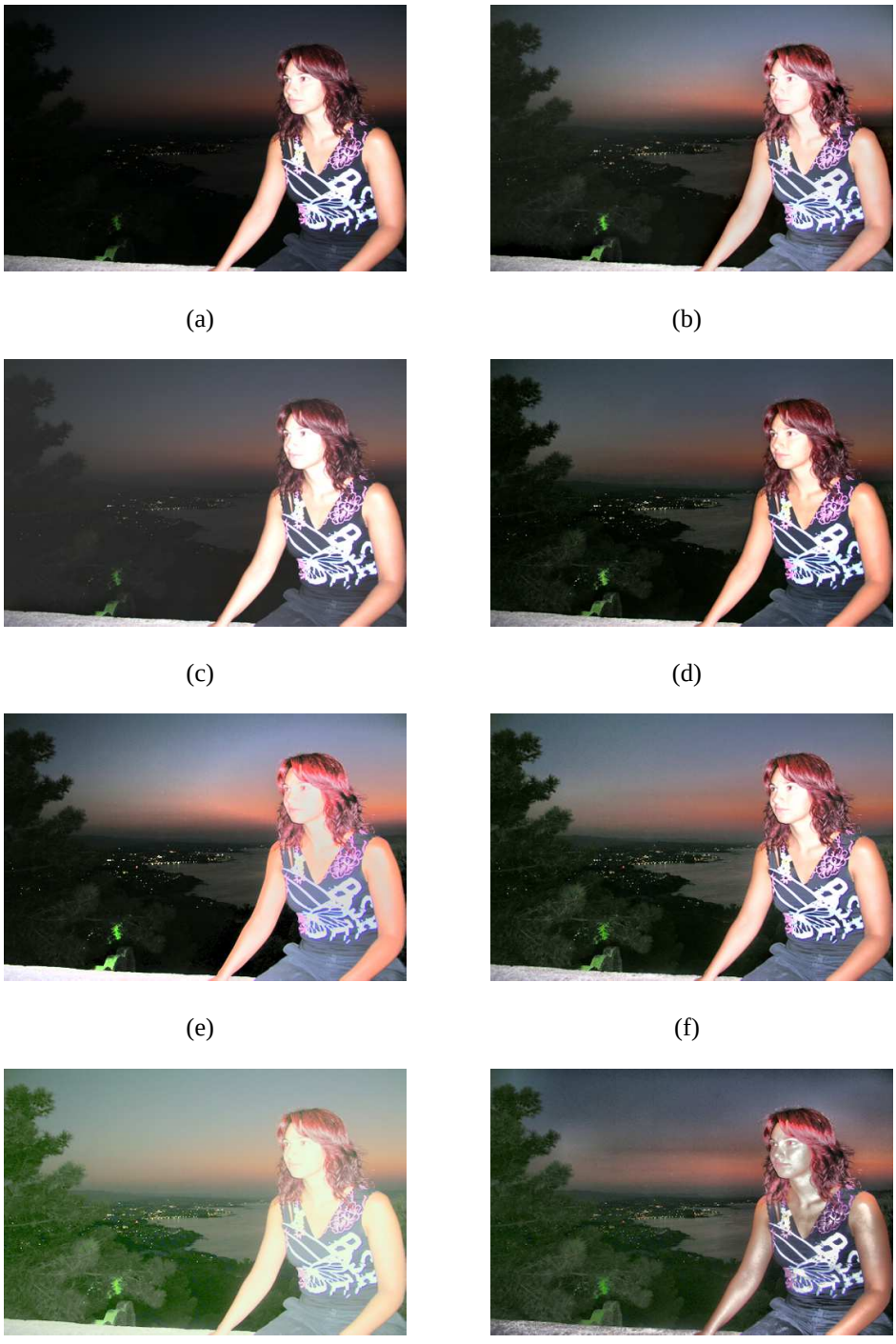

(a) (b) (c) (d) (e) (f) (g) (h)

Figure A.1: Image comparison with the existing method: (a) input image, (b) LVCEHP [25], (c) LVCE [22], (d) FCSM [1], (e) MSRCP [13], (f) MEF [11], (g) MSRCR [8], (h) CLAHE [3]

(a) (b) (c) (d) (e) (f) (g) (h)

Figure A.2: Image comparison with the existing method: (a) input image, (b) LVCEHP [25], (c) LVCE [22], (d) FCSM [1], (e) MSRCP [13], (f) MEF [11], (g) MSRCR [8], (h) CLAHE [3]

(a) (b)

(c) (d)

(e) (f)

(g) (h)

Figure A.3: Image comparison with the existing method: (a) input image, (b) LVCEHP [25], (c) LVCE [22], (d) FCSM [1], (e) MSRCP [13], (f) MEF [11], (g) MSRCR [8], (h) CLAHE [3]

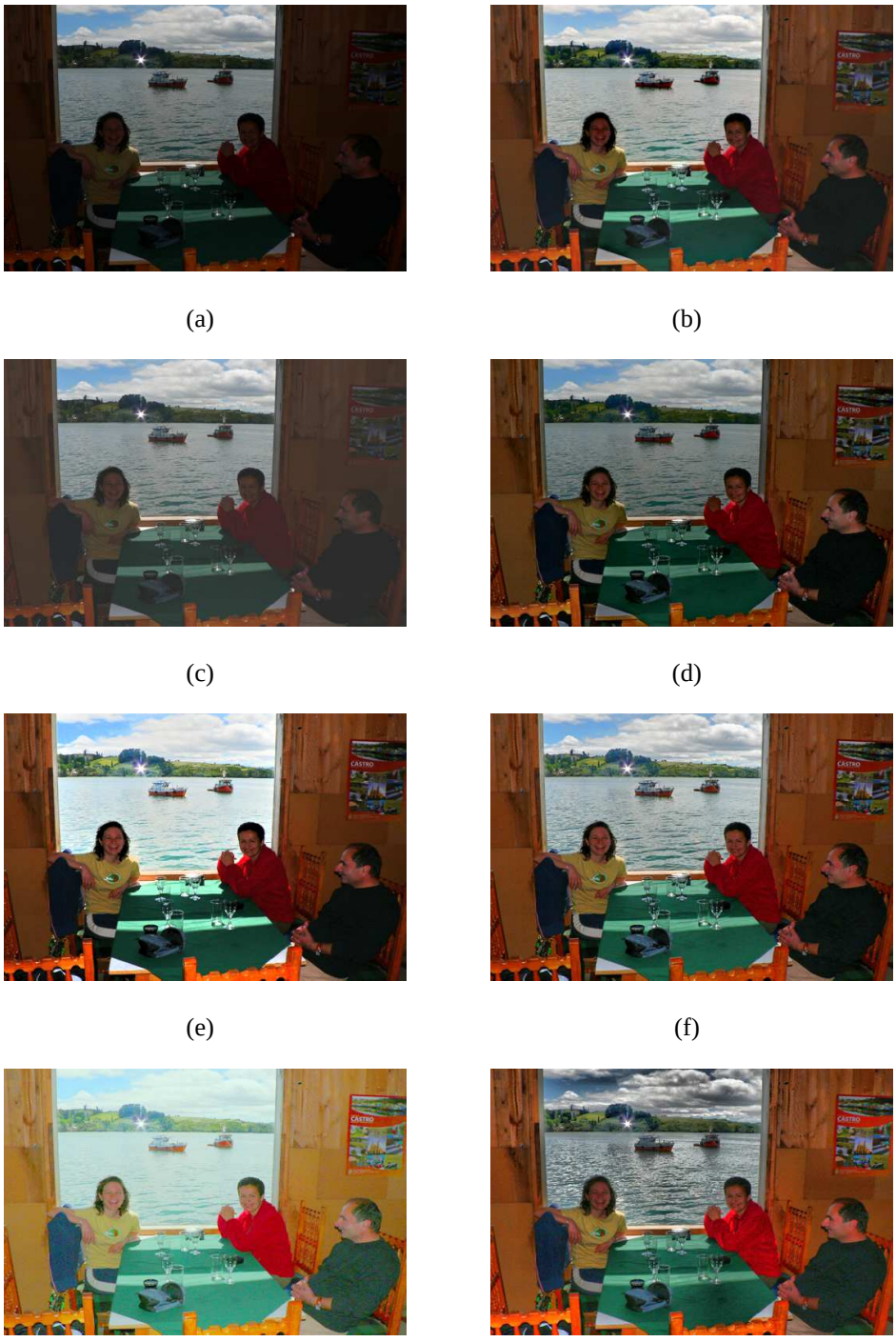

(a) (b)

(c) (d)

(e) (f)

(g) (h)

Figure A.4: Image comparison with the existing method: (a) input image, (b) LVCEHP [25], (c) LVCE [22], (d) FCSM [1], (e) MSRCP [13], (f) MEF [11], (g) MSRCR [8], (h) CLAHE [3]

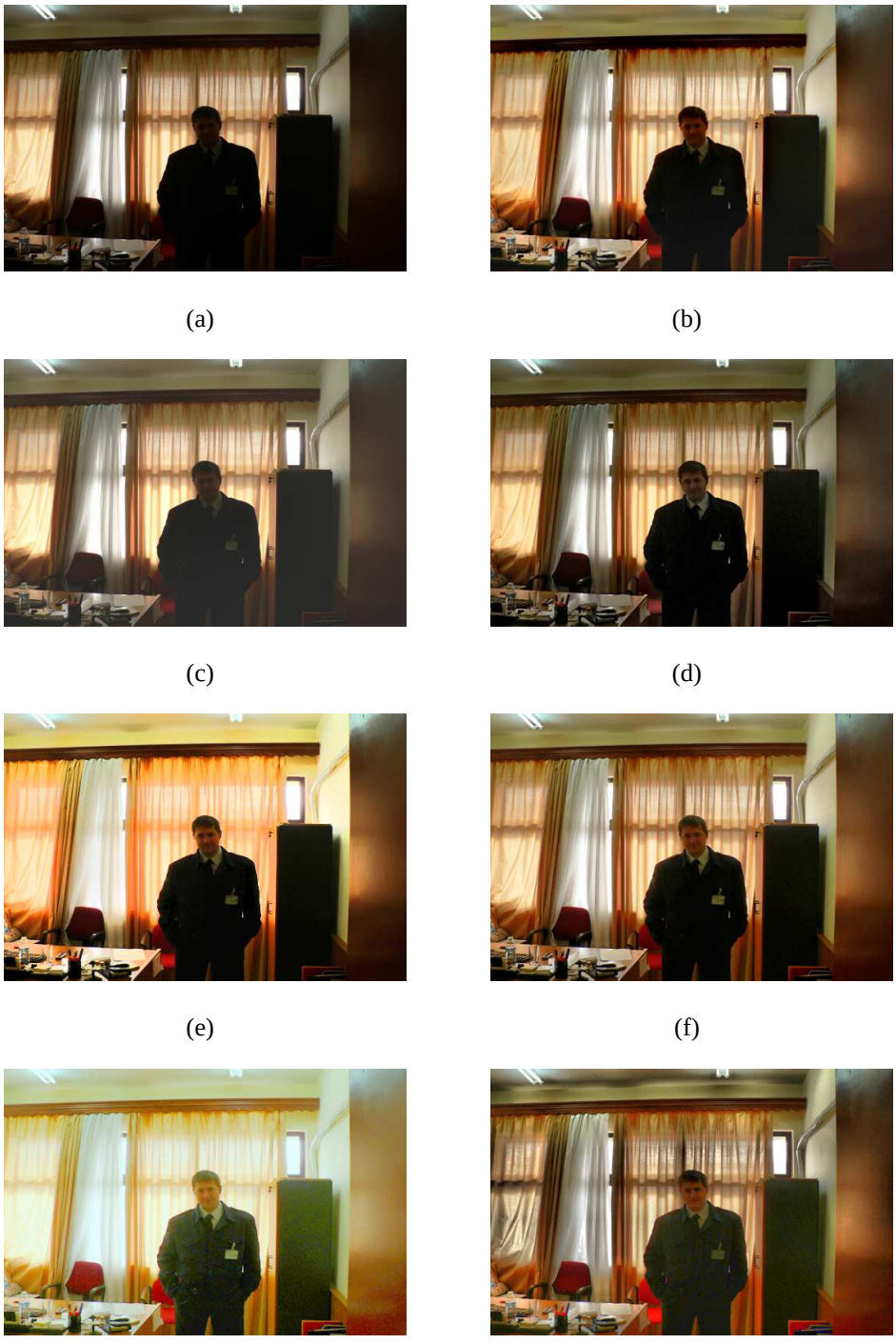

(a) (b) (c) (d) (e) (f) (g) (h)

Figure A.5: Image comparison with the existing method: (a) input image, (b) LVCEHP [25], (c) LVCE [22], (d) FCSM [1], (e) MSRCP [13], (f) MEF [11], (g) MSRCR [8], (h) CLAHE [3]

(a) (b) (c) (d) (e) (f) (g) (h)

Figure A.6: Image comparison with the existing method: (a) input image, (b) LVCEHP [25], (c) LVCE [22], (d) FCSM [1], (e) MSRCP [13], (f) MEF [11], (g) MSRCR [8], (h) CLAHE [3]

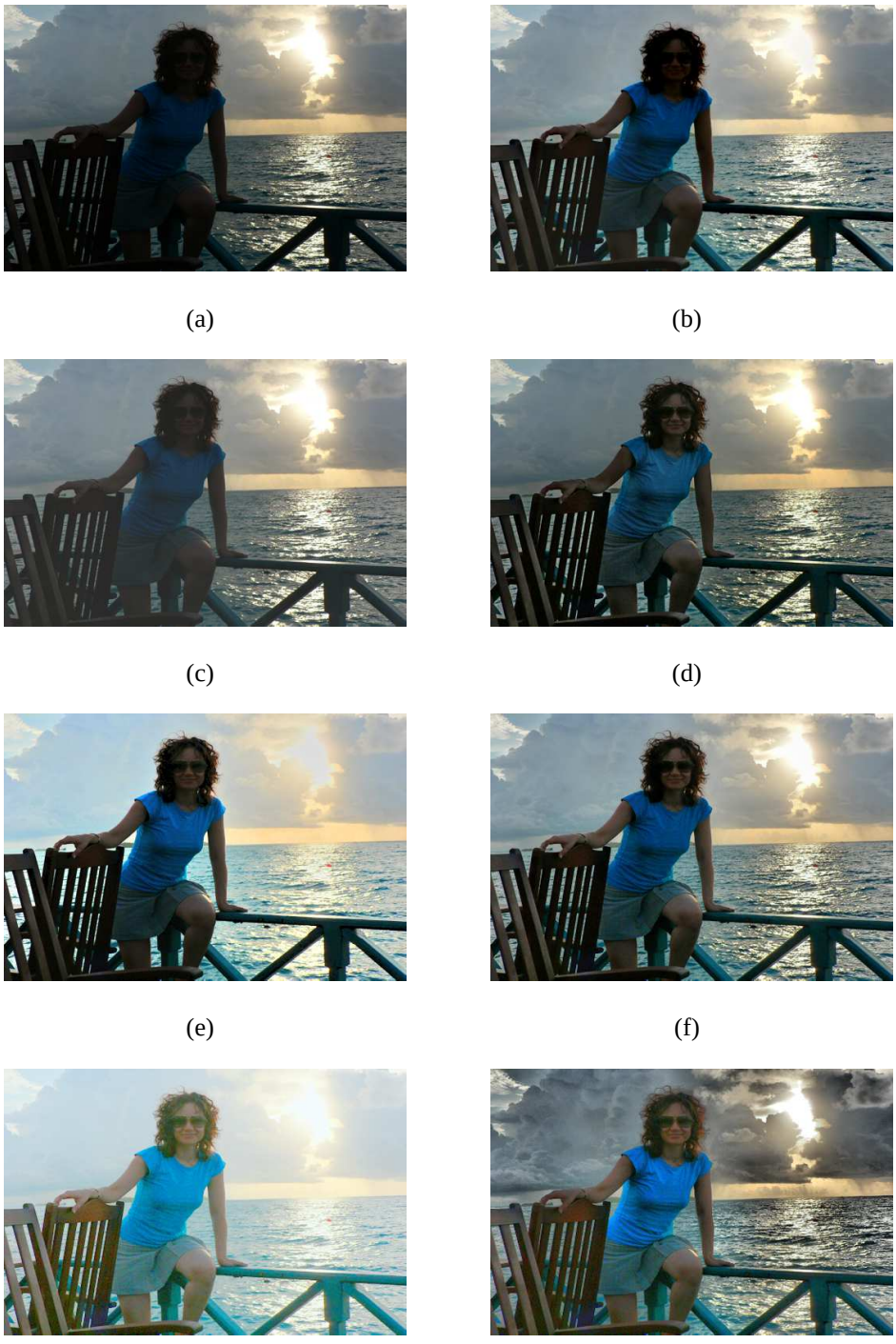

(a) (b) (c) (d) (e) (f) (g) (h)

Figure A.7: Image comparison with the existing method: (a) input image, (b) LVCEHP [25], (c) LVCE [22], (d) FCSM [1], (e) MSRCP [13], (f) MEF [11], (g) MSRCR [8], (h) CLAHE [3]

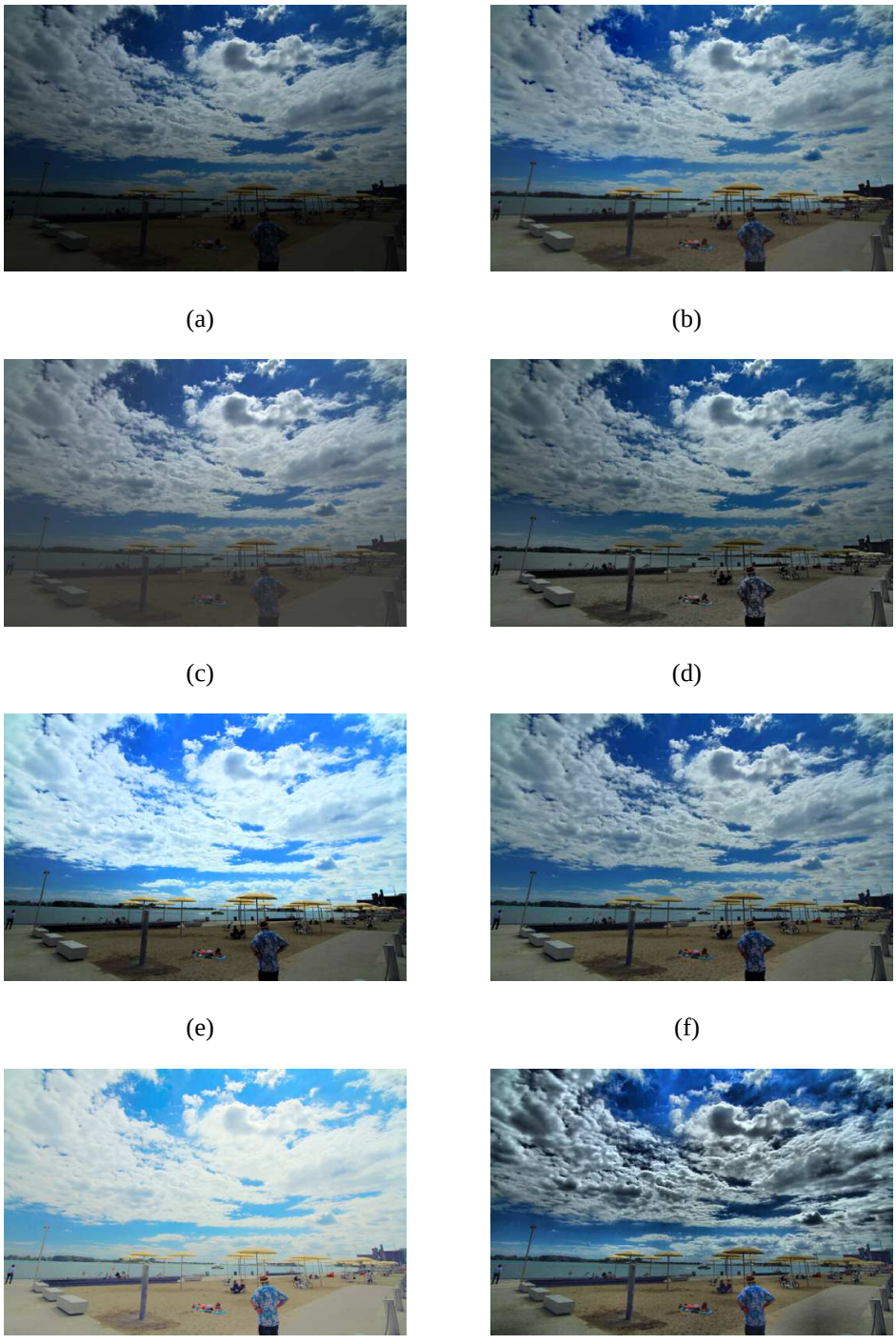

(a) (b) (c) (d) (e) (f) (g) (h)

Figure A.8: Image comparison with the existing method: (a) input image, (b) LVCEHP [25], (c) LVCE [22], (d) FCSM [1], (e) MSRCP [13], (f) MEF [11], (g) MSRCR [8], (h) CLAHE [3]

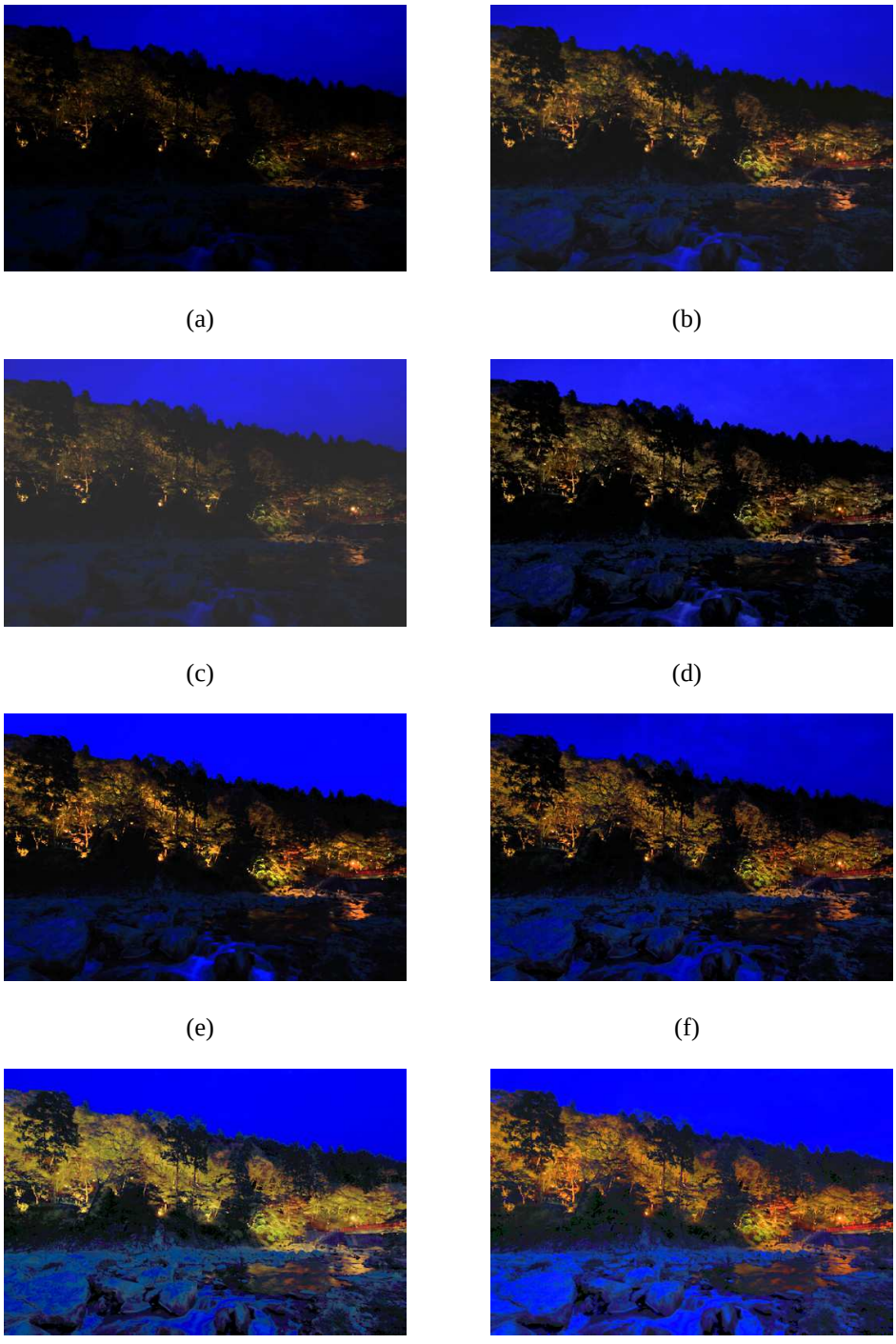

(a) (b) (c) (d) (e) (f) (g) (h)

Figure A.9: Image comparison with the existing method: (a) input image, (b) LVCEHP [25], (c) LVCE [22], (d) FCSM [1], (e) MSRCP [13], (f) MEF [11], (g) MSRCR [8], (h) CLAHE [3]

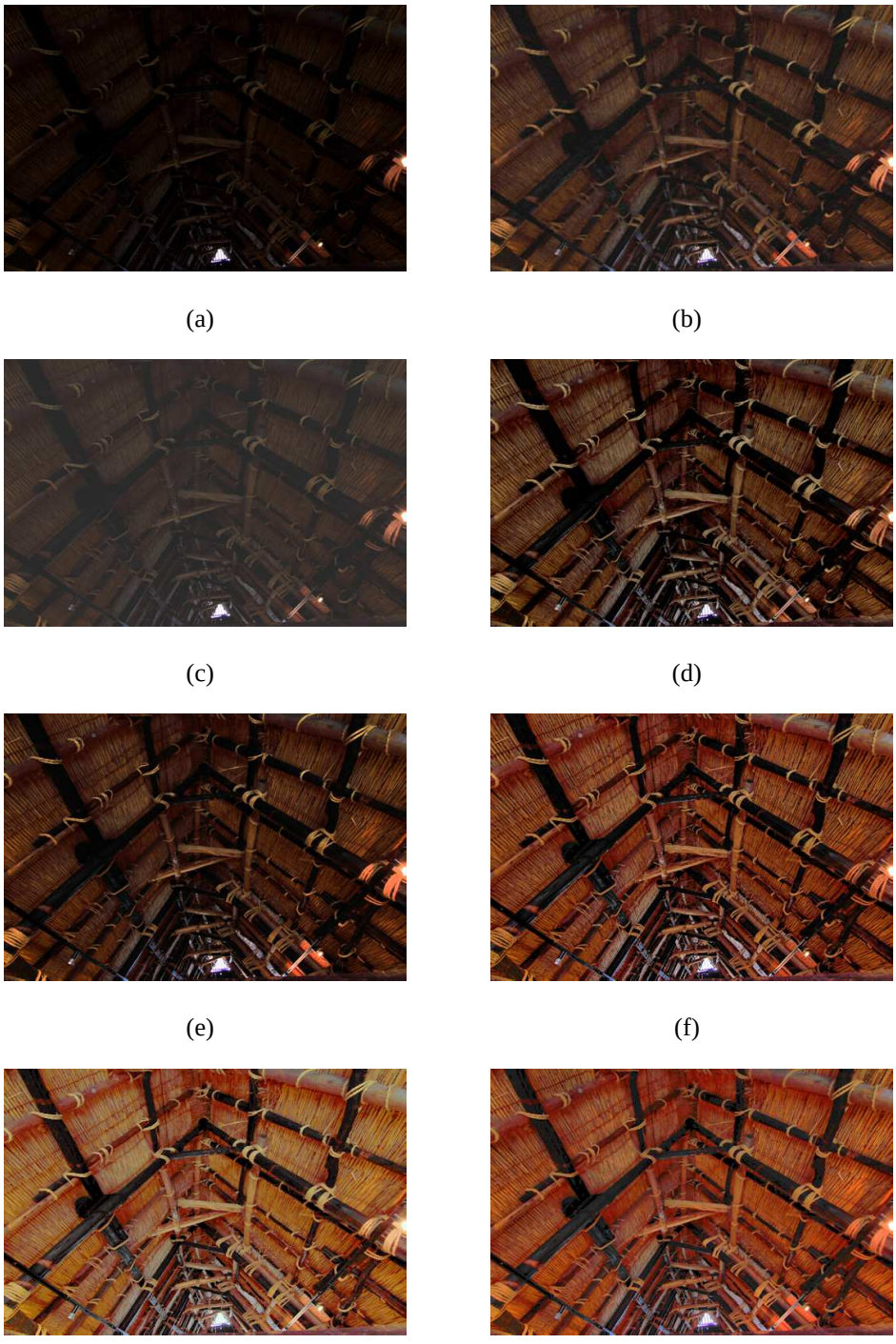

(a) (b)

(c) (d)

(e) (f)

(g) (h)

Figure A.10: Image comparison with the existing method: (a) input image, (b) LVCEHP [25], (c) LVCE [22], (d) FCSM [1], (e) MSRCP [13], (f) MEF [11], (g) MSRCR [8], (h) CLAHE [3]

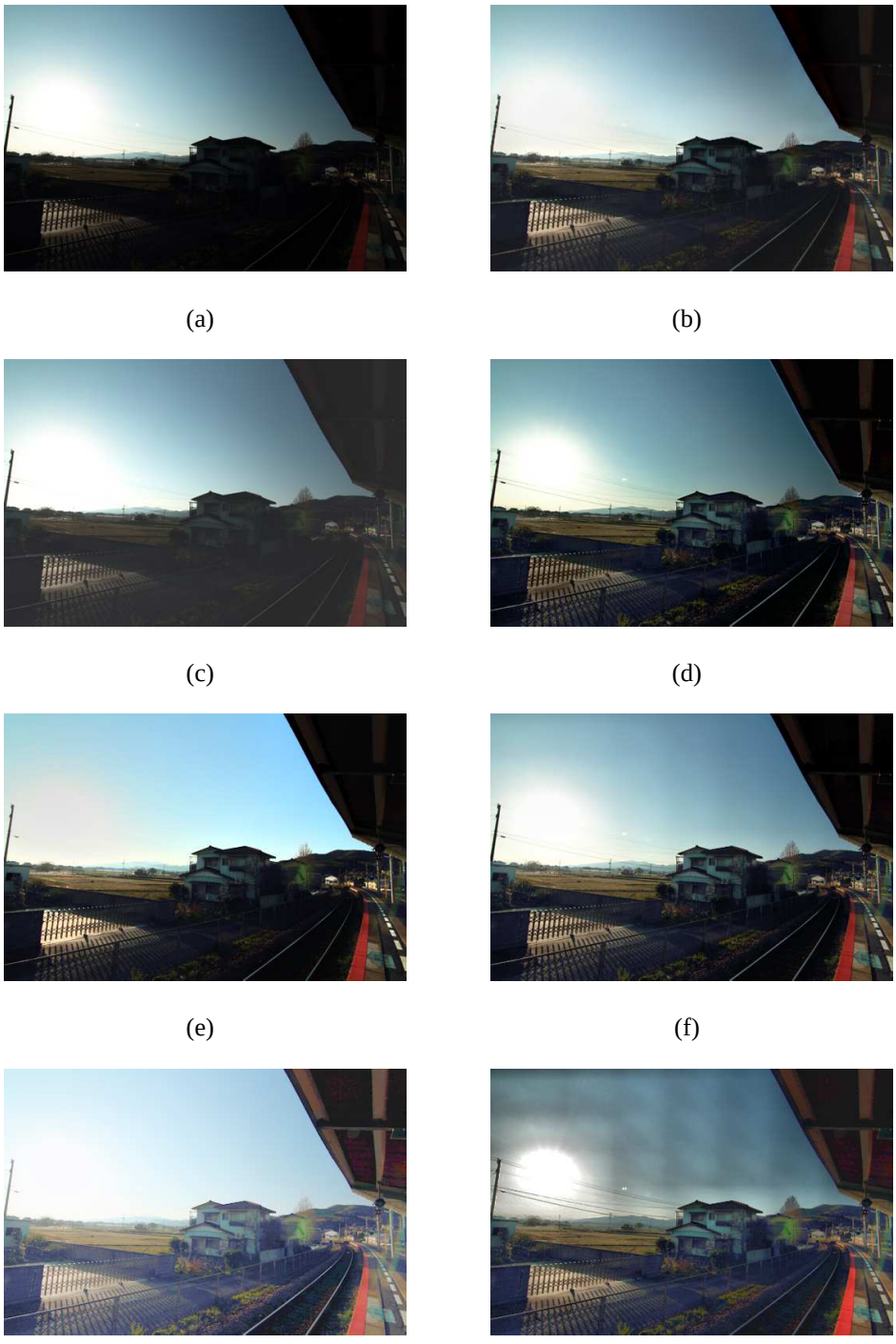

(a) (b) (c) (d) (e) (f) (g) (h)

Figure A.11: Image comparison with the existing method: (a) input image, (b) LVCEHP [25], (c) LVCE [22], (d) FCSM [1], (e) MSRCP [13], (f) MEF [11], (g) MSRCR [8], (h) CLAHE [3]

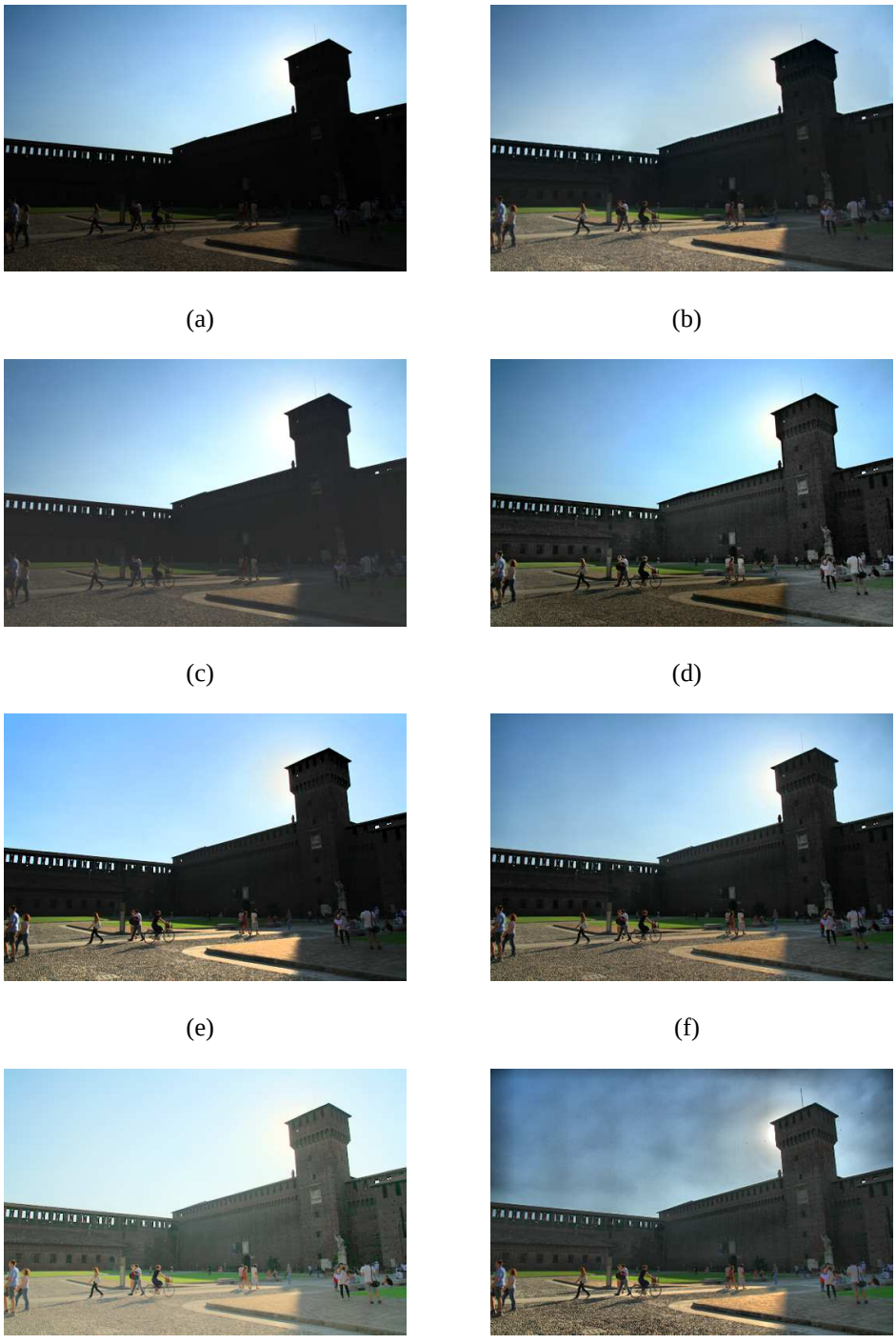

(a) (b) (c) (d) (e) (f) (g) (h)

Figure A.12: Image comparison with the existing method: (a) input image, (b) LVCEHP [25], (c) LVCE [22], (d) FCSM [1], (e) MSRCP [13], (f) MEF [11], (g) MSRCR [8], (h) CLAHE [3]

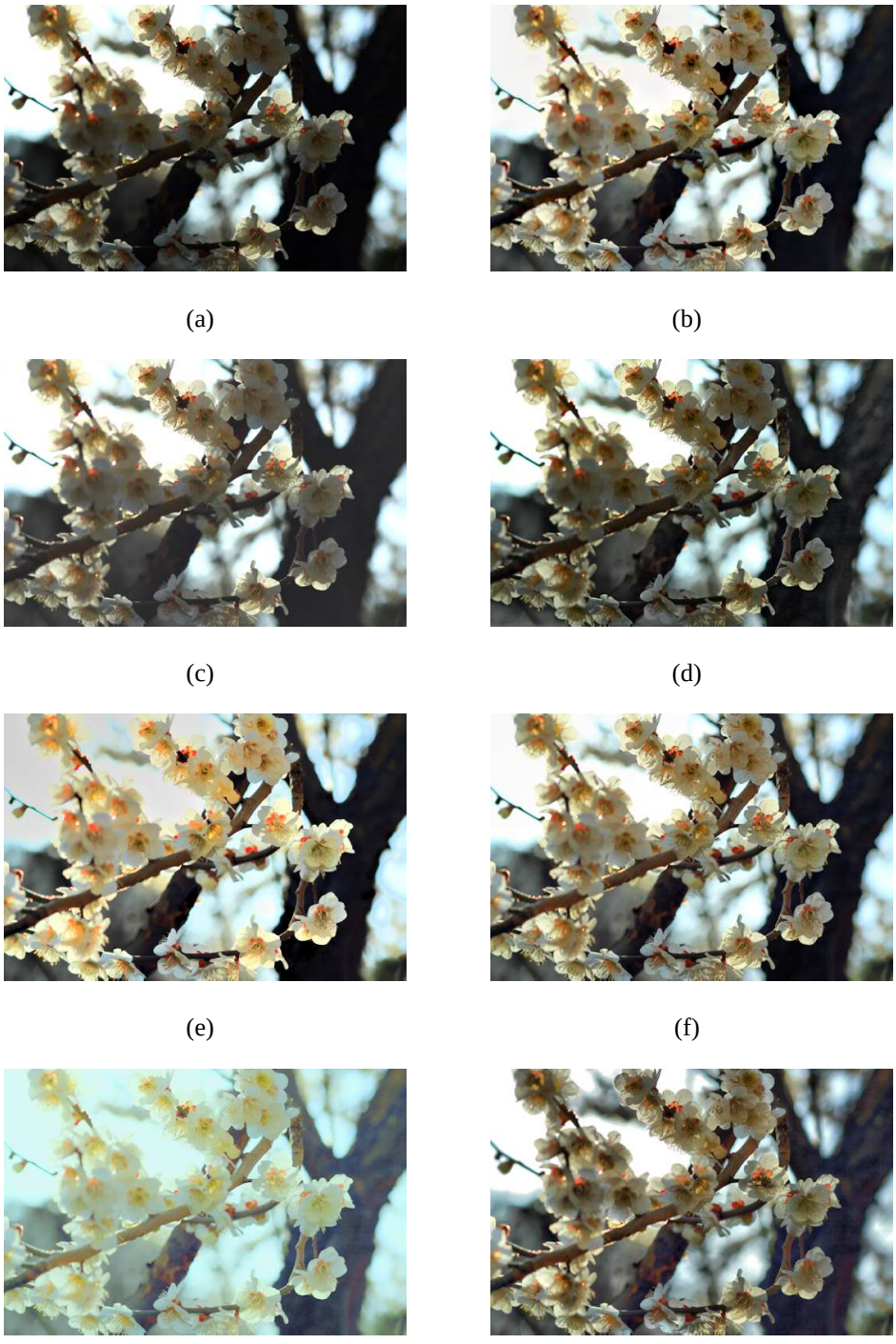

(a) (b) (c) (d) (e) (f) (g) (h)

Figure A.13: Image comparison with the existing method: (a) input image, (b) LVCEHP [25], (c) LVCE [22], (d) FCSM [1], (e) MSRCP [13], (f) MEF [11], (g) MSRCR [8], (h) CLAHE [3]

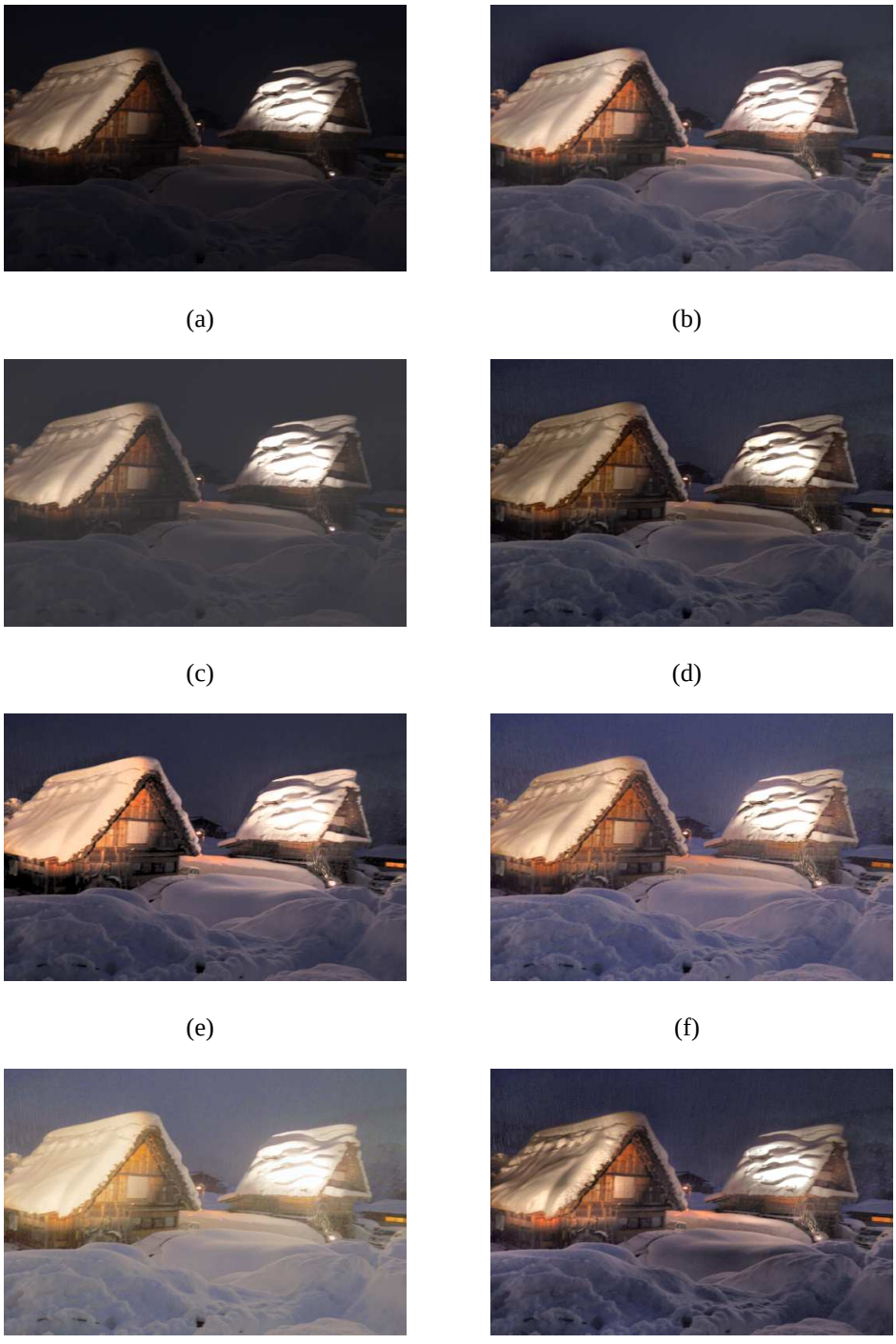

(a) (b) (c) (d) (e) (f) (g) (h)

Figure A.14: Image comparison with the existing method: (a) input image, (b) LVCEHP [25], (c) LVCE [22], (d) FCSM [1], (e) MSRCP [13], (f) MEF [11], (g) MSRCR [8], (h) CLAHE [3]

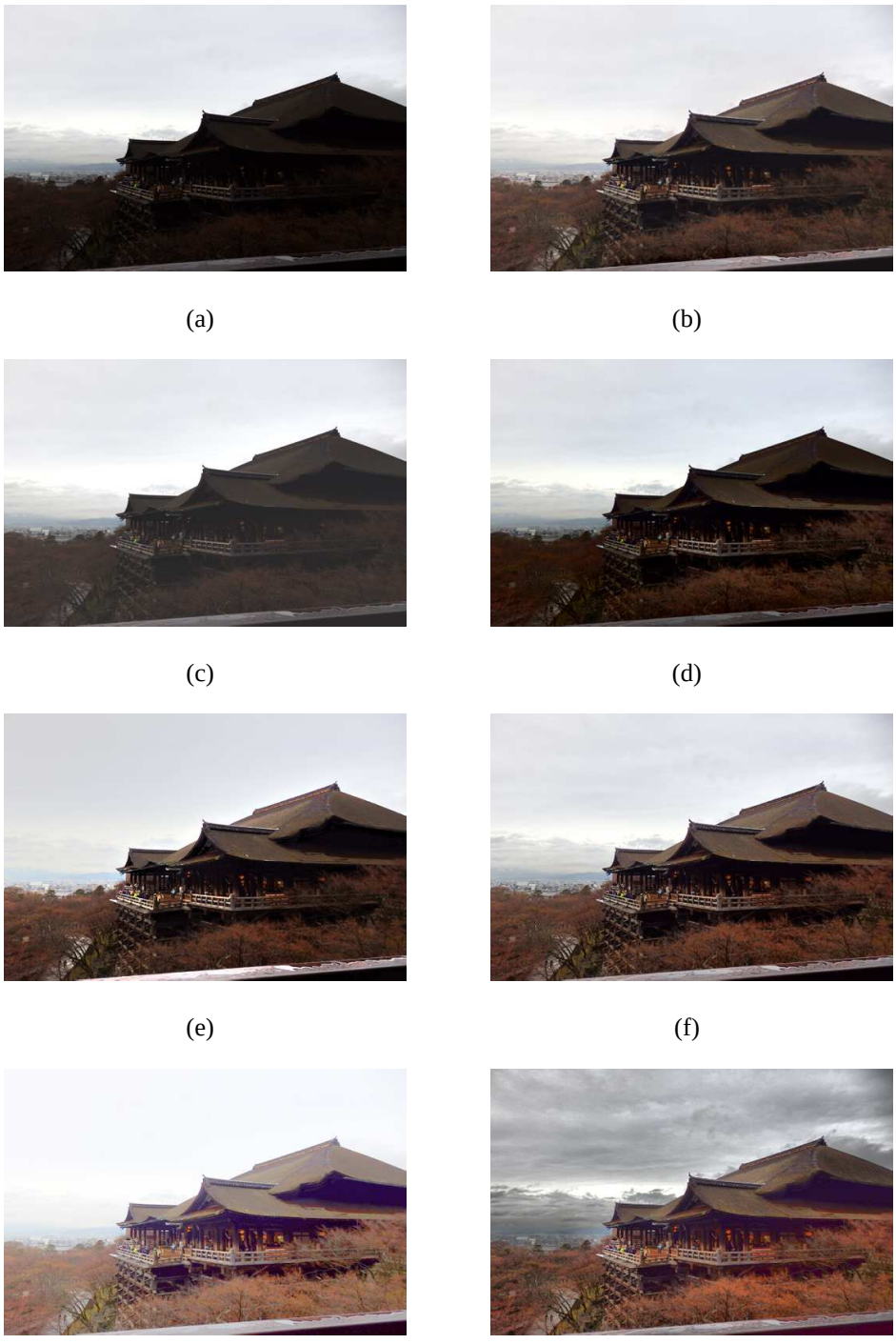

(a) (b) (c) (d) (e) (f) (g) (h)

Figure A.15: Image comparison with the existing method: (a) input image, (b) LVCEHP [25], (c) LVCE [22], (d) FCSM [1], (e) MSRCP [13], (f) MEF [11], (g) MSRCR [8], (h) CLAHE [3]

(a) (b) (c) (d) (e) (f) (g) (h)

Figure A.16: Image comparison with the existing method: (a) input image, (b) LVCEHP [25], (c) LVCE [22], (d) FCSM [1], (e) MSRCP [13], (f) MEF [11], (g) MSRCR [8], (h) CLAHE [3]

(a) (b) (c) (d) (e) (f) (g) (h)

Figure A.17: Image comparison with the existing method: (a) input image, (b) LVCEHP [25], (c) LVCE [22], (d) FCSM [1], (e) MSRCP [13], (f) MEF [11], (g) MSRCR [8], (h) CLAHE [3]

(a) (b) (c) (d) (e) (f) (g) (h)

Figure A.18: Image comparison with the existing method: (a) input image, (b) LVCEHP [25], (c) LVCE [22], (d) FCSM [1], (e) MSRCP [13], (f) MEF [11], (g) MSRCR [8], (h) CLAHE [3]

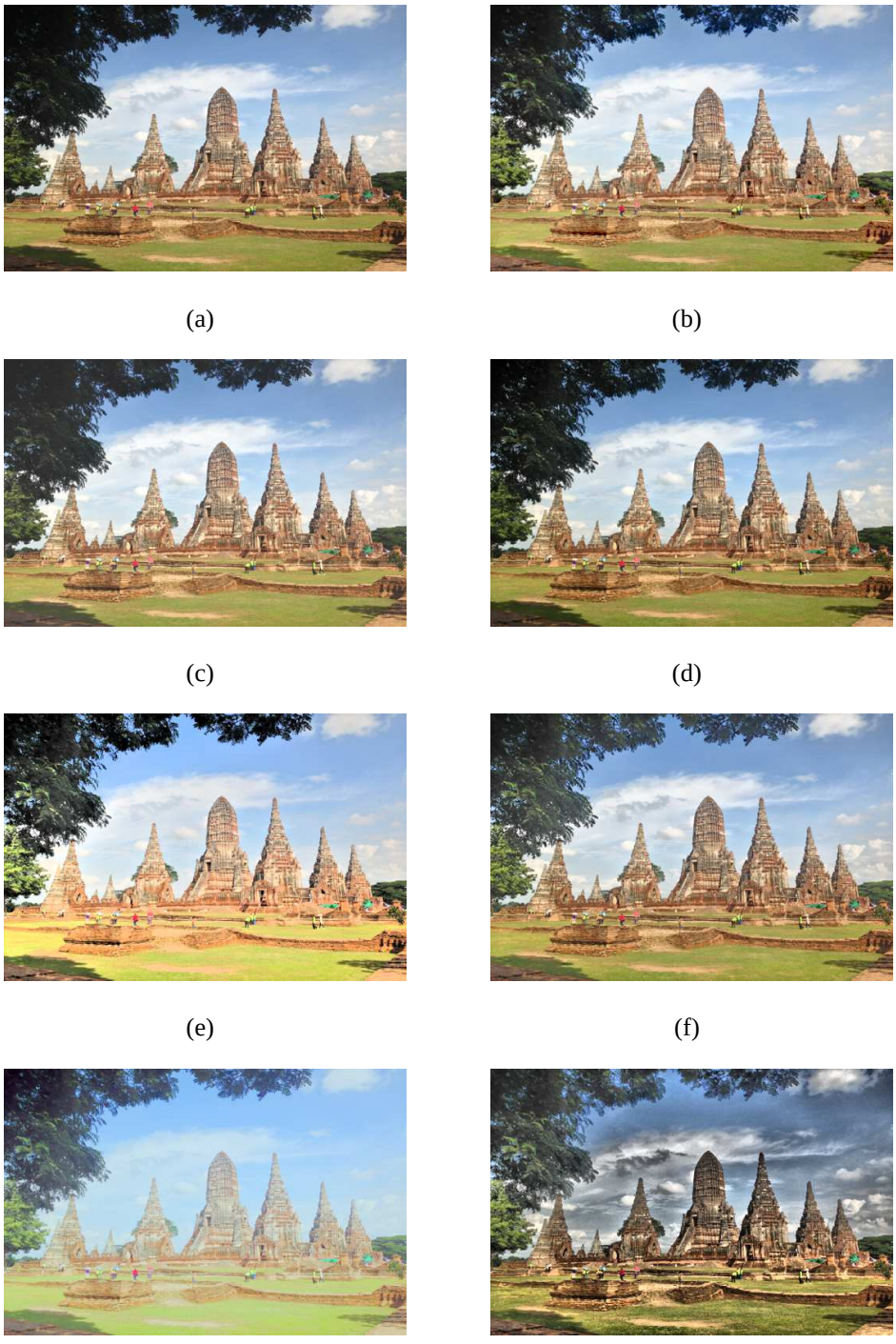

(a) (b) (c) (d) (e) (f) (g) (h)

Figure A.19: Image comparison with the existing method: (a) input image, (b) LVCEHP [25], (c) LVCE [22], (d) FCSM [1], (e) MSRCP [13], (f) MEF [11], (g) MSRCR [8], (h) CLAHE [3]

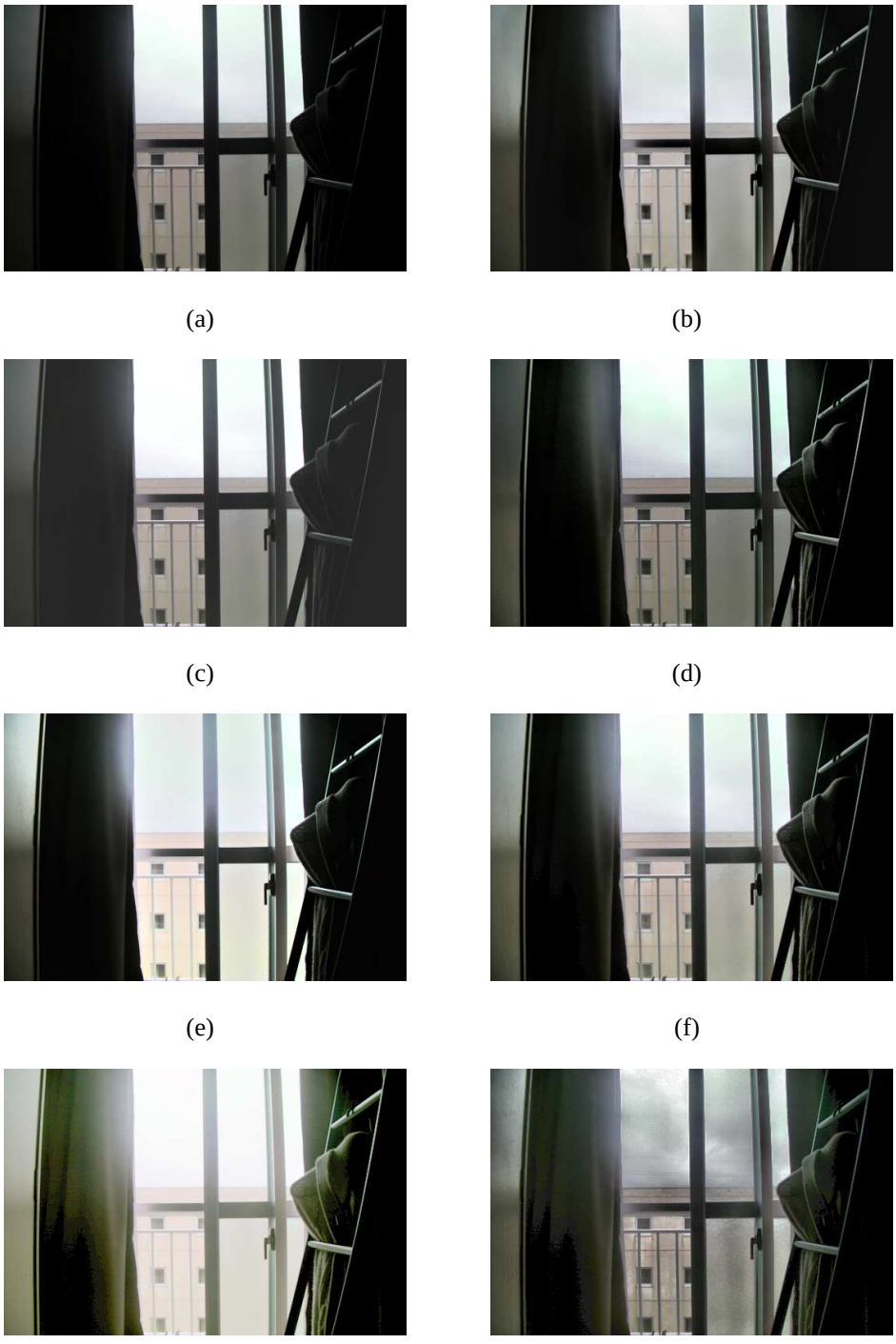

(a) (b)

(c) (d)

(e) (f)

(g) (h)

Figure A.20: Image comparison with the existing method: (a) input image, (b) LVCEHP [25], (c) LVCE [22], (d) FCSM [1], (e) MSRCP [13], (f) MEF [11], (g) MSRCR [8], (h) CLAHE [3]

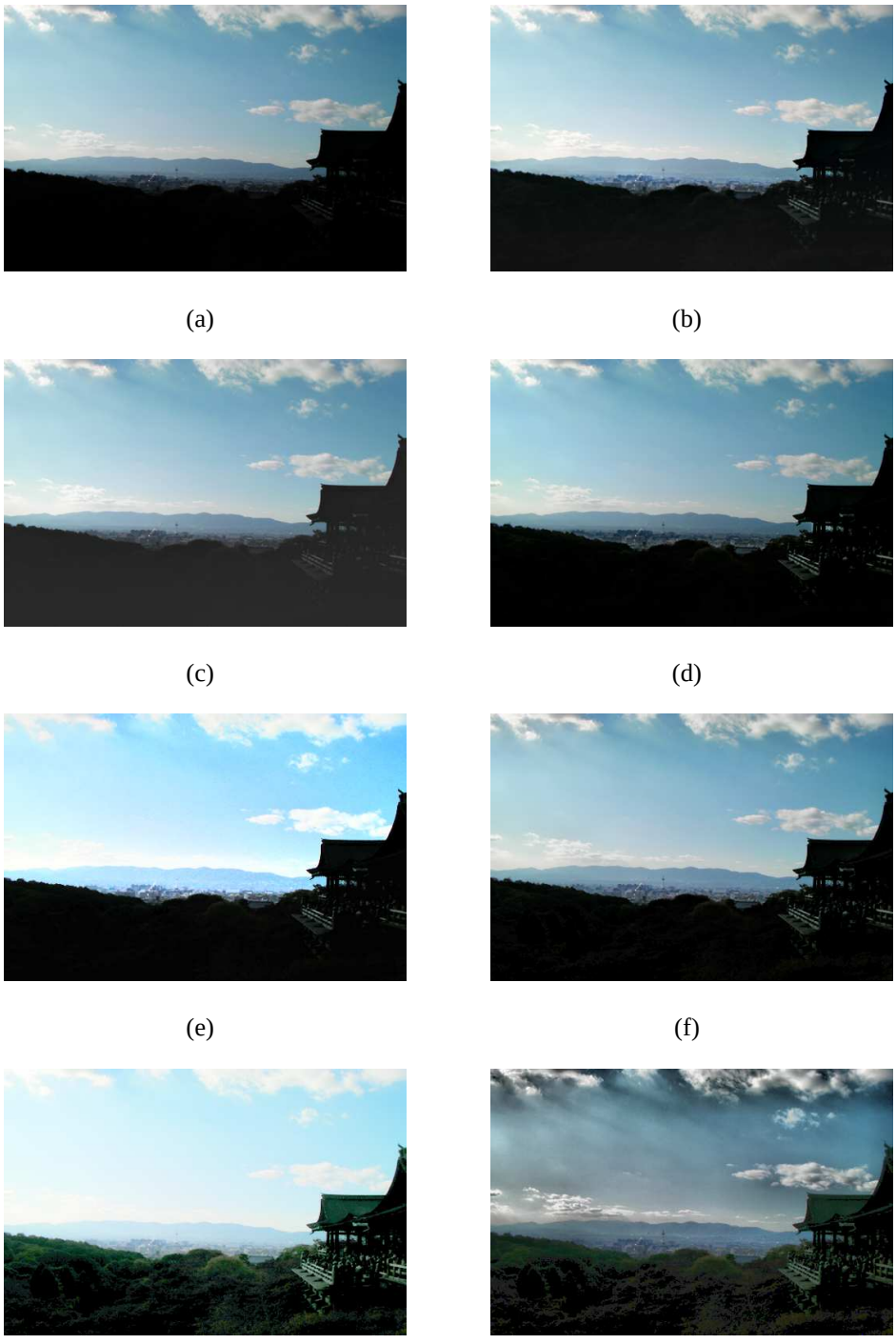

(a) (b) (c) (d) (e) (f) (g) (h)

Figure A.21: Image comparison with the existing method: (a) input image, (b) LVCEHP [25], (c) LVCE [22], (d) FCSM [1], (e) MSRCP [13], (f) MEF [11], (g) MSRCR [8], (h) CLAHE [3]

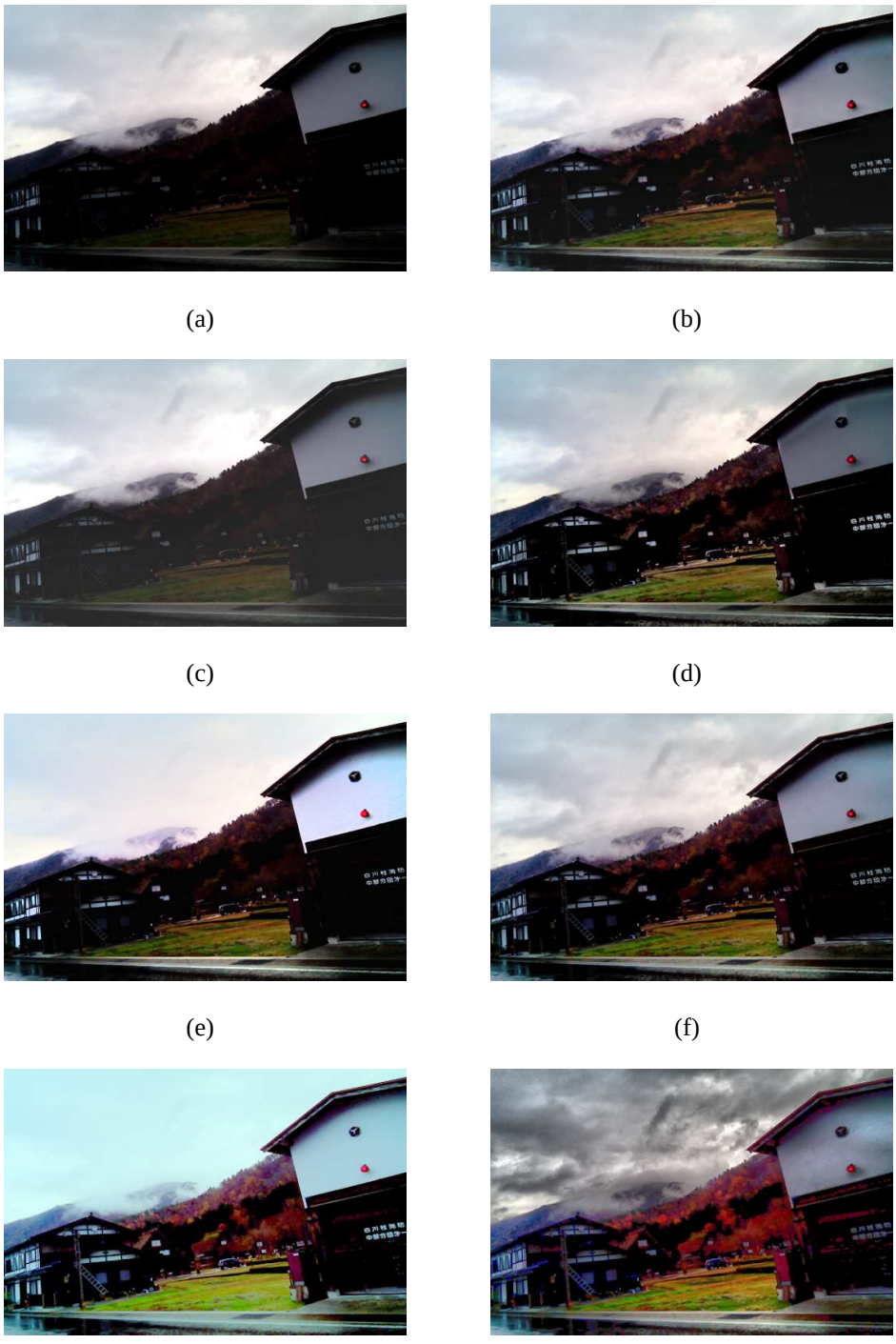

(a) (b)

(c) (d)

(e) (f)

(g) (h)

Figure A.22: Image comparison with the existing method: (a) input image, (b) LVCEHP [25], (c) LVCE [22], (d) FCSM [1], (e) MSRCP [13], (f) MEF [11], (g) MSRCR [8], (h) CLAHE [3]

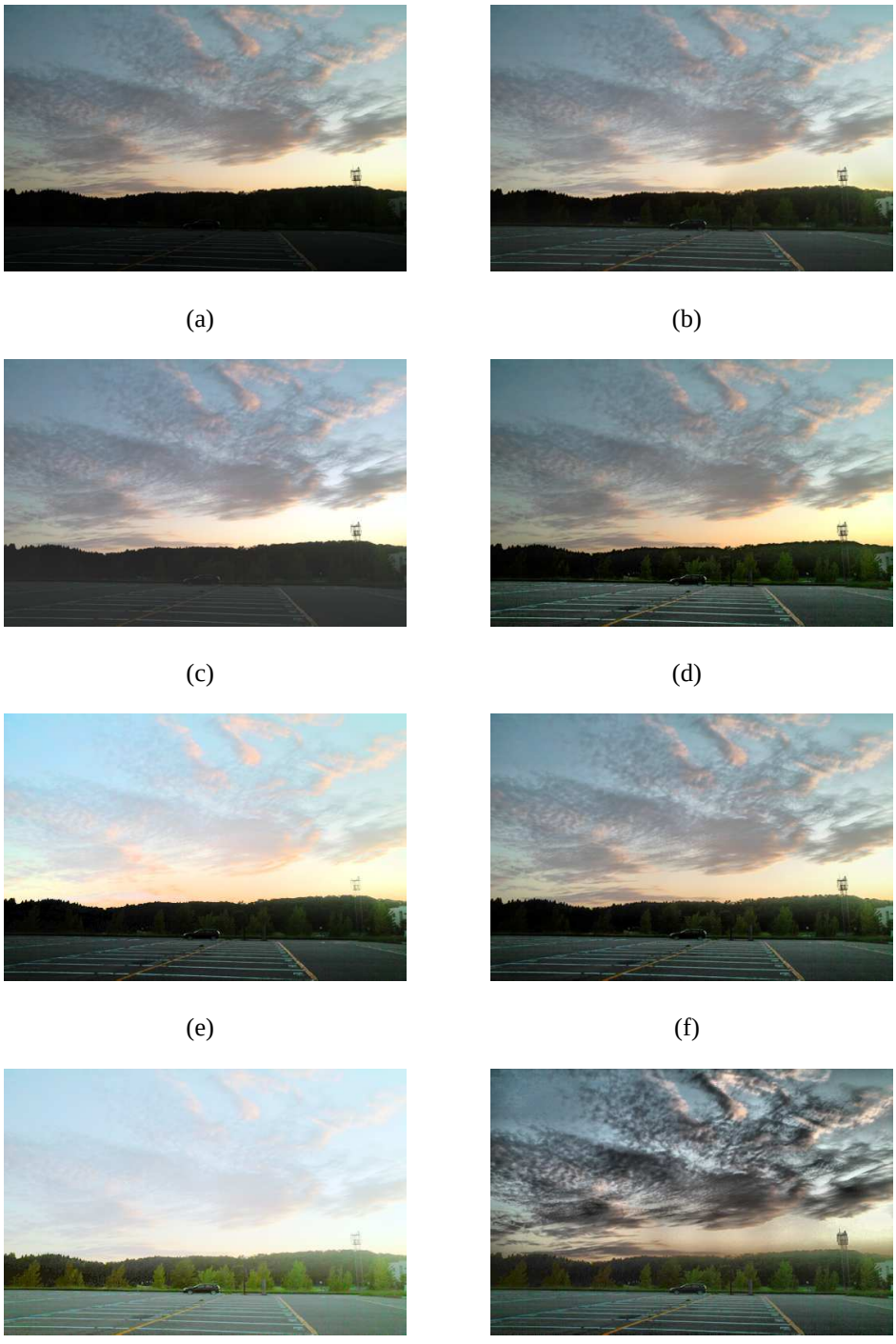

(a) (b) (c) (d) (e) (f) (g) (h)

Figure A.23: Image comparison with the existing method: (a) input image, (b) LVCEHP [25], (c) LVCE [22], (d) FCSM [1], (e) MSRCP [13], (f) MEF [11], (g) MSRCR [8], (h) CLAHE [3]

(a) (b)

(c) (d)

(e) (f)

(g) (h)

Figure A.24: Image comparison with the existing method: (a) input image, (b) LVCEHP [25], (c) LVCE [22], (d) FCSM [1], (e) MSRCP [13], (f) MEF [11], (g) MSRCR [8], (h) CLAHE [3]

(a) (b)

(c) (d)

(e) (f)

(g) (h)

Figure A.25: Image comparison with the existing method: (a) input image, (b) LVCEHP [25], (c) LVCE [22], (d) FCSM [1], (e) MSRCP [13], (f) MEF [11], (g) MSRCR [8], (h) CLAHE [3]

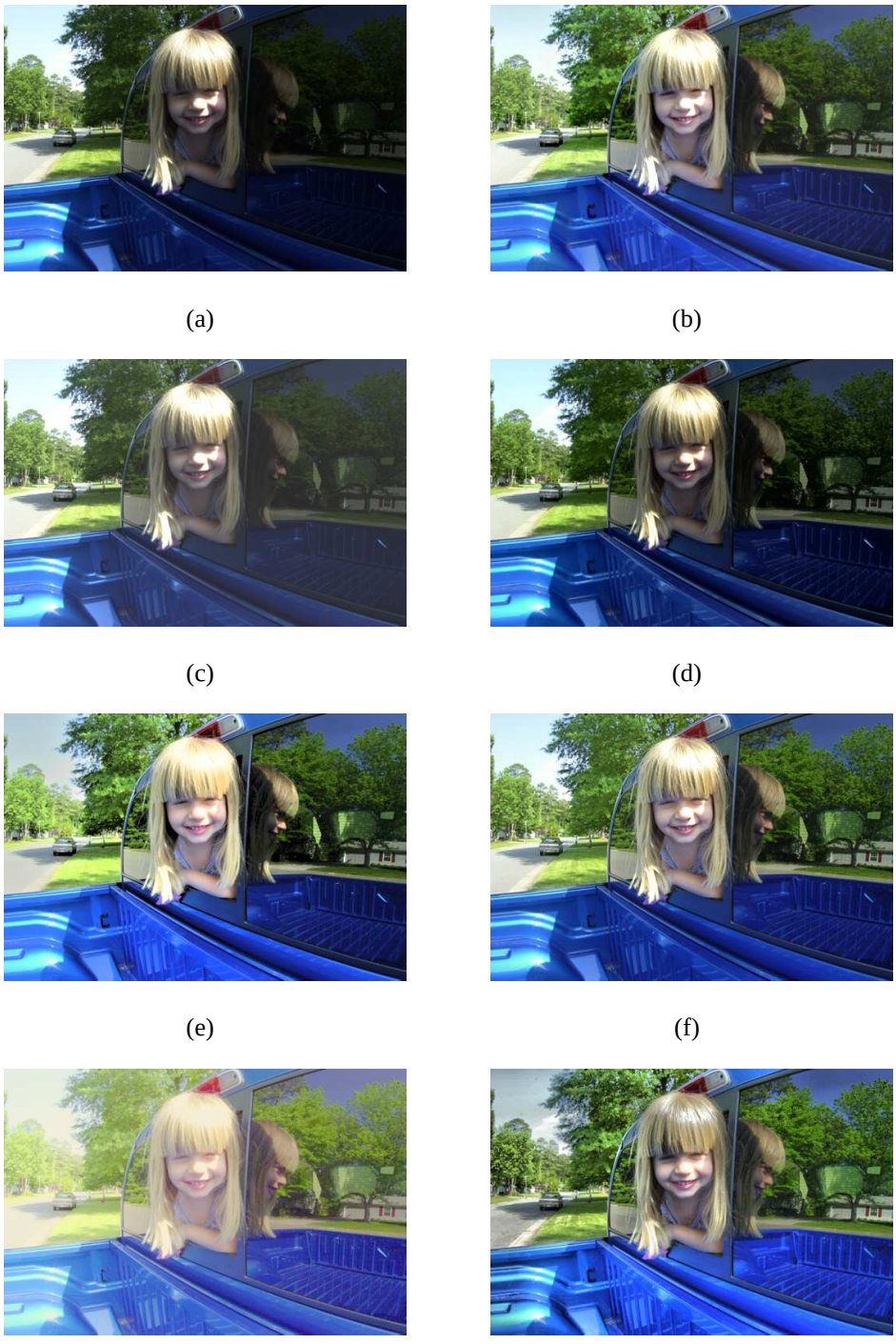

(a) (b) (c) (d) (e) (f) (g) (h)

Figure A.26: Image comparison with the existing method: (a) input image, (b) LVCEHP [25], (c) LVCE [22], (d) FCSM [1], (e) MSRCP [13], (f) MEF [11], (g) MSRCR [8], (h) CLAHE [3]

(a) (b)

(c) (d)

(e) (f)

(g) (h)

Figure A.27: Image comparison with the existing method: (a) input image, (b) LVCEHP [25], (c) LVCE [22], (d) FCSM [1], (e) MSRCP [13], (f) MEF [11], (g) MSRCR [8], (h) CLAHE [3]

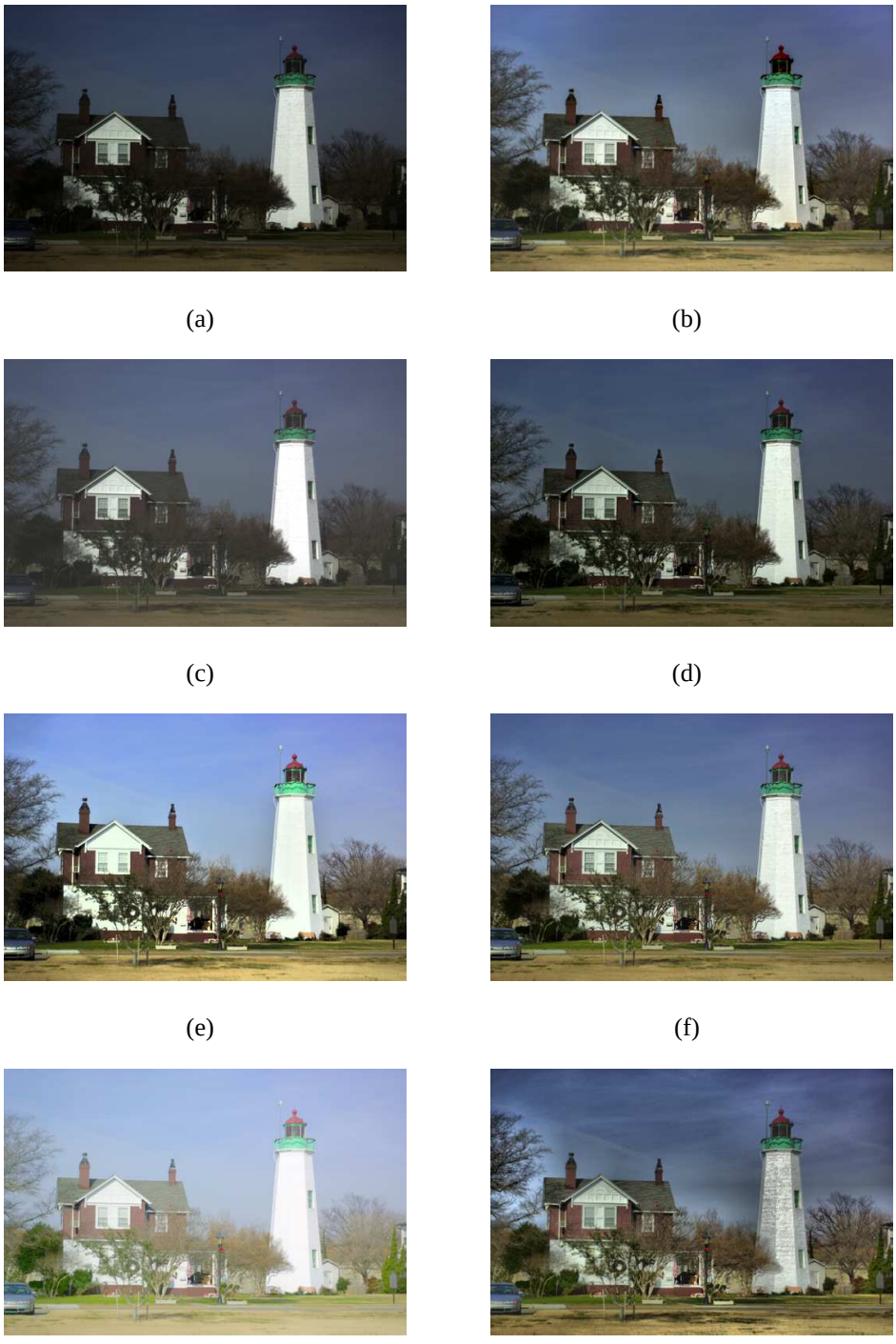

(a) (b) (c) (d) (e) (f) (g) (h)

Figure A.28: Image comparison with the existing method: (a) input image, (b) LVCEHP [25], (c) LVCE [22], (d) FCSM [1], (e) MSRCP [13], (f) MEF [11], (g) MSRCR [8], (h) CLAHE [3]

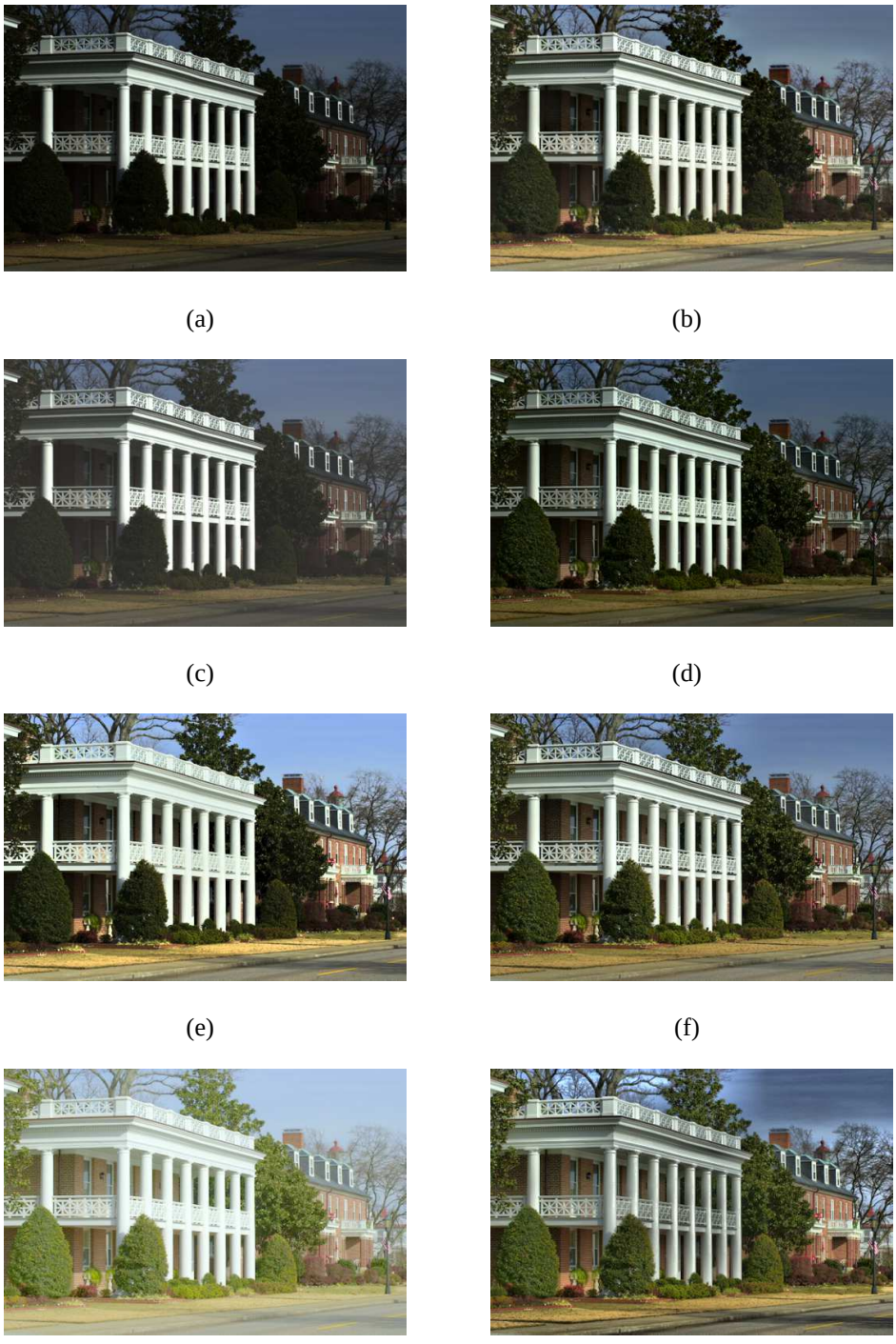

(a) (b) (c) (d) (e) (f) (g) (h)

Figure A.29: Image comparison with the existing method: (a) input image, (b) LVCEHP [25], (c) LVCE [22], (d) FCSM [1], (e) MSRCP [13], (f) MEF [11], (g) MSRCR [8], (h) CLAHE [3]

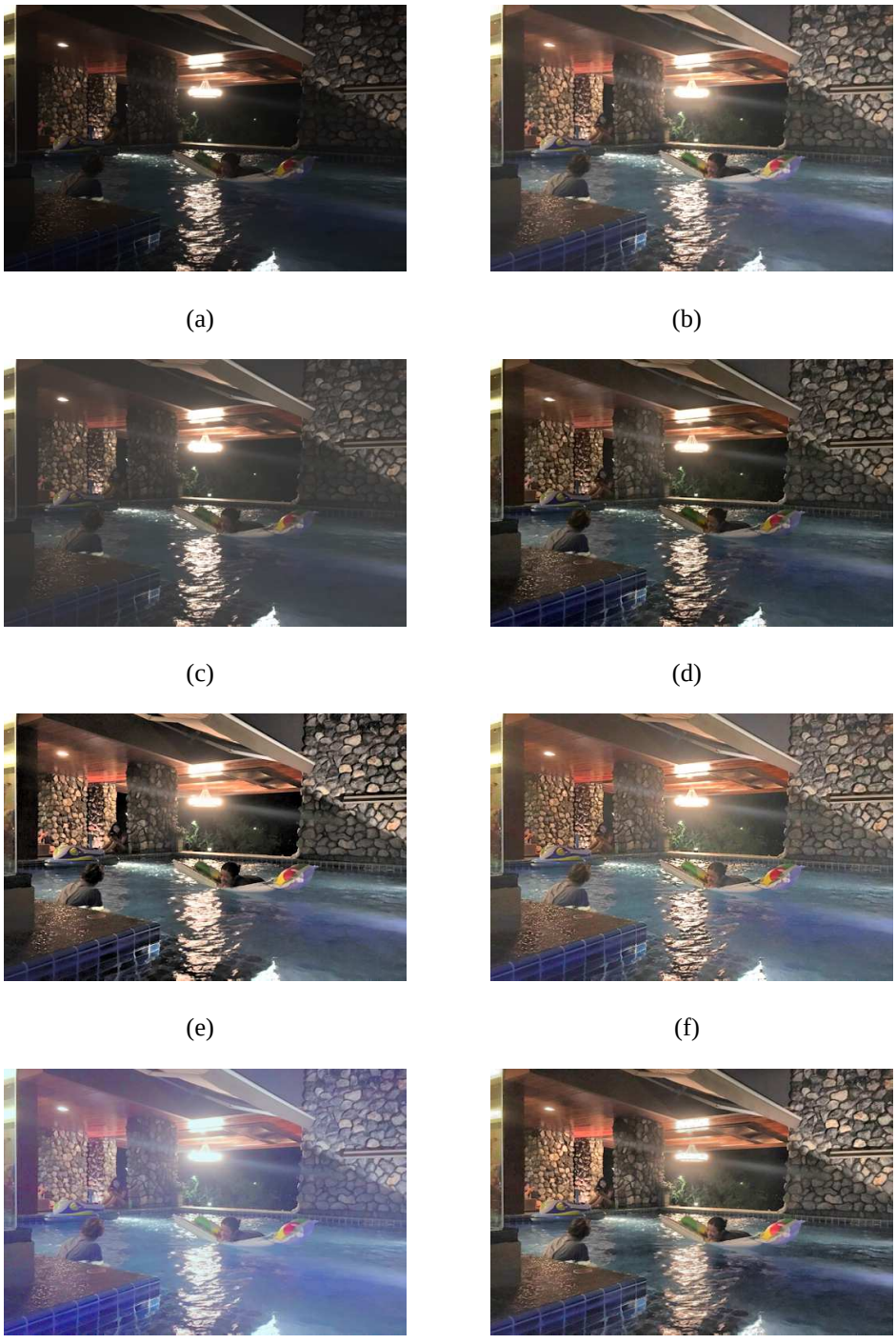

(a) (b) (c) (d) (e) (f) (g) (h)

Figure A.30: Image comparison with the existing method: (a) input image, (b) LVCEHP [25], (c) LVCE [22], (d) FCSM [1], (e) MSRCP [13], (f) MEF [11], (g) MSRCR [8], (h) CLAHE [3]

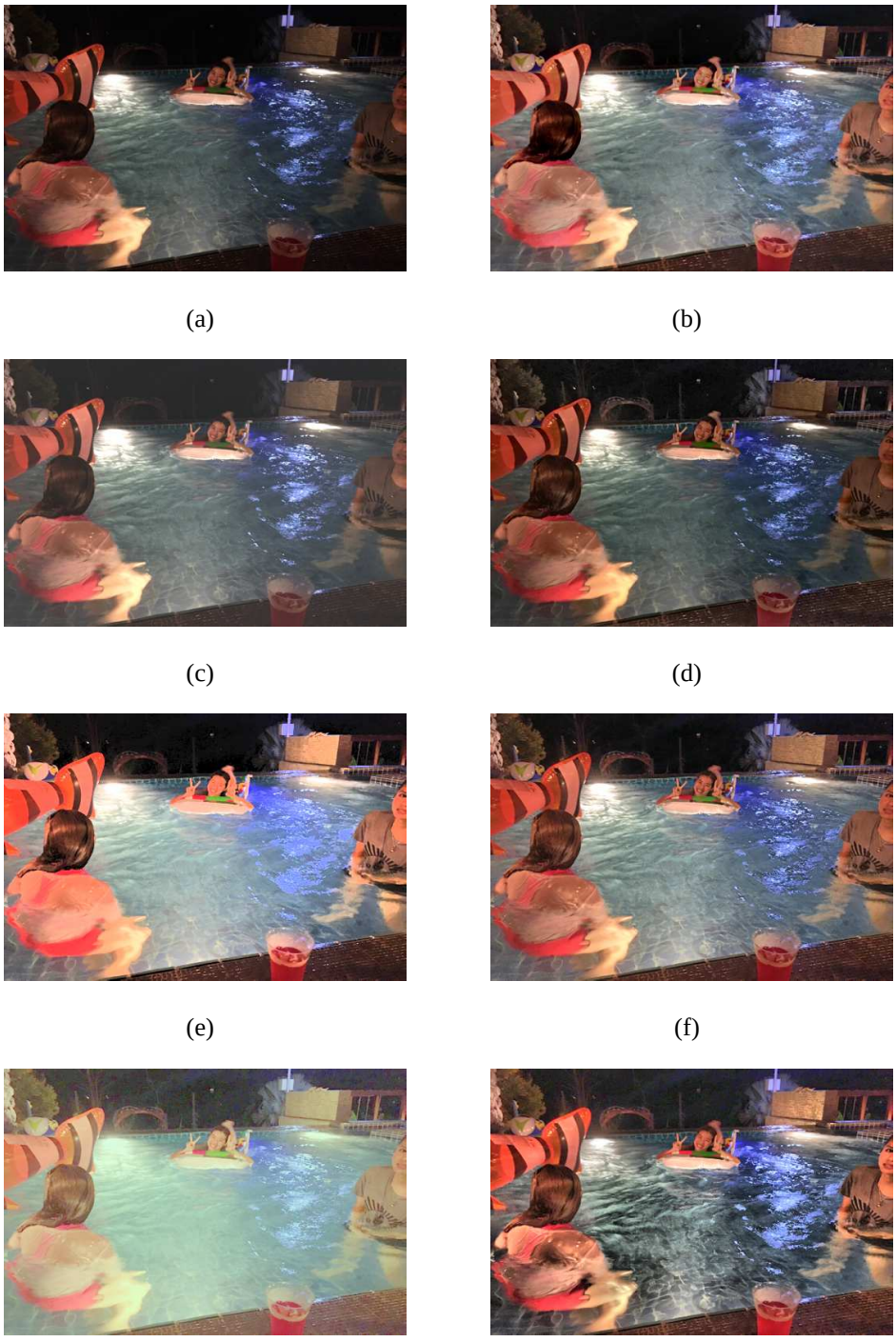

(a) (b) (c) (d) (e) (f) (g) (h)

Figure A.31: Image comparison with the existing method: (a) input image, (b) LVCEHP [25], (c) LVCE [22], (d) FCSM [1], (e) MSRCP [13], (f) MEF [11], (g) MSRCR [8], (h) CLAHE [3]

(a) (b)

(c) (d)

(e) (f)

(g) (h)

Figure A.32: Image comparison with the existing method: (a) input image, (b) LVCEHP [25], (c) LVCE [22], (d) FCSM [1], (e) MSRCP [13], (f) MEF [11], (g) MSRCR [8], (h) CLAHE [3]

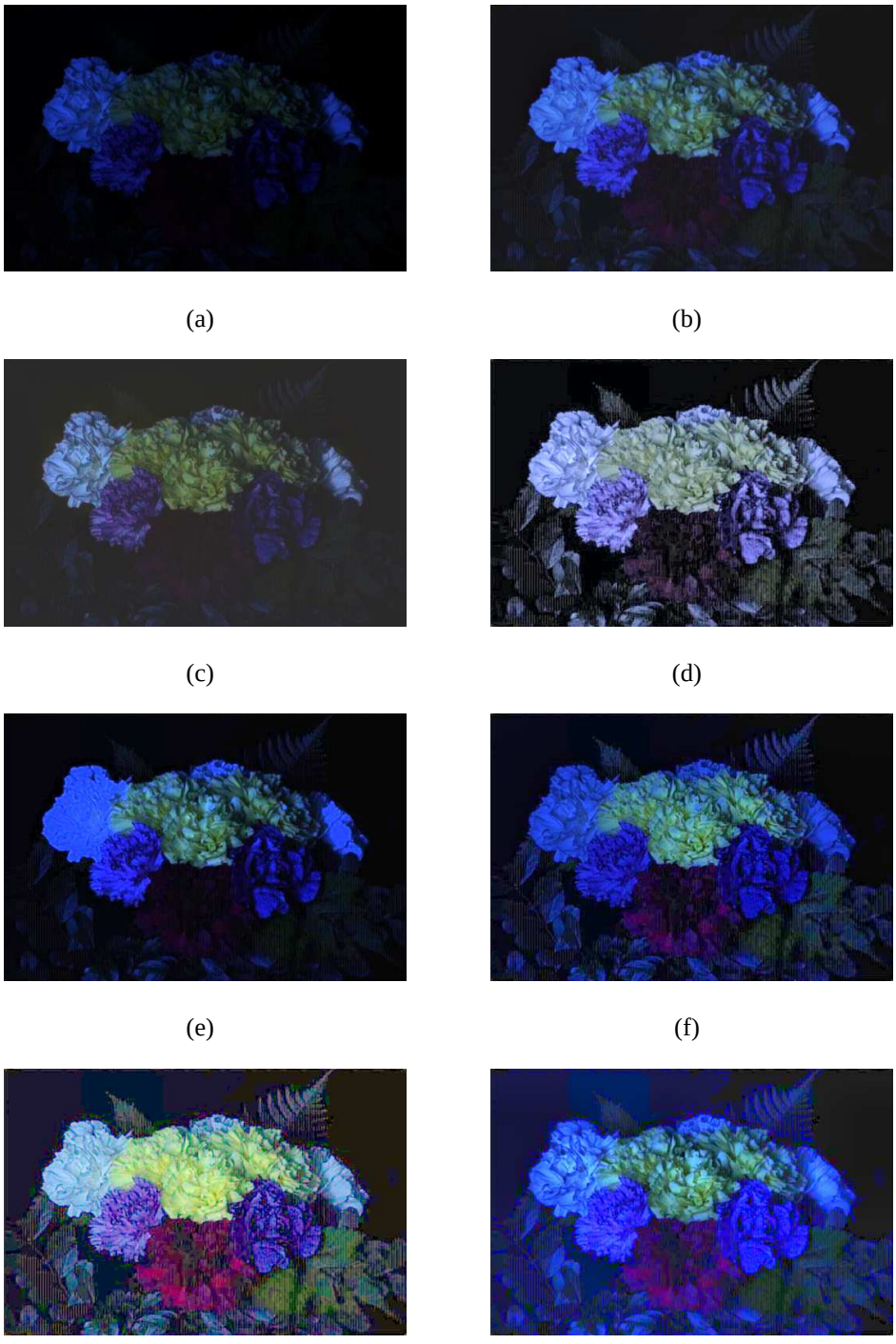

(a) (b) (c) (d) (e) (f) (g) (h)

Figure A.33: Image comparison with the existing method: (a) input image, (b) LVCEHP [25], (c) LVCE [22], (d) FCSM [1], (e) MSRCP [13], (f) MEF [11], (g) MSRCR [8], (h) CLAHE [3]

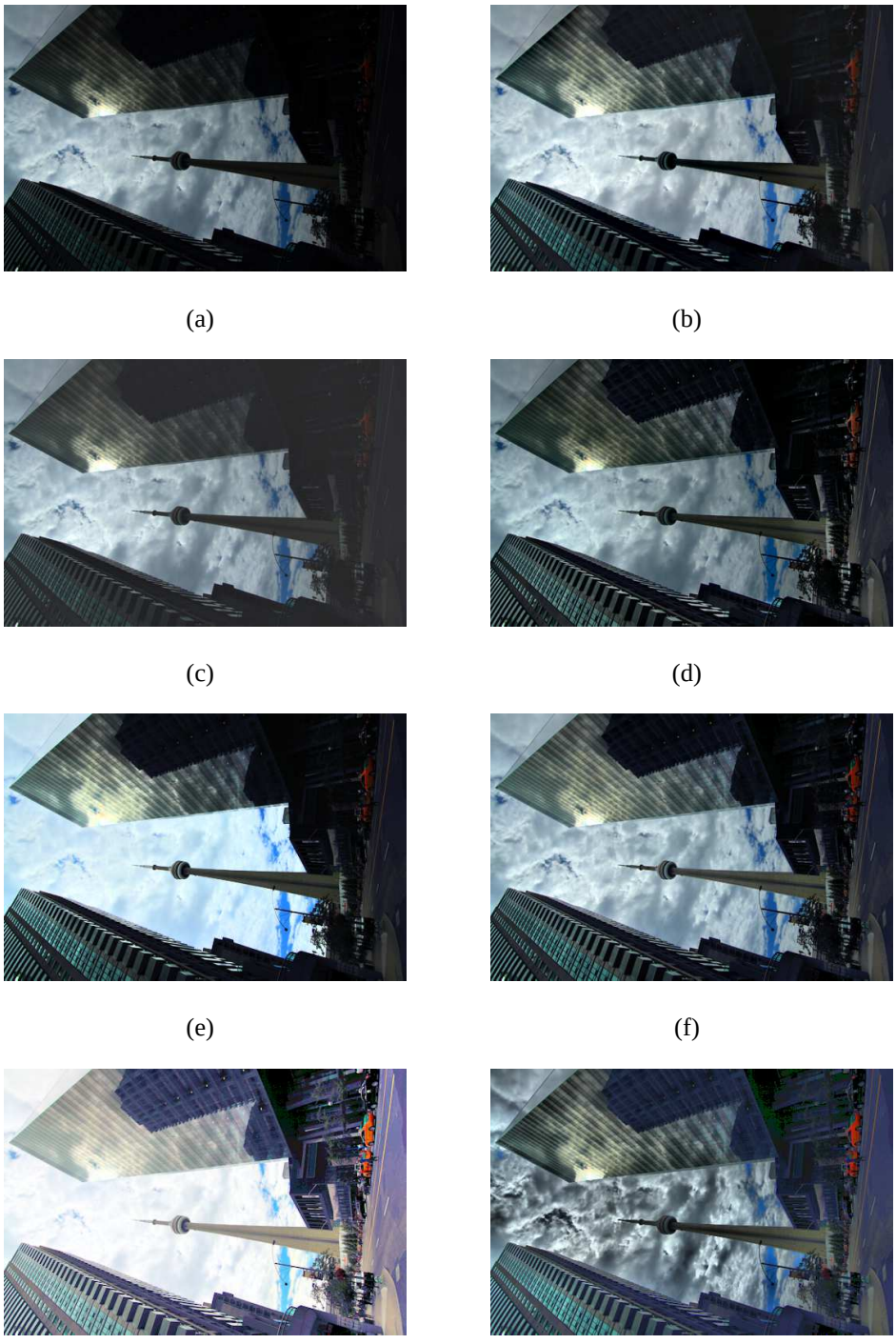

(a) (b) (c) (d) (e) (f) (g) (h)

Figure A.34: Image comparison with the existing method: (a) input image, (b) LVCEHP [25], (c) LVCE [22], (d) FCSM [1], (e) MSRCP [13], (f) MEF [11], (g) MSRCR [8], (h) CLAHE [3]

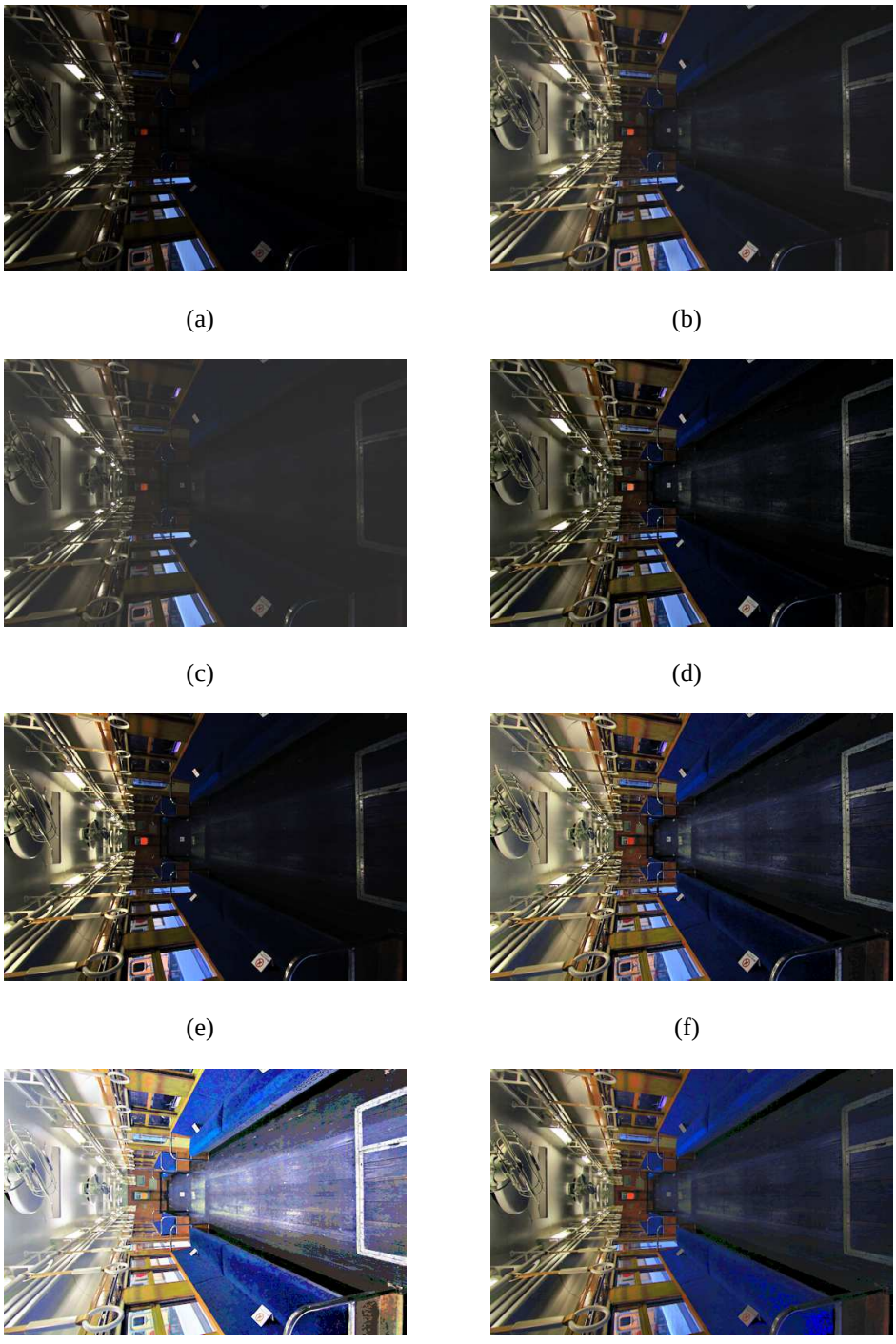

(a) (b) (c) (d) (e) (f) (g) (h)

Figure A.35: Image comparison with the existing method: (a) input image, (b) LVCEHP [25], (c) LVCE [22], (d) FCSM [1], (e) MSRCP [13], (f) MEF [11], (g) MSRCR [8], (h) CLAHE [3]

(a) (b) (c) (d) (e) (f) (g) (h)

Figure A.36: Image comparison with the existing method: (a) input image, (b) LVCEHP [25], (c) LVCE [22], (d) FCSM [1], (e) MSRCP [13], (f) MEF [11], (g) MSRCR [8], (h) CLAHE [3]

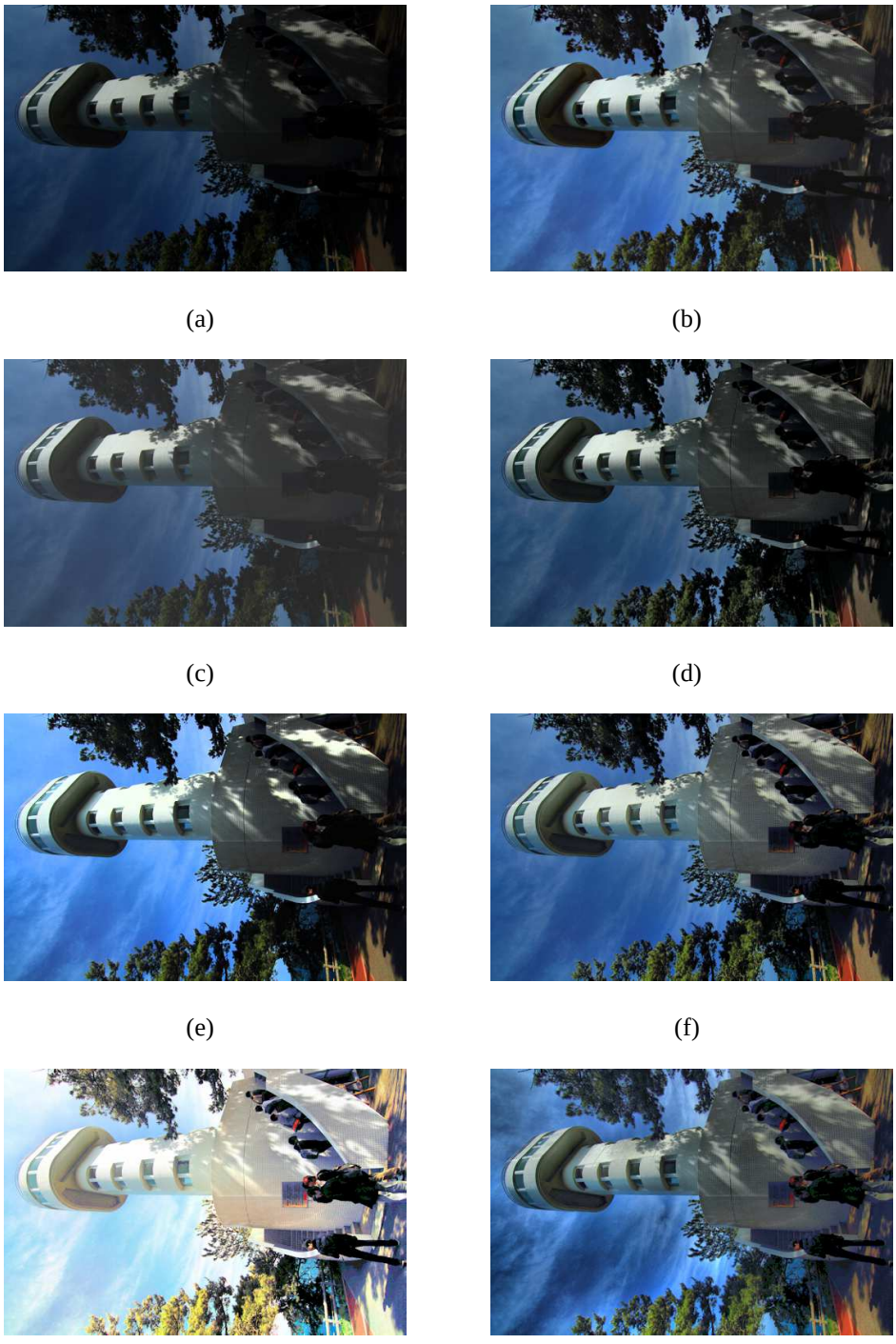

(a) (b) (c) (d) (e) (f) (g) (h)

Figure A.37: Image comparison with the existing method: (a) input image, (b) LVCEHP [25], (c) LVCE [22], (d) FCSM [1], (e) MSRCP [13], (f) MEF [11], (g) MSRCR [8], (h) CLAHE [3]

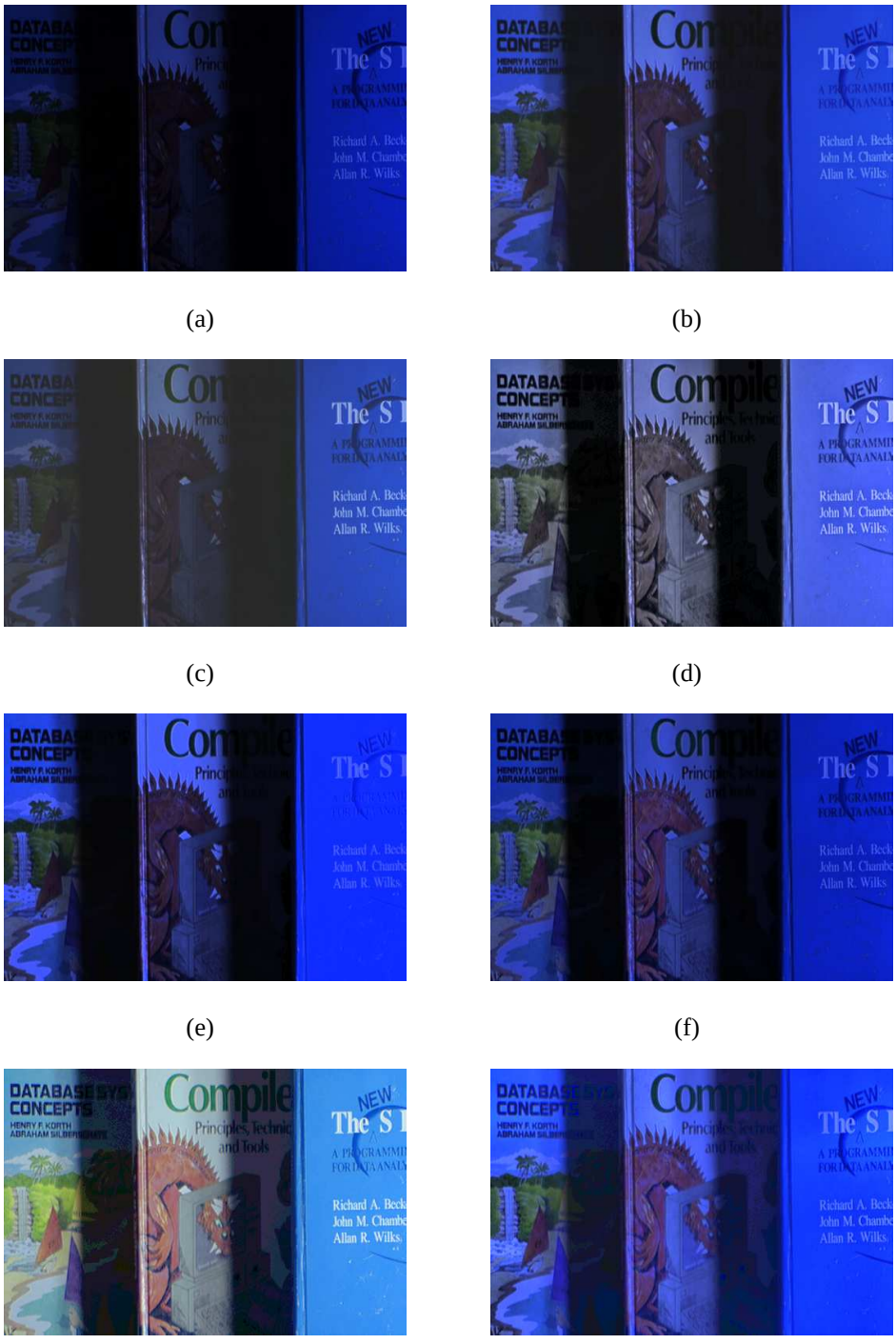

(a) (b) (c) (d) (e) (f) (g) (h)

Figure A.38: Image comparison with the existing method: (a) input image, (b) LVCEHP [25], (c) LVCE [22], (d) FCSM [1], (e) MSRCP [13], (f) MEF [11], (g) MSRCR [8], (h) CLAHE [3]

Bibliography

[1] V. Vonikakis, I. Andreadis, and A. Gasteratos, "Fast centre-surround contrast modification," *IET Image Processing*, vol. 2, pp. 19–34, Feb 2008.

[2] R. C. Gonzalez and R. E. Woods, *Digital Image Processing (3rd Edition)*. Upper Saddle River, NJ, USA: Prentice-Hall, Inc., 2006.

[3] K. Zuiderveld, "Graphics gems iv," ch. Contrast Limited Adaptive Histogram Equalization, pp. 474–485, San Diego, CA, USA: Academic Press Professional, Inc., 1994.

[4] Y.-T. Kim, "Contrast enhancement using brightness preserving bi-histogram equalization," *IEEE Transactions on Consumer Electronics*, vol. 43, pp. 1–8, Feb 1997.

[5] A. Majumder and S. Irani, "Perception-based contrast enhancement of images," *ACM Trans. Appl. Percept.*, vol. 4, Nov. 2007.

[6] D. J. Jobson, Z. Rahman, and G. A. Woodell, "Properties and performance of a center/surround retinex," *IEEE Transactions on Image Processing*, vol. 6, pp. 451–462, Mar 1997.

[7] Z. Rahman, D. J. Jobson, and G. A. Woodell, "Multi-scale retinex for color image enhancement," in *Image Processing, 1996. Proceedings., International Conference on*, vol. 3, pp. 1003–1006 vol.3, Sep 1996.

[8] D. J. Jobson, Z. Rahman, and G. A. Woodell, "A multiscale retinex for bridging the gap between color images and the human observation of scenes," *IEEE Transactions on Image Processing*, vol. 6, pp. 965–976, Jul 1997.

[9] S. Bhattacharya, S. Gupta, and V. K. Subramanian, “Localized image enhancement,” in *Communications (NCC), 2014 Twentieth National Conference on*, pp. 1–6, Feb 2014.

[10] H. Demirel, G. Anbarjafari, and M. N. S. Jahromi, “Image equalization based on singular value decomposition,” in *Computer and Information Sciences, 2008. ISCIS ’08. 23rd International Symposium on*, pp. 1–5, Oct 2008.

[11] X. Fu, D. Zeng, Y. Huang, Y. Liao, X. Ding, and J. Paisley, “A fusion-based enhancing method for weakly illuminated images,” *Signal Process.*, vol. 129, pp. 82–96, Dec. 2016.

[12] E. H. Land and J. J. McCann, “Lightness and retinex theory,” *J. Opt. Soc. Am.*, vol. 61, pp. 1–11, Jan 1971.

[13] A. B. Petro, C. Sbert, and J.-M. Morel, “Multiscale Retinex,” *Image Processing On Line*, pp. 71–88, 2014.

[14] B. Funt, F. Ciurea, and J. Mccann, “Retinex in matlab,” in *Journal of Electronic Imaging*, pp. 112–121, 2000.

[15] P. Burt and R. Kolczynski, “Enhanced image capture through fusion,” in *Computer Vision, 1993. Proceedings., Fourth International Conference on*, pp. 173–182, May 1993.

[16] S. Keerativittayanun, T. Kondo, K. Kotani, and T. Phatrapornnant, “An innovative of pyramid-based fusion for generating the hdr images in common display devices,” in *Machine Vision Applications (MVA), 2015 14th IAPR International Conference on*, pp. 53–56, May 2015.

[17] T. Mertens, J. Kautz, and F. V. Reeth, “Exposure fusion,” in *Computer Graphics and Applications, 2007. PG ’07. 15th Pacific Conference on*, pp. 382–390, Oct 2007.

[18] S. Corchs and F. Gasparini, *Enhancing Underexposed Images Preserving the Original Mood*, pp. 125–136. Berlin, Heidelberg: Springer Berlin Heidelberg, 2011.

[19] K. Konstantinides, B. Natarajan, and G. S. Yovanof, “Noise estimation and filtering using block-based singular value decomposition,” *Trans. Img. Proc.*, vol. 6, pp. 479–483, Mar. 1997.

[20] C.-H. Chou and Y.-C. Li, "A perceptually tuned subband image coder based on the measure of just-noticeable-distortion profile," *IEEE Transactions on Circuits and Systems for Video Technology*, vol. 5, no. 6, pp. 467–476, 1995.

[21] X. Zhang, W. Lin, and P. Xue, "Just-noticeable difference estimation with pixels in images," *Journal of Visual Communication and Image Representation*, vol. 19, no. 1, pp. 30–41, 2008.

[22] S. Keerativittayanun, K. Kotani, T. Kondo, T. Phatrapornnant, and J. Karnjana, "Less-visible contrast enhancement based on non-linear scaling function and singular value decomposition," in *Digital Image Computing: Techniques and Applications (DICTA), 2016*, [To appear].

[23] "Orasis image enhancement software: Bridging the gap between what you see and what the camera captures." `http://vonikakis.com/`. Accessed: 2017-09-20.

[24] "Multiscale retinex." `http://demo.ipol.im/demo/107/?` Accessed: 2017-09-13.

[25] S. Keerativittayanun, K. Kotani, T. Kondo, T. Phatrapornnant, and J. Karnjana, "Less-visible contrast enhancement based on the human visual perception," *Optik - International Journal for Light and Electron Optics*, vol. 157, no. Supplement C, pp. 467 – 483, 2018.

[26] J. V. L and R. Gopikakumari, "Article: Iem: A new image enhancement metric for contrast and sharpness measurements," *International Journal of Computer Applications*, vol. 79, pp. 1–9, October 2013.

[27] Z. Wang and A. C. Bovik, "A universal image quality index," *IEEE Signal Processing Letters*, vol. 9, pp. 81–84, March 2002.

[28] Y. Hu, C. x. Zhao, and H. n. Wang, "Directional analysis of texture images using gray level co-occurrence matrix," in *Computational Intelligence and Industrial Application, 2008. PACIIA '08. Pacific-Asia Workshop on*, vol. 2, pp. 277–281, Dec 2008.

Publications

Journal

[1] S. Keerativittayanun, K. Kotani, T. Kondo, T. Phatrapornnant, J. Karnjana, Less-visible contrast enhancement based on the human visual perception, Optik, Vol. 157, March, 2018, Pages 467-483.

International Conference

[2] S. Keerativittayanun, T. Kondo, K. Kotani and T. Phatrapornnant, ”An innovative of pyramid-based fusion for generating the HDR images in common display devices,” 2015 14th IAPR International Conference on Machine Vision Applications (MVA), Tokyo, 2015, pp. 53-56.

[3] S. Keerativittayanun, K. Kotani, T. Kondo, T. Phatrapornnant and J. Karnjana, ”Less-Visible Contrast Enhancement Based on Non-Linear Scaling Function and Singular Value Decomposition,” 2016 International Conference on Digital Image Computing: Techniques and Applications (DICTA), Gold Coast, QLD, 2016, pp. 1-8.